

**Influence of strain-hardening on the wear resistance of
metallic materials**

by

Aakash Kumar

A thesis submitted in partial fulfillment of the requirements for the degree of

Master of Science

in

Materials Engineering

Department of Chemical and Materials Engineering

University of Alberta

Abstract

Keywords: sliding wear, cold work, strain hardening, wear resistance, hardness, Young's modulus.

Although it is known that strain-hardening helps improve the wear resistance of metallic materials, puzzles or inconsistent phenomena still exist regarding the effect of strain-hardening on the wear resistance of metallic materials. It was reported that strain-hardening showed little or limited benefits to the wear resistance of some carbon steels. Besides, if the strain-hardening works, its benefit to the wear resistance may not be as large as expected. In this thesis, a study on the influence of strain hardening on the wear resistance of cold worked metallic materials is reported in three parts.

In part 1, the effects of strain-hardening (cold work) on dry sliding wear of Cu and Mg were investigated. The dry sliding wear tests were performed under different contact loads of 2N, 5N, 8N, and 12N, respectively, at room temperature. It was demonstrated that the strain-hardening decreased Young's moduli of Cu and Mg samples due to deteriorated crystalline integrity, which reduced the benefit of strain-hardening to their wear resistance. The strain-hardening benefited the FCC Cu more than the HCP Mg, and the effectiveness of strain-hardening decreased with increasing the contact load. Relevant mechanisms were elucidated from the viewpoint of wearing energy consumption.

In part 2, we investigated the wear behaviors of strain-hardened Cu and Mg and demonstrated that the H/E (H=Hardness, E=Young's modulus) ratio markedly

overestimated the wear resistance of these pure metals. The H/E ratio is often used as an index to represent the wear resistance of materials and coatings. The larger the H/E ratio, the higher the wear resistance. However, though this ratio is shown to be a measure of the wear resistance for reported cases, whether it can be generalized as an index of wear resistance is questionable. Although the cold work increases hardness, it deteriorates the material integrity with introduced lattice imperfections, which negatively influence the atomic bonding, thus decreasing the benefit of strain-hardening to the wear resistance. As a result, the H/E ratio should not be generalized as a measure of wear resistance.

In part 3, we investigated the influence of the Bauschinger effect on the wear behavior of cold worked Cu and Mg under unidirectional and bidirectional sliding wear conditions. The Bauschinger effect has been studied for a long time, which influences the wear of materials under the unidirectional sliding wear and reciprocating wear conditions. The Bauschinger effect could be altered during the wear of cold worked metals with different crystal structures such as Cu (FCC) and Mg (HCP). The strain-hardened Cu had dislocation pileups while strain-hardened Mg had vacancies, pores, or micro-cracks with fewer dislocations. Volume losses of the cold worked metals are higher caused by unidirectional sliding than those caused by bidirectional sliding, attributed to the fact that during bidirectional sliding, reversible movement dislocations may occur, and dislocations with opposite signs may cancel each other due to the reversal of the wearing stress, leading to lowered wear damage.

Preface

No part of this work was taken from other people's or party's work without their consent, except otherwise noted as cited works used in this scope alone.

Portions of this work have been published in scientific forums and journals/communications:

1. 'Clarification of the Puzzled Effects of Cold work on Wear of Metals from the Viewpoint of Wearing Energy Consumption'. Aakash Kumar, D. Y. Li, **Tribology Letters**, Volume 70, Article number: 3 (2022).
2. 'Can the H/E ratio be generalized as an index for the wear resistance of materials?', *Aakash Kumar, D. Y. Li, Materials Chemistry and Physics*, Volume 275, January 2022, 125245.
3. 'Influence of Bauschinger effect in the wear behavior of cold worked pure Cu and Mg during unidirectional and bidirectional sliding wear'. *Manuscript being prepared for submission.*

All rights reserved. No part of this publication may be reproduced, distributed, or transmitted in any form or by any means, including photocopying, recording, or other electronic or mechanical methods, without the prior written permission of the author, except in the case of brief quotations embodied in critical reviews and specific other non-commercial uses if permitted by the Canadian copyrights law.

Dedications

*To my father Ashok Kumar Sahni
In loving memory of my brother Vikash &
my mother.*

Acknowledgments

This work was done to provide an insight into the effect of strain hardening (cold working) on the wear behavior of pure metals from the viewpoint of energy consumption and can be further extended to other types of materials like alloys, composites, etc.

I would like to give my thanks and appreciation to the following persons:

Dr. Dongyang Li for his excellent oversight and consistent mentoring. His knowledge of tribological characteristics and metal physics in general, as well as his approach to them, are among the best in the area. I had a great time being guided by him.

My cohorts Zhang Dong, Mingyu Wu, Yuzhuo Luo, Guijiang Diao, Xu Zhen, Raymond Christopher Setiawan, Mohammadjavad Palimi always give me helpful thoughts on how to improve my experiments and avoid falling into technical traps.

My father, Ashok Kumar Sahni, for always believing in me and inspiring me.

Unfortunately, I cannot mention all my friends and families one by one here. However, do remember that you are always in my mind, and my thanks will always be yours.

This thesis is not the pinnacle of my quest for knowledge. I understand that this is only a little portion of my lengthy journey, but I have always treasured every step along the route. Thank you, University of Alberta, for every cherished memory I penned and friendly acquaintances I made, for every emotion I felt and for every laugh I shared!

The University of Alberta acknowledges that we are located on Treaty 6 territory, and respects the histories, languages, and cultures of First Nations, Métis, Inuit, and all First Peoples of Canada, whose presence continues to enrich our vibrant community.

L'Université de l'Alberta reconnaît qu'elle est située sur les terres du Traité 6 et respecte les histoires, les langues et les cultures des Premières Nations, des Métis, des Inuits et de tous les peuples autochtones du Canada, dont la présence continue d'enrichir notre communauté si vivante.

Author
Winter 2022

Funding Disclosure:

The author is grateful for the continuing support from the Natural Science and Engineering Research Council (NSERC) Canada.

Declaration of Competing Interest:

I acknowledge that this work in its entirety is free from any form of conflicting or competing interests.

COVID-19 Protocol:

Because of the global COVID-19 epidemic, several aspects of this research were conducted remotely wherever feasible. Due to the nature of this investigation, which included some physical presence at the laboratory, this work was carried out in strict accordance with the university's COVID-19 dissemination prevention policy.

The author, as the study's principal executor, strictly followed the instructions and bylaws issued by the Alberta and federal governments regarding establishment closure and restriction to entry (March 2020, December 2020, and May 2021), and performed no laboratory work on or within the perimeter of the university establishments during those times.

This thesis is registered under the *Theses Canada* program.

Contents

Title page	I
Abstract.....	ii
Preface	iv
Dedications	v
Acknowledgments	vi
Funding Disclosure	vii
Contents.....	viii
List of Tables.....	xi
List of Figures	xii
List of Abbreviations	xv
List of Symbols	xvi
Chapter I: Introduction	1
1.1. Motivations.....	1
1.1.1. Review of the Archard Wear model.....	1
1.1.2. Limitations of the Archard Wear model.....	3
1.1.3. Review of the Wearing energy model	4
1.1.4. Part I: Clarification of the puzzled effects of cold work on wear of metals from the viewpoint of wearing energy consumption	5
1.1.5. Part II: Generalization of the H/E ratio as an index for wear resistance of materials.....	6
1.1.6. Part III: Influence of Bauschinger effect in the wear behavior of Cold worked pure Cu and Mg during unidirectional and bidirectional sliding wear.....	6
1.2. Timeline	7
1.3. Outline of this thesis	7
Chapter II: Theoretical Background	8
2.1. Wear	8
2.2. Wear classification	9
2.2.1. Adhesive wear	10
2.2.2. Abrasive wear	11
2.2.3. Corrosive wear.....	12

2.2.4. Surface fatigue wear	13
2.2.5. Some other types of wear	13
2.3. Strengthening mechanisms	14
2.3.1. Strain hardening.....	15
2.3.2. Grain size reduction	16
2.3.3. Solid solution strengthening.....	17
2.3.4. Precipitation strengthening.....	18
2.3.5. Dispersion strengthening	19
2.3.6. Fiber strengthening	19
2.3.7. Martensite strengthening	19
2.4. Electron Work Function (EWF).....	20
2.4.1. Definition.....	20
2.4.2. EWF and Young's modulus	20
2.4.3. EWF measurement using Kelvin Probe Method.....	21
2.5. Bauschinger effect and its mechanism	22
2.5.1. Bauschinger effect	22
2.5.2. Mechanisms of the Bauschinger effect	23
2.5.2.1. Internal stress theory	23
2.5.2.2. Composite model	24
2.5.2.3. Dislocation theory.....	25

Chapter III: Clarification of the puzzled effects of cold work on wear of metals from the viewpoint of wearing energy consumption..... 26

3.1. Experimental.....	31
3.1.1. Materials	31
3.1.2. Sample preparation.....	31
3.1.3. Sliding wear test setup	32
3.1.4. Mechanical testing	33
3.2. Results and discussions.....	34
3.2.1. Mechanical properties and cold work-induced changes in hardness and Young's modulus	34
3.2.2. Wear behavior.....	39
3.3. Conclusion	48

Chapter IV: The unsuitability of generalizing the H/E ratio as an index for the wear resistance of materials..... 49

4.1. Experimental 51
4.1.1. Materials and sample preparation 51
4.1.2. Mechanical testing..... 52
4.1.3. Sliding wear test 52
4.2. Results and Discussion..... 53
4.2.1. Mechanical properties 53
4.2.2. Microstructural characterization..... 54
4.2.3. Wear behavior 56
4.3. Conclusion 61

Chapter V: Influence of Bauschinger effect in the wear behavior of cold worked pure Cu and Mg during unidirectional and bidirectional sliding wear. 62

5.1. Experimental..... 65
5.1.1. Materials and methodology 65
5.1.2. Sliding wear test and Characterization 67
5.2. Results and Discussion..... 68
5.2.1. Mechanical properties 68
5.2.2. Microstructural characterization 68
5.2.3. Wear characteristics 71
5.3. Conclusion 79

Chapter VI: General Conclusions..... 81

6.1. Part I: Clarification of the puzzled effects of cold work on wear of metals from the viewpoint of wearing energy consumption 81
6.1.1. Concluding results 81
6.1.2. Future recommendations..... 82
6.2. Part II: Generalization of the H/E ratio as an index for wear resistance of materials 83
6.2.1. Concluding results..... 83
6.2.2. Future recommendations 83
6.3. Part III: Influence of Bauschinger effect in the wear behavior of cold worked pure Cu and Mg during unidirectional and bidirectional sliding wear..... 84
6.3.1. Concluding results 84
6.3.2. Future recommendation 86

Bibliography	87
Appendix.....	101

List of Tables

Table 1.1. Timeline of this study	7
--	---

Table 3.1. Mechanical properties determined by tension and impact tests.....	34
---	----

Table 3.2. Hardness (MPa) and Young's Modulus (GPa) for Cu and Mg samples with at 0%, 10%, 20%, 30%, 40% reduction in thickness.	39
---	----

List of Figures

Figure 2.1. Mechanism of Adhesive wear 10

Figure 2.2. Mechanism of Abrasive wear 11

Figure 2.3. Mechanism of Corrosive wear 12

Figure 2.4. Mechanism of surface fatigue wear 13

Figure 2.5. Stress-strain curve of a metallic alloy with strain hardening & variation of tensile properties of low carbon steel in terms of % of Cold work 16

Figure 2.6. Schematic illustration of the grain size effect on the stress-strain curves on a metallic material. 17

Figure 2.7. Schematic representation of the effect of alloy content in the tension properties of a solid solution metallic alloy..... 18

Figure 2.8. Correlation between a material’s EWF and its bulk moduli 21

Figure 2.9. Schematic representation of the principle of Kelvin Probe Microscopy 22

Figure 2.10. Schematic illustration of the Bauschinger effect in metallic materials. Compressive plastic deformation reduces the tensile strength, leading to yielding under lower tensile stress..... 22

Figure 3.1. Relative wear resistance ($=1/\text{volume loss}$) versus hardness for metals 29

Figure 3.2. (a) Charpy impact energy and (b) stress-strain curves of the as-received Mg and Cu..... 35

Figure 3.3. Variations in Rockwell hardness and Young’s modulus with respect to cold work reduction: (a) Magnesium and (b) Copper..... 38

Figure 3.4. (a) Mg sample without cold work, (b) Mg sample cold worked by 20% reduction in thickness, (c) Cu sample without cold work, (d) Mg sample cold worked by 20% reduction in thickness; all samples were polished and then etched. 39

Figure 3.5. (a) Mg sample without cold work, (b) Mg sample cold worked by 20% reduction in thickness, (c) Cu sample without cold work, (d) Mg sample cold worked by 20% reduction in thickness; all samples were polished and then etched.

.....	40
Figure 3.6. (a-d) Curves of relative wear resistance of non-deformed deformed Mg samples versus apparent hardness, predicted by Archard’s equation. Experimentally measured data points are presented, which were used to determine the η value in the wearing energy model. Wear resistance ~ hardness curves given by eq. (3.2) are presented by dashed purple lines; Variations in Young’s modulus with respect to hardness are also given. The wear tests were performed under (a) 2N, (b) 5N, (c) 8N, (d) 12N for samples with 0%, 10%, 20%, 30%, 40% reduction in thickness, respectively.	43
Figure 3.7. (a-d) Curves of relative wear resistance of non-deformed and deformed Cu samples versus apparent Rockwell hardness, predicted by Archard’s Model. Experimentally measured data points are presented, which were used to determine the η value in the wearing energy model [eq. (3.2)]. Wear resistance ~ hardness curves given by eq. (3.2) are presented by dashed purple lines; Variations in Young’s modulus with respect to hardness are also given. The wear tests were performed under (a) 2N, (b) 5N, (c) 8N, (d) 12N for samples with 0%, 10%, 20%, 30%, 40% reduction in thickness, respectively.	46
Figure 3.8. Variations in η value versus with the applied load for (a)Mg (HCP) and (b)Cu (FCC)	47
Figure 4.1. Variations in H, E, and EWF of (a) Cu and (b) Mg, with respect to the reductions in the thickness of 0%, 10%, 20%, 30%, and 40%, respectively	54
Figure 4.2. SEM images of (a) non-deformed Mg, (b) Mg with 20% reduction in thickness, (c) Mg with 40% reduction in thickness; (d) non-deformed Cu, (e) Cu with 20% reduction in thickness, and (f) Cu with 40% reduction in thickness. The surfaces were etched	55
Figure 4.3. Standardized wear resistances determined experimentally, corresponding H/E ratios and those predicted by Archard’s equation versus the apparent hardness for cold worked Cu and Mg tested at two loads: (a) Cu_5N, (b) Cu_8N, (c) Mg_5N, and (d) Mg_8N.	58
Figure 4.4. Plastic deformation may introduce dislocations, vacancies, and micro-voids or micro-cracks that may be initiated from vacancy clusters during severe plastic deformation. The lattice imperfections lose the crystal lattice, leading to	

	weakened atomic bonding and correspondingly decreased Young's modulus.	59
Figure 5.1.	Schematic representation of Bauschinger effect in metallic materials	63
Figure 5.2.	Schematic representation of unidirectional and bidirectional sliding wear tests	67
Figure 5.3.	SEM images of etched (a) undeformed Cu (400X), (b) undeformed Cu (5200X), (c) cold worked Cu up to 40% reduction in thickness (400X), (d) cold worked Cu up to 40% reduction in thickness (5200X).	69
Figure 5.4.	SEM images of etched (a) undeformed Mg, (b) cold worked Mg up to 40% reduction in thickness, (c) Micro voids present cold worked Mg (40%).	70
Figure 5.5.	Wear volume (mm ³) versus CN (Cyclic number) for Cu and Mg of 0%, 10%, 20%, 30%, 40% reduction in thickness.	73
Figure 5.6.	(a) SEM image of wear track of cold worked Cu (20%) during bidirectional sliding (CN=30), (b) oxygen composition of the wear track cold worked Cu during bidirectional sliding, (c) EDX map and spectrum of cold worked Cu during bidirectional sliding, (d) SEM image of wear track of cold worked Cu (20%) during unidirectional sliding, (e) oxygen composition of the wear track cold worked Cu during unidirectional sliding, (f) EDX map and spectrum of cold worked Cu during unidirectional sliding.	75
Figure 5.7.	SEM images and EDX analysis of wear track of (a, b) cold worked Mg (40%) in unidirectional sliding and (c, d) cold worked Mg in bidirectional sliding (CN=30)	77
Figure 5.9.	3D profile of the wear tracks along with the wear width and depth curve for (a) Cu 0% [CN=0], (b) Cu 0% [CN=30], (c) Cu 40% [CN=0], Cu 40% [CN=30].	78
Figure 5.10.	3D profile of the wear tracks along with the wear width and depth curve for (a) Mg 0% [CN=0], (b) Mg 0% [CN=30], (c) Mg 40% [CN=0], Mg 40% [CN=30].	79

List of Abbreviations

1.	CN	Cyclic Number
2.	EDS/EDX	Energy-dispersive X-ray spectroscopy
3.	EWF	Electron Work Function
4.	eV	Electron Volt
5.	FCC	Face Centered Cubic
6.	HCP	Hexagonal Close Packed
7.	HRB	Rockwell Hardness B Scale
8.	HRE	Rockwell Hardness E Scale
9.	KP	Kelvin Probe
10.	MgCO ₃	Magnesium Carbonate
11.	MgO	Magnesium Oxide
12.	RFDA	Resonance Frequencies and Damping Analysis
13.	SEM	Scanning Electron Microscope
14.	Si ₃ N ₄	Silicon Nitride
15.	SiC	Silicon Carbide
16.	UTM	Ultimate Tensile Machine

List of Symbols

1.	E	Young's modulus
2.	E_0	Young's modulus of undeformed specimen
3.	H	Hardness
4.	d	Grain size
5.	V	Volume loss during wear
6.	K	Wear coefficient
7.	L	Applied load
8.	σ	Stress
9.	σ_Y	Yield stress
10.	σ_{UTS}	Ultimate tensile stress
11.	η	Constant from the wearing energy model
12.	J	Charpy impact energy
13.	u	Strain energy density
14.	ε	Strain
15.	ε_b	Atomic bond strength
16.	e	Charge of an electron

Chapter I:

Introduction

This chapter outlines the issues that we are addressing along with the motivation, significance, and elementary principles of this study. It also includes general approaches for the problem presented and outlines the criteria for the study's success. The general outline for this study consists of three parts; the first part deals with the study of the effect of strain hardening on the wear resistance of cold worked pure Cu and Mg metals from the viewpoint of the wearing energy model which is a modified Archard model considering the energy consumed during sliding wear.

The second part investigates the application and generalization of the commonly used H/E ratio for ranking materials according to their wear resistance.

The third part determines the Influence of the Bauschinger effect in the wear behavior of cold worked pure Cu and Mg under unidirectional and bidirectional sliding wear conditions. Strain hardened pure Cu and Mg were used for all the above-mentioned three studies.

1.1. Motivation

1.1.1. Review of Archard Wear model

For the development of wear models and wear estimation of materials, a very common assumption was used that the volume loss during wear is directly proportional to the normal force and sliding distance. As an observed assumption, this law was proposed by Reye in 1860 [1] but it took almost a century for wear models and equations to get widely accepted and experimentally validated for their

specific applications mainly due to the complex phenomenon of wear which includes plastic deformation, crack nucleation and propagation, tribochemical reactions, material transfer between contact surfaces [2-6], etc.

In the 1950s, Kruschov conducted extensive experimental studies on abrasive wear of metals [7, 8]. Around the same time, J. Archard carried out his classical studies of contact mechanics of rough metal surfaces in dry conditions without any lubricant [9, 10] and developed his very famous and commonly used wear law based on prior works of Holm [11], Burwell [12]. This sliding wear equation is referred to as Archard's equation, which was derived after Bowden and Tabor presented a friction theory where adhesion occurs at the asperity contacts and the contact force plastically deforms the asperities of the softer metal [13-14]. This classical wear equation was extended by Rabinowicz for more generalized cases of abrasive wear [15]. Therefore, this equation is widely used to describe material removal caused by sliding wear resulting from tearing due to adhesion, plowing, or a cutting mechanism by a harder counter-face with asperities [16-18].

Interestingly, both laws of Kruschov and Archard have the same mathematical form and state that the wear volume V is proportional to the normal force F_N and the sliding distance D and inversely proportional to the hardness of the softer material.

$$V = K \frac{F * D}{H}$$

V: Volume loss

F: Normal contact force

H: Hardness

D: Sliding distance

K: Wear coefficient

1.1.2. Limitations of the Archard wear model

Because the Archard wear model was designed utilizing asperity contact geometry rather than directly dealing with the wearing energy, it is difficult to accurately represent wear under certain situations, such as strain-hardened materials, for which relevant reasons have never been elucidated [24]. The material hardness, which controls the asperity contacts, local mechanical interactions, and adhesive force in the asperity contact region under the applied load, is a major factor in the damage caused by sliding wear. By affecting mechanical deformation, plowing, fracture, oxidation, and adhesive tearing at the contacts, these factors influence the wear damage to materials in dynamic contact [19-21].

Hardness is a controlling parameter in the model for calculating the contact area that is worn over when a load is applied. In addition to mechanical damages, wear at the asperity contacts may include frictional heating [22-23], material softening, and improved material transfer between rubbing surfaces. However, while potential impacts of these factors on wear might be considered in the wear coefficient (K), the way they affect wear is not quantified. Therefore, to look at it in another way, the model provides ideas but not technical information. When constructing the sliding model, the focus is mostly on determining the contact area, with little consideration given to the wearing stress and energy dissipation during wear. Archard's equation is commonly used to deal with wear and is widely used in industry to predict the service life of machinery and facilities that are subjected to

wear. As previously stated, this contact geometry-based approach is unrelated to the wearing stress or strain and associated energy consumption since it primarily considers geometrical parameters with minimal physical consideration. As a result, the impact of a material's mechanical behavior on its wear is simply tied to the contact area's dependency on hardness. In dealing with the wearing process, there is insufficient physical framework and specifics. As a result, the sliding model described by Archard's equation is insufficient to give unambiguous hints to unravel the underlying wear mechanisms and explain some wear occurrences, such as the failure to anticipate wear of cold worked materials as previously discussed.

1.1.3. Review of the Wearing energy model

To address the wear damage from the perspective of energy consumption, which is the deformation energy absorbed up to failure, a wearing energy model was developed [24]. Although the apparent hardness of a material increases owing to the strain-hardening effect, the new flaws weaken atomic bonding, reducing the positive effect of such increased hardness on the wear resistance. The ratio of residual strain in the pre-deformed state (ϵ_p) to the failure strain (ϵ_f) as (ϵ_p / ϵ_f) may be associated to the change in Young's modulus (E) via its interaction with electron work function (ϕ) [24, 25].

Dislocations are formed during plastic deformation, lowering the material's density, and weakening its atomic bond strength [26-29]. Because the elastic modulus is determined by the strength of interatomic bonding, the weakening of atomic bonds caused by cold work reduces Young's modulus [30-32]. By using the relationships between Young's modulus, electron work function, and strain energy,

the ratio can be related to the ratio of Young's modulus of plastically deformed material (E) to that of strain-free one (E_0). The derived wearing energy model is expressed as

$$V = K \frac{F L}{H[1 + \eta \ln\left(\frac{E}{E_0}\right)]}$$

where V is the volume loss, K is the wear coefficient, L is the load applied, D is the sliding distance, H is the hardness of the material, E and E_0 are Young's moduli of plastically deformed material and strain-free one, respectively, and η is a coefficient which expresses the extent to which a reduction in Young's modulus has a detrimental impact on wear resistance.

1.1.4. Part I: Clarification of the puzzled effects of cold work on wear of metals from the viewpoint of wearing energy consumption

As discussed earlier the limitations of the classical Archard's model, in this part of the study the newly developed wearing energy model was used to investigate the wear behavior of cold worked pure Cu and Mg. Efforts were made to provide some meaningful significance to η (eta) which is a coefficient in the wearing energy model. The variations in η with load and the intensity of cold work were also established in this part. The effect of strain hardening on the wear resistance of cold worked pure Cu and Mg and the benefits of strain hardening after cold working was discussed.

1.1.5. Part II: The unsuitability of generalizing the H/E ratio as an index for the wear resistance of materials

Both hardness and Young's modulus of any material determine its response to wear. In this study, we discussed the generalization of a frequently used Hardness (H) to Young's modulus (E) ratio, (H/E), as an index of the wear resistance in ranking materials and coatings in terms of their wear resistance. We investigated the wear behavior of cold worked Cu and Mg and showed that the ratio should not be generalized as a measure to rank or index materials, as cold work increases hardness by strain hardening but lowers Young's modulus, thus leading to exaggerated high wear resistance.

1.1.6. Part III: Influence of Bauschinger effect on the wear behavior of cold worked Cu and Mg under unidirectional and bidirectional sliding wear conditions

Bauschinger's effect on the mechanical behavior of materials has been studied for a long time, which also influences the response of materials to wear. In this study, we investigated the effects of two different sliding conditions, unidirectional sliding, and bidirectional sliding, on the wear of cold worked Cu and Mg. The effect of the reversal of the wearing stress on wear was discussed for both the sliding conditions along with different frequencies of the reversal of wearing stress. Percentage wear volume changes for both the materials were different, which shows that they responded to the reversal of wearing stress differently. The study demonstrated that the Bauschinger effect on their wear resistances was influenced by different types of defects or imperfections introduced by cold work.

1.2. Timeline

Table 1.1. *Timeline of this study.*

<i>Project description</i>	Timeline
<i>Preparation of the layout</i>	Sept. 2019 – Oct. 2019
<i>Part I</i>	Nov. 2019 – Oct. 2020
<i>Part II</i>	Nov. 2021 – May 2021
<i>Part III</i>	May 2021 – Nov 2021
<i>Project closing</i>	Nov. 2021

1.3. Outline of this thesis

This thesis consists of 6 (six) chapters:

Chapter I: Introduction

Chapter II: Theoretical Background

Chapter III: Clarification of the puzzled effects of cold work on wear of metals from the viewpoint of wearing energy consumption

Chapter IV: The unsuitability of generalizing the H/E ratio as an index for the wear resistance of materials

Chapter V: Influence of Bauschinger effect on the wear behavior of cold worked Cu and Mg under unidirectional and bidirectional sliding wear conditions

Chapter VI: General Conclusions and recommended future work.

Chapter II:

Theoretical Background

This chapter discusses all the basic definitions of the parameters, characterization techniques used in this thesis. Firstly, the different types of wear and their classifications with the underlying mechanisms are discussed followed by the hardening mechanism which covers strain hardening. Characterization techniques and equipment are also briefly discussed along with some more terminologies that are frequently used in the thesis.

2.1. Wear

The unwanted but unavoidable removal of material from rubbing surfaces is referred to as wear. Even though the amount of material removed from the surface is tiny, it changes the dimensions of dynamic components in facilities, reduces operational efficiency, and could trigger the entire failure of the facilities. Replacement or repair of worn components and overhauling of machinery on a more frequent basis could cost a lot of money in terms of labor, machine downtime, and energy in the manufacturing of replacements. The term "wear" refers to the gradual deterioration of a surface's shape, which is often accompanied by a loss of weight and the formation of debris. Although wear appears to be simple at first glance, the real process of material removal is quite complicated. This is due to a variety of factors that affect wear [33].

The entire wear mechanism is complex and depends on several factors, including the surface composition and geometry, the contact cycle, the surrounding environment, and the contact forces involved. Highly strained localized contact spots are created when two surfaces are in dynamic contact. At these concentrated contact areas, fracture, shearing, or flow occurs, and bits of the material is taken from the surface and become debris [34].

Due to the harsh local circumstances and numerous types of processes occurring simultaneously at the contact, wear is a very complex phenomenon. The following arguments can be used to assess the problem's complexity. Wear alters the composition and properties of surfaces and near-surface regions; the material that separates two sliding surfaces can be considered a separate 'third-body' with its evolutionary history and attributes, which will frequently change over the system's lifespan. Surface topology changes when the material is removed or displaced during wear. Furthermore, the mechanisms that cause wear are frequently complicated, including a combination of mechanical and chemical processes. These reactions can produce a variety of tribochemical compounds such as composites and oxides.

2.2. Wear classification

The most commonly seen types of wear have been covered in this section of the thesis [35-37]. Wear can occur in a specific mode or two or more modes simultaneously. For instance, adhesive wear involves material tearing off the soft one involving large adhesive force, while abrasive wear of material is caused by hard asperities of a hard rough counter-face or hard abrasives. These two types of wear may be active at the same time. The following are the basic categories of wear.

2.2.1. Adhesive wear

As seen in Figure 2.1, this type of wear happens when two surfaces are slid over each other and fragments are torn off from the softer surface by adhesive force to cling to the other. These fragments may later partially come away from the surface, or they may form loose wear particles. At the contact surface, a large amount of stress develops, and the fragment deforms. The loose particle arises when the tension release associated with the particle departing the contact zone is stronger than the adhesive bond [38].

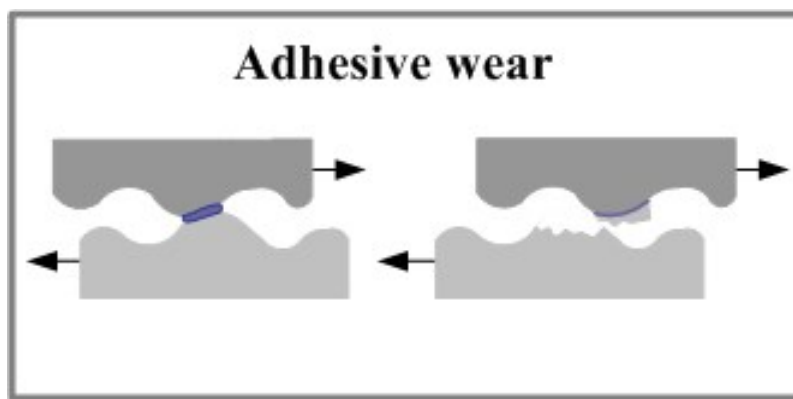


Figure 2.1. *Mechanism of Adhesive wear* [42]

Galling, scuffing, scoring, and seizing wear are all types of adhesive wear that depend on the degree of the action. This is one of the fundamental types of wear. It involves micro welds formed between the surface asperities that bear the load between two mated surfaces shearing. High temperatures, pressures, and sliding velocities usually promote adhesive wear.

2.2.2. Abrasive wear

This is the type of wear that occurs when a rough hard surface slides on a relatively soft surface and digs up a series of depressions in it. The material displaced by these depressions or grooves is in the form of wear particles, which are usually loose. Abrasive wear may also be caused by hard foreign particles, such as metal grit, metallic oxides, and dust and grit from the environment, which are present between the two surfaces in contact and result in abrasion. The first situation is usually referred to as two-body abrasive, while the second one is referred to as three-body abrasive wear. Figure 2.2 illustrates these two forms of abrasive wear.

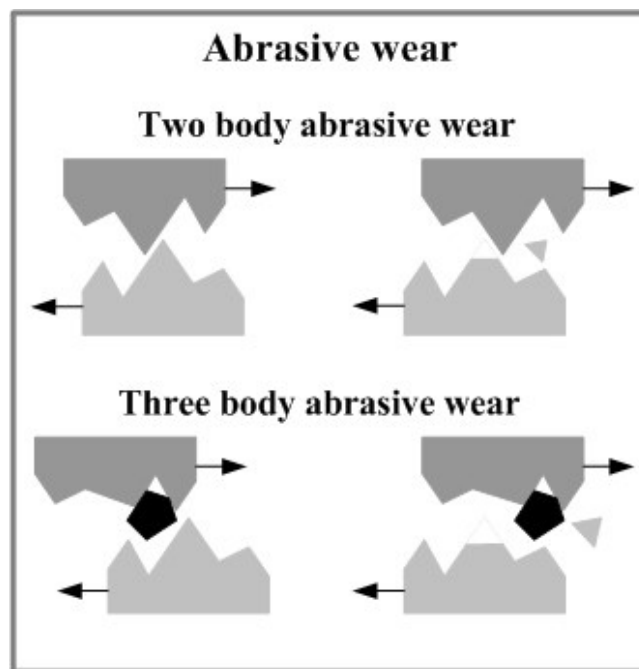


Figure 2.2. *Mechanism of Abrasive wear* [42]

The asperities on the tougher surface led the softer material to wear down in this scenario. During three-body wear, the abrasive particles may be partly immersed in one of the mating materials or maybe free. Abrasive wear is also called gouging,

grinding, or scratching abrasion depending on its intensity. Abrasive wear is one of the most prevalent forms of wear seen in engineering practice, and in many machine applications, it is likely the most common single source of wear [39].

2.2.3. Corrosive wear

It is the wear process that occurs when sliding in a corrosive environment. Without slippage, corrosion products (e.g., oxides) could form a film on surfaces, usually less than a micrometer thick, which would slow down or even stop corrosion, but the sliding motion damages the film causing more corrosion to occur. Since an oxygen-rich atmosphere is a typical environment for this wear process, oxidative wear is one of the most common types of corrosive wear [40]. If there is no oxide film formed on the material when the solution is very corrosive (usually acidic), the generated plastic deformation makes the material more anodic, which also accelerates the wear damage [40].

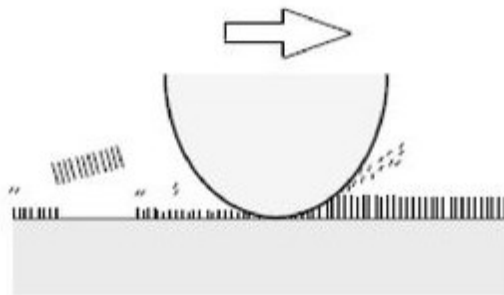


Figure 2.3. *Mechanism of Corrosive wear* [42]

2.2.4. Surface fatigue wear

Repeated sliding or rolling over a track causes this type of wear. The repetitive loading and unloading cycles to which the materials are subjected may cause the

creation of a surface or subsurface fatigue and fracture, which will finally result in the surface breaking apart with the formation of huge shards and enormous pits, as seen in figure 2.4. Pitting, spalling, and cause crushing are some of the terms used to describe this type of wear [41]. If the amplitude of cyclic displacement at the contact point is small, the fatigue wear is usually called fretting.

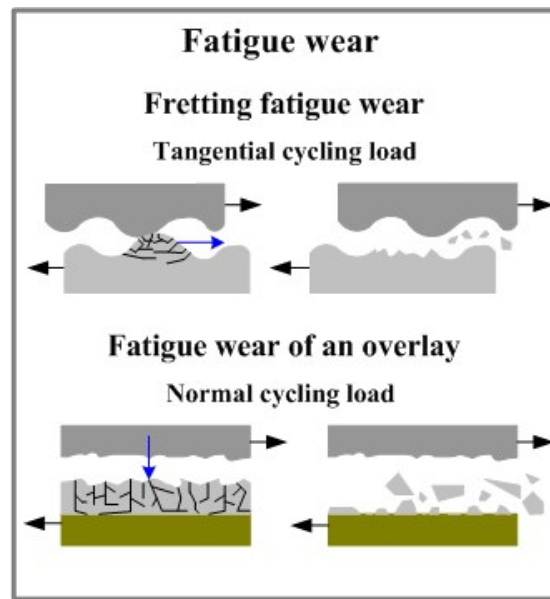


Figure 2.4. Mechanism of surface fatigue wear [42]

2.2.5. Some other types of wear

With the understanding of the above-mentioned elementary wear types, there are several other types of wear namely: impact wear, oxidative wear, erosion, and cavitation [42].

2.3. Strengthening mechanisms

Strengthening materials is defined as enhancing the mechanical strength of materials to increase their capacity to bear loads and withstand external stresses

without failing; particularly, it is accomplished by increasing the yield strength while maintaining, or even improving, ductility. Toughness, or the amount of energy or stress multiplied by strain required to deform a material before it fractures, is the attribute that best represents the mechanical behavior. Because hardness is directly connected to yield strength, strengthening is sometimes referred to as "hardening." A hard material such as zircon is not resistant to mechanical processing because it can be easily broken with a hammer; On the other hand, materials labeled as "high strength" or "tough" have high hardness values but also high ductility, which makes them strong and resistant to mechanical work [43].

Dislocations are introduced during plastic deformation, and their interaction with one another is a complicated process due to the large number of dislocations traveling in diverse directions throughout multiple slip systems. Dislocations traveling in parallel planes can annihilate or cancel each other, leaving vacancies or interstitial holes, but dislocations traveling in non-parallel planes constrain each other's movement by forming abrupt breaks — jog (break out of slip plane), kink (break in slip plane). Dislocation motion is also hampered by interstitial and substitutional atoms, grain boundaries, and foreign particles. Stopping dislocation motion can improve material strength [44].

The following are some of the several approaches to prevent dislocation motion/strengthening mechanisms:

In single-phase materials

2.3.1 Strain hardening

Strain hardening/work hardening is the process of strengthening any metallic material by plastic deformation. Dislocations, which are tiny imperfections in metallic crystal lattices, relate to plastic deformation. Interactions between nearby dislocations produce strain hardening during plastic deformation. The rate of strain hardening slows down as the temperature rises. As a result, materials are strain hardened at low temperatures, a process known as cold working. The density of dislocations rises because of plastic deformation. As a result of their interplay, the yield stress increases.

Dislocations are generally generated by changes in local stress fields inside a material, which cause atomic rearrangement in the crystal lattice due to dislocation movement. Dislocations can also be created by multiplying dislocations [45]. They collect and interact with one another as dislocation movement increases. This results in the formation of multiple pinning sites inside the lattice, which obstructs dislocation motion, resulting in material strengthening and a loss in ductility [46]. The phrase "percent Cold work" refers to the greatest plastic deformation that material may achieve before becoming fully brittle in the following load cycle.

Physical parameters change during strain hardening, in addition to mechanical attributes: a slight loss in density and a significant decrease in electrical conductivity. Chemical reactivity was boosted resulting in a decrease in corrosion resistance and a slight increase in the thermal coefficient of expansion.

The influences of cold work on the material properties can be mitigated by heating the material to an appropriate temperature below its melting point, which is called annealing. Annealing at appropriate temperatures can restore the material's

original qualities. Recovery, recrystallization, and grain growth are the three types of annealing. Most metals are deformed to a large amount in the industry using alternate cycles of strain hardening and annealing [47].

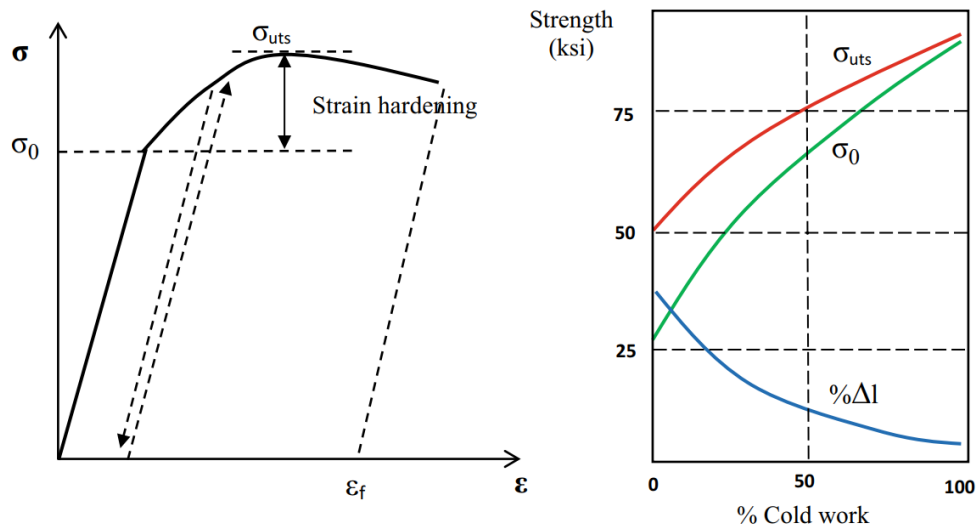


Figure 2.5. Stress-strain curve of a metallic alloy with strain hardening & variations in tensile properties of low carbon steel with respect to cold work [43].

2.3.2 Grain size-reduction

The movement of dislocations in polycrystalline materials would encounter obstacles when attempting to migrate from one grain to the next. There are two sorts of hindrances: forced slip direction shift and discontinuous slip plane. A dislocation frequently faces obstacles when grain size decreases. The material's yield strength will be increased [48]. The Hall Petch relationship links the yield strength to the grain size (diameter, d):

$$\sigma_y = \sigma_i + kd^{-1/2}$$

Regulated cooling or plastic deformation followed by suitable heat treatment can be used to alter grain size.

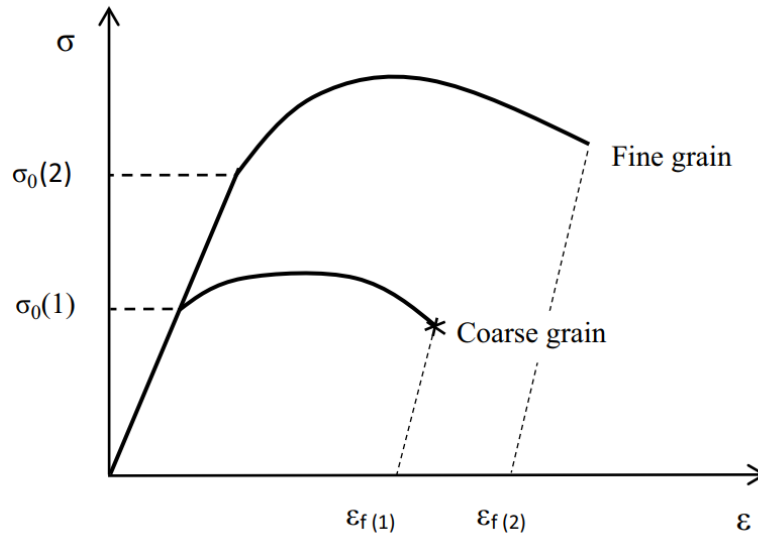


Figure 2.6. Schematic illustration of the grain size effect on the stress-strain curve of a metallic material [43].

2.3.3 Solid solution strengthening

When impurity atoms or solutes enter the solution and stay in substitutional or interstitial positions, the localized strain fields created by the impurity atoms interact with the compressive and tensile strain fields caused by dislocations. Based on the respective atomic sizes of the solute and solvent atoms, the impurity strain field is either compressive or tensile. If the impurity atom is smaller than the host atom, the strain field puts the surrounding atoms under stress as the bonds are stretched. The impurity atom will ultimately diffuse into a compressive field created by a dislocation to lower the system's energy, resulting in a reduction in the total

stress field, thus pinning the dislocation. A bigger atom would diffuse to a dislocation's tensile field, lowering the total stress field, thus pinning, and consequently making the crystal tougher [49].

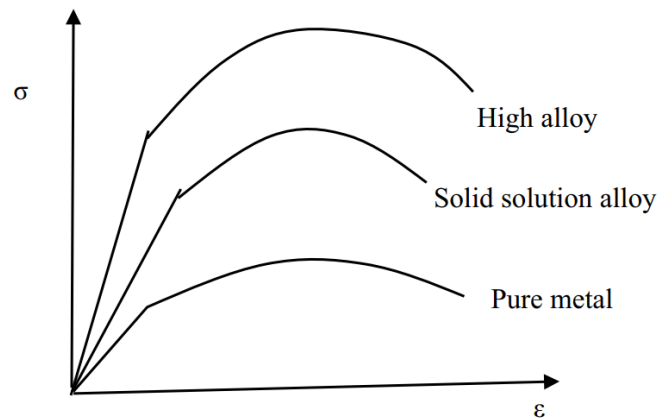


Figure 2.7. Schematic representation of the effect of alloy content in the tension properties of a solid solution metallic alloy [43].

In multi-phase materials

2.3.4 Precipitation strengthening

Since strength increases with aging, precipitation hardening is also termed age hardening. The second phase for precipitation-hardening is soluble at high temperatures but precipitates when quenched and aged at lower temperatures [50]. Al-alloys, Cu-Be alloys, Mg-Al alloys, and Cu-Sn alloys are examples of precipitation strengthening.

Natural aging may happen when aging occurs at ambient temperature. If the material needs to be heated throughout the aging process, it is referred to as artificial aging.

2.3.5 Dispersion strengthening

When fine second-phase particles are combined with matrix powder, homogenized, and pressed in powder metallurgy operations, it is called dispersion hardening. At all temperatures, the second phase must have a very low solubility for dispersion hardening to take place. Oxides, carbides, nitrides, borides are a few examples. Dislocations traveling through a matrix including foreign particles can either cut through or wrap around the particles [51].

2.3.6 Fiber strengthening

Fibers can also be used to introduce the second phase into the matrix. Fiber-strengthening prerequisite: High strength and modulus fiber material Matrix material are ductile and non-reactive, and it is combined with fiber material to create a composite. Fiber materials, such as Al_2O_3 , boron, graphite, metals, and glass, are examples. Metals and polymers make up the matrix material.

Different from other approaches, the mechanism of strengthening is unique. The load is carried by higher modulus fibers, which are distributed to fibers by a ductile matrix. As a result, the interface between the matrix and the fibers is critical [52].

2.3.7 Martensite strengthening

The production of the hard martensitic phase from the retained high-temperature phase at temperatures lower than the equilibrium invariant transition temperature is the basis for this strengthening process. Martensite platelets develop at a rapid rate (1/3rd the speed of sound), requiring less activation energy for growth.

As a result, the nucleation rate determines the volume percentage of martensite that exists. Martensite's exceptional strength is attributable to its distinctive twin structure and high dislocation density [53].

2.4. Electron Work Function (EWF)

2.4.1 Definition

The minimal energy necessary to move an electron at the Fermi level inside material to its surface without kinetic energy is described as the electron work function (EWF) [54]. Assume that the stated electron has evacuated to a point near to the material's surface, where it is no longer impacted by the nuclear attraction force emanating from the material's bulk interior. The critical distance is defined as the equivalent distance in this scenario. The EWF is the amount of energy necessary to move one electron from the inner cavity of an atom to this critical distance.

$$\phi = -e\phi_{vacuum} - E_{Fermi}$$

E_{Fermi} is the energy at the Fermi Level [55], where e is the elementary charge and Φ is the electrostatic potential in the vacuum immediately outside the solid's surface.

2.4.2 EWF and Young's modulus

Previous research has shown that the Electron Work Function (EWF) may be used as a probe to evaluate material characteristics [56, 57]. A crystalline material with temperature-dependent properties, such as Young's modulus, is of special interest. Young's modulus has been found to have a sixth power relationship with the EWF. e.g., $E \propto \phi^6$.

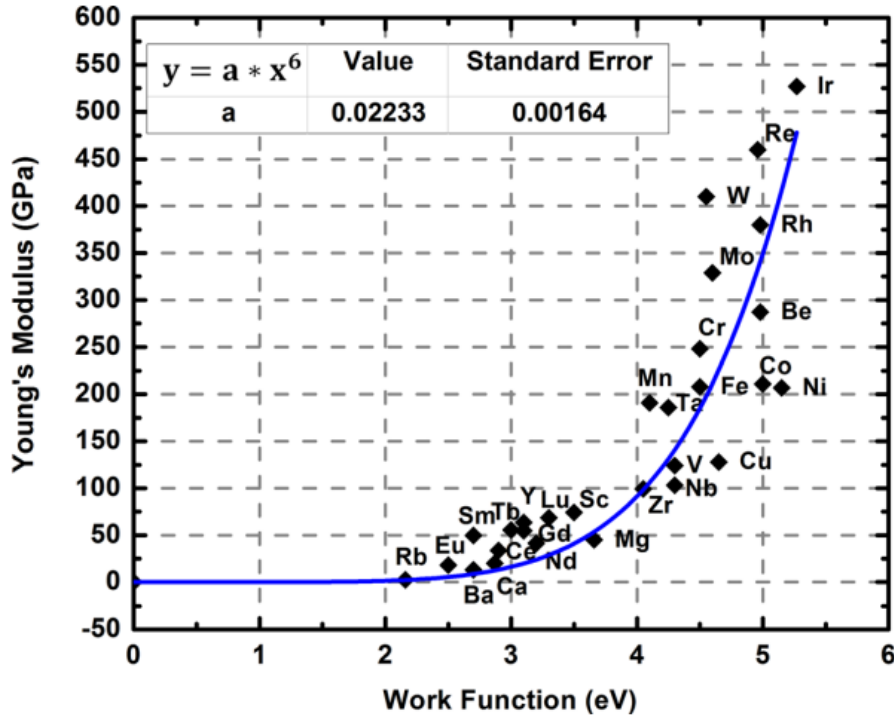


Figure 2.8. Correlation between EWF and Young's modulus of materials [57].

2.4.3 EWF measurement using Kelvin Probe Method

The Kelvin Probe (KP) is a technique for determining the surface work function of a material. The probe is perpendicular to the surface and is positioned quite near to it. The probe vibrates along the z-axis, with z representing the average distance traveled. The probe acts as a parallel plate capacitor since it is conducting. Because the Fermi levels of the two materials must be separate, the probe must be made from a different material than the sample's surface [25, 58, 59].

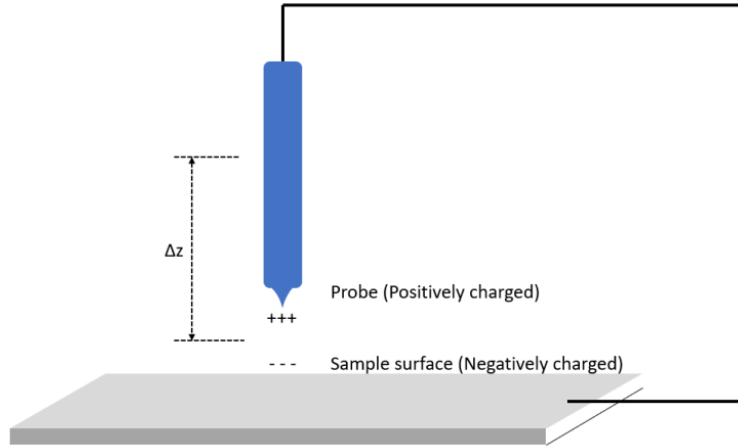


Figure 2.9. *Schematic representation of the principle of Kelvin Probe Microscopy*

2.5. Bauschinger effect and its mechanism

2.5.1 Bauschinger effect

When materials are put into the plastic regime uniaxially in one direction (e.g., in tension). When loaded to zero stress and subsequently reloaded in the opposite way (for example, in compression), they may yield at a lower stress level than if reloaded in the original direction as Fig. 2.10 illustrates.

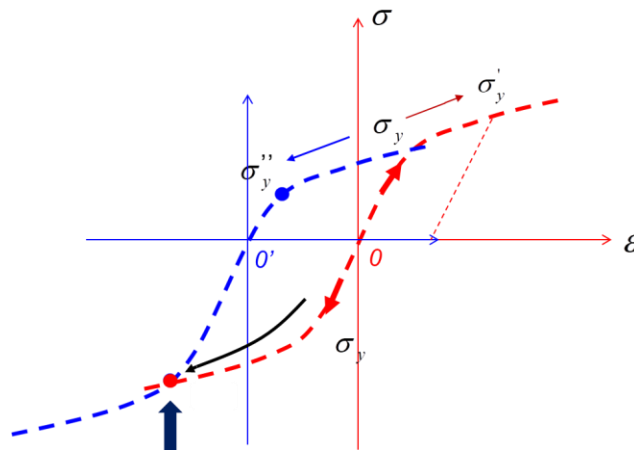


Figure 2.10. *Schematic illustration of the Bauschinger effect in metallic materials. Compressive plastic deformation reduces the tensile strength, leading to yielding under lower tensile stress.*

The Bauschinger effect is named after Johann Bauschinger, who originally described this direction-dependent, asymmetrical yield behavior in 1886 [60]. Since then, this impact has been extensively researched. It is now obvious that Bauschinger's findings only covered a portion of the phenomena at hand, and that directed behavior in the stress-strain connection is far more complicated than previously imagined. The Bauschinger effect has been seen in a wide range of materials since J. Bauschinger's discovery, including single crystals, polycrystals, pure metals, alloys, and dispersion hardened metals. The Bauschinger effect was more evident in FCC materials than in BCC materials, according to Woolley [61].

2.5.2 Mechanisms of the Bauschinger effect

Since the discovery of the Bauschinger effect, several investigations have been conducted to understand the mechanism. Internal stresses and macroscopic residual stresses created owing to non-homogeneous deformation of individual grains of a polycrystalline metal were thought to be the origin of the Bauschinger effect in the beginning. Orowan [62], on the other hand, proposed an alternative theory based on anisotropy of the driving force for dislocation motion as a result of pre-strain. In order to explain the Bauschinger effect, internal stress and dislocation theories are two primary schools of thought. Besides, a composite model, initially presented by Masing [63, 64], can also be used to explain the Bauschinger effect. These models are briefly described as follows.

2.5.2.1 Internal stress theory

Heyn (1918) [65] proposed a model to explain the reduction in yield stress observed after load reversal, with the following three assumptions:

- (1) Different volume components have different elastic limitations.
- (2) The material is made up of tiny volume parts with a perfect stress-strain curve: at a constant stress level, the elastic response transforms into a non-hardening plastic extension.
- (3) The absolute value of any volume element's elastic limit is independent of deformation direction, i.e., it is the same in tension and compression.

The theory explains that there is a curvature in the initial stress-strain curve during the elastic-plastic transition based on these assumptions. In the loading region, strain is homogenous throughout deformation. The stress distribution during plastic deformation is not uniform; as a result, residual stresses emerge after unloading, which is responsible for the yield-lowering impact following load reversal. Schmid and Boas [66] described the Bauschinger effect as the result of internal tensions locked up in cold worked metal.

2.5.2.2 Composite model

When two phases (matrix and second phase, for example) or two components with differing mechanical characteristics exist in a single specimen, the Bauschinger effect may also be explained using a composite model. Masing was the first to propose this mechanism [67]. According to the model, a specimen has two phases or components, each with the same elastic constant but differing elastic limits.

When the specimen is pre-strained in the same direction. Plastic deformation will occur in the phase or component with the lower elastic limit if the strain is sufficiently strong, while the other will behave elastically. When the applied load is zero during unloading, one phase or component will be under tensile stress while the

other is in compressive residual stress. Both will act elastically when reloaded in the same direction, to the same stress level; but, when reloaded in the opposite way, the residual stress in the 'softer' phase or component will aid the applied stress in causing premature give. As a result, the system's behavior is asymmetrical, and it's softer for reverse loading than it was in its pristine form. Masing's model is also applicable to materials with varied Young's modulus and hardening behavior in the matrix and second phase.

2.5.2.3 Dislocation theory

When the findings of several studies demonstrating the presence of the Bauschinger effect in single crystals are considered, the internal stress theory is severely weakened; as a result, a new approach to explain the Bauschinger effect is needed. Two different dislocation theories were proposed to elucidate the Bauschinger effect. The first approach was given by Mott [68] and later refined by Seeger [69]. It has been proposed that during pre-straining, a long-range tension is built up through dislocation pile-up at obstacles. Grain boundaries, for example, are strong enough to stop dislocations from moving. As a result, the accumulated back strains caused by dislocations will aid mobility in the opposite direction.

Orowan [62] proposed the second approach, proposing that when deformation is reversed, the entire stress-strain curve moves in the negative stress direction, resulting in permanent softening of the material rather than the Bauschinger effect. The degree of persistent softening demonstrates that the impact of back stress is minimal. All signs of the Bauschinger effect vanish when a prestrained sample is unloaded and heated above its recrystallization temperature.

Chapter III:

Clarification of the puzzled effects of cold work on wear of metals from the viewpoint of wearing energy consumption

Predicting the wear rate of materials in various applications is crucial for the maintenance of industrial machinery and facilities which suffer from wear attacks. However, wear is a complicated process, influenced by various factors such as deformation, hardness, atomic bonding, strain-hardening, wearing stress, strain rate, microstructure, and its variations during wear, etc. [70-72]. It is challenging to predict the damage to materials caused by such a complicated process with the desired accuracy since mutual influences of mechanical, physical, and/or electrochemical sub-processes are involved in wear [4]. Efforts have long been made to develop wear models, which may capture the main factors that dominate the wear damage. Various wear models and equations can be found in the literature. However, many of them are either for wear processes under specific conditions or complicated with multiple variables, making it less easy to elucidate mechanisms for the predicted wear behavior. One of the most used sliding wear models is known as the Archard equation proposed by J. F. Archard in 1953, which is expressed as [9].

$$V = K \frac{L \cdot D}{H} \quad (3.1)$$

where V is the volume loss of a material caused by wear, L is the applied load, D is the sliding distance, H is the hardness of the material, and K is a constant known as the wear coefficient. This classic sliding wear equation is often referred to Archard's equation [9,14,15,73-74], which was derived after Bowden and Tabor proposed a friction theory that took account of adhesion at the asperity contacts and the contact force that deformed the asperities of the softer metal, accompanied with the asperity junctions cold welding and shear failure of the welded junctions [9,10,13].

In 1958, another important development was made by Rabinowicz who proposed a criterion through more analysis on adhesion, which determined the minimum size of wear particles by considering the elastic energy stored in the asperities and the amount of work done to separate a wear fragment from the surface [75-76]. Based on the asperity or particle penetration and contact geometry, Rabinowicz and his colleagues also derived a model to deal with abrasive wear, which has a mathematically identical form as the Archard equation [15, 77-78]. As a result, this equation or Archard equation has been widely used to describe material removal caused by sliding wear, which includes adhesive wear and abrasive wear or a mixture of both, involving tearing due to adhesion, or plowing and cutting by a harder counter-face with asperities [15,17-18, 74].

Archard equation is frequently adopted in industry to estimate the effective lifespan of machinery and facilities under abrasive wear attack. However, this equation was developed based on the geometry of contact between two surfaces under an applied load [15, 19] without involving wearing stress or wearing energy.

Thus, the model is rather simplified with little thought given to the physical attributes and processes like interatomic bonding and energy consumption during wear, which does not provide definitive clues to understand some fundamental issues and elucidate relevant wear mechanisms. As an example [79] (see Fig. 3.1), Archard's equation cannot explain why the increased hardness by cold work or heat treatment show no benefit or less benefit to the wear resistance of carbon steel, compared to the clear dependence of the wear resistance of metals on their inherent hardness.

Different from the inherent hardness of a metal, which is determined by the atomic bond strength and the slip systems, the hardness increment by cold work or strain-hardening results from interactions among dislocations associated with strain-induced plastic deformation. The cold work introduces lattice imperfections, which can increase apparent hardness through their mutual interactions such as dislocation tangling. But on the other hand, the lattice imperfections can deteriorate the crystal integrity with reduced electron density, which decreases the electron-nuclei interactions and thus weakens the metallic bond strength, leading to decreased Young's modulus [10]. Archard model with application to abrasive wear shows the benefit from the increase in apparent hardness but does not consider the associated deterioration of the crystal integrity or the decrease in Young's modulus caused by cold work.

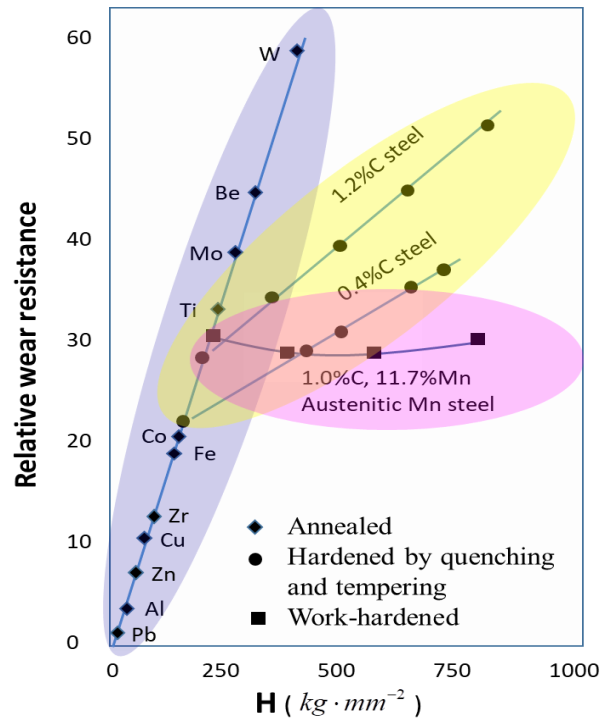


Figure 3.1. Relative wear resistance (=1/volume loss) versus hardness for metals (the relative wear resistance – H relationships are illustrated using a part of data values reported in [79]).

Elastic modulus or Young's modulus is correlated with the atomic bonding [75, 76] and is of importance to the wear resistance since it influences the resistance to elastic deformation [77-78] and is related to the barriers to dislocation generation and movement [16, 18]. Young's Modulus was previously incorporated into Archard Equation [19,26,79] for improved accuracy. However, such incorporation is mainly by taking account of the effect of elastic deformation on the contact geometry, which still cannot explain why the benefit of cold work to the wear resistance is not as much as the Archard equation predicts. A recently proposed wearing energy model [24] provides a different view on the issue and demonstrates an important role that

Young's modulus plays in affecting the wear of strain-hardened materials, which is represented by the following equation (see appendix),

$$V = K \frac{L \cdot D}{H[1 + \eta \ln(E/E_0)]} \quad (3.2)$$

where V is the volume loss, K is the wear coefficient, L is the load applied, D is the sliding distance, H is the hardness of the material, E and E_0 are Young's moduli of plastically deformed material, and strain-free one respectively. η is a coefficient that reflects the degree or severity of the negative influence of decreased Young's modulus on the wear resistance.

The effect of cold work or strain-hardening on wear can be captured by looking at the deterioration of the crystal integrity caused by the cold work or plastic deformation. Since materials having different crystal structures behave differently during plastic deformation, depending on the number of slip systems and atomic bonding strength, they would show different responses to the strain-hardening and thus different variations in the wear resistance. In this study, we investigate abrasive wear behaviors of two metals having different crystal structures, Mg (HCP) and Cu (FCC), with the objectives of 1) looking into effects of cold work on their wear resistances, 2) investigating how the crystalline structures of Cu (with 12 slip systems) and Mg (with 3 slip systems) affect the benefits of strain-hardening to their wear resistance, and 3) elucidating underlying mechanisms.

3.1. Experimental

3.1.1. Materials

Materials used for this study are Cu (FCC, 99.99% pure) plates and Mg (HCP, 99.8% pure) cylinders in the annealed state without pre-deformation. The Cu plates and Mg cylinders were cut into small rectangular plates using a wire-cutting machine.

3.1.2. Sample preparation

To plastically deform the samples, Cold work was applied to both the metals using a setup in which a metal plate (Cu or Mg) was placed in the center between two cylindrical cast iron blocks (40 mm in diameter) and hammered with a hammer weighted 10 lbs. at a speed of 6~7 m/s, which had a flat surface with its area almost equal to the surface area of the cast iron blocks. As Cu and Mg are relatively soft, they are easily deformed using the above-mentioned process. A vernier caliper was used to measure the change in thickness after every cycle of hammering (1 cycle =5 hammering steps) to get the desired percentage reduction in thickness (10, 20, 30, 40%). The entire process was done in such a way that the hammering force was homogeneously applied to the Cu or Mg plate, which was transferred through the cast iron block to the metal plate. Hardness measurement showed that the deformed plate was smooth with homogeneously distributed hardness values, indicating that the cold work was homogeneously applied to the metal plates. The samples were polished with silicon carbide (SiC) emery papers up to 1200 grit, cleaned using acetone solution, and then etched for 3-5 seconds. The etchant for Cu was a mixture of 50 ml distilled water and 50 ml nitric acid, and that for Mg was a mixture of 10ml

acetic acid, 70 ml ethanol, 10 ml distilled water and 6 grams of picric acid. After etching, samples were thoroughly washed under flowing water, and dried quickly with a compressed air flow.

3.1.3. Sliding wear test setup

Samples for sliding wear tests were cut from the deformed plates with size of 15 mm x 30 mm, which were also polished with silicon carbide (SiC) emery papers up to 1200 grit followed by ultrasonic cleaning using acetone solution before being tested. Dry sliding wear tests were performed using a computerized pin-on-disc tribometer (CSM Instruments) at room temperature. Silicon nitride (Si_3N_4) balls of radius 6 mm were used as the pin. The wear tests were performed at a sliding speed of 2 cm/s over 2000 laps corresponding to a sliding distance of 12.5 m. The volume loss of a sample caused by wear was determined by measuring the dimensions of wear track using a 3D Optical Surface Profilometer made by Zygo Corporation (Middlefield, CT, USA). All the samples were also examined under an EVO MA10 Scanning Electron Microscope equipped with an Energy Dispersive Spectrometer (EDS).

For the wear tests, the applied normal loads were 2N, 5N, 8N, and 12N, respectively. At least three repeated tests were performed for each type of sample with which an average was obtained. Eq. (3.2) was used to calculate the volume loss of individual samples with known normal force (L), total sliding distance (D), measured hardness (H), and Young's modulus (E). The relative wear resistance is $1/V$. Volume losses of the cold worked and strain-free samples under four applied loads or normal forces, 2N, 5N, 8N, and 12N, respectively, over the same sliding

distance were calculated. The experimental data points were used to determine the value in the wearing energy model [eq. (3.2)], with which the relative wear resistance \sim hardness curves from the model can be drawn. Wear coefficient (K) was calculated from the strain-free sample based on its volume loss, hardness, applied normal load, and sliding distance.

3.1.4. Mechanical testing

Young's moduli of all specimens were measured using a non-destructive acoustic instrument with RFDA basic software provided by IMCE (Genk, Belgium) under flexural mode. The hardness of the samples was determined using a Zwick Roell Indentec Hardness Testing Machine. Rockwell scale E (HRE) of Mg samples was determined using a $1/8$ in (3.18 mm diameter) steel ball as an indenter under a load of 100kgf. Rockwell scale B (HRB) of Cu samples was determined using a $1/16$ in (1.59 mm diameter) steel ball as an indenter under a load of 100kgf. Indentations were made across the rectangular samples and a minimum of 20 measurements were taken to get the mean value. The obtained Rockwell hardness values were converted into SI units (MPa) and are presented in Table 2.

For more information on mechanical properties of the as-received Mg and Cu, tensile tests were performed using a UTM (Test Resources Inc., USA), following the ASTM E8 standard. The strain rate was set at 0.5 mm/min and the extensometer gauge length was 2 inches. Plain strain fracture toughness of the as-received metals was determined following the ASTM E399 [80]. The strain rate was fixed at 0.5 mm/min, which is like that of the tensile tests. Conditional KQ value was determined from the 5% secant line of the load vs displacement curve. Charpy impact test was

also performed, following ASTM E23 on undeformed samples (10 X 10 X 55 mm) using an Impact tester at room temperature, from which the impact energy was determined.

3.2. Results and discussions

3.2.1. Mechanical properties and cold work induced changes in hardness and Young's modulus

In order to determine the mechanical properties of non-deformed Mg and Cu samples and their capabilities to absorb the deformation energy up to failure, uniaxial tensile and Charpy impact tests were performed. Results of the measurements are shown in Table 3.1. The tests were performed three times with which average values were obtained. Figs. 3.2 (a) and (b) illustrate the Charpy Impact energy (J) and typical tensile curves of the Cu and Mg samples, respectively.

Table 3.1. *Mechanical properties determined by tension and impact tests*

Material	Cu	Mg
Charpy Impact energy (J)	97.2	8.5
Fracture Toughness (MPa.m ^{1/2})	42.8	14.4
Tensile strength (MPa)	219.7	100.3
Yield strength (MPa)	201.9	89.0
Young's Modulus (GPa)	146.0	45.0
Fracture strain (%)	29.2	8.4
Strain energy density (u) (MPa)	5979	646

As Figs. 3.2 (a) and (b) illustrate, copper with an FCC structure has significantly higher impact energy, larger ductility or fracture strain, higher strength, which help absorb much more energy up to failure than Mg. Mg having an HCP structure with limited slip systems shows relatively brittle behavior, evidenced by its low impact energy and low ductility.

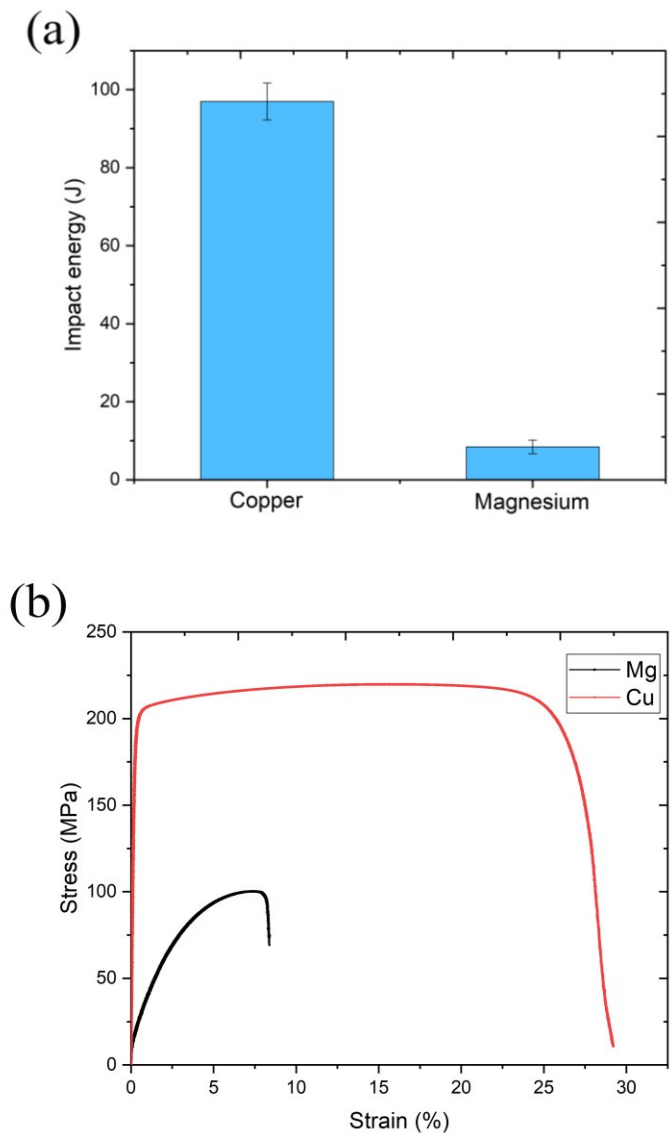


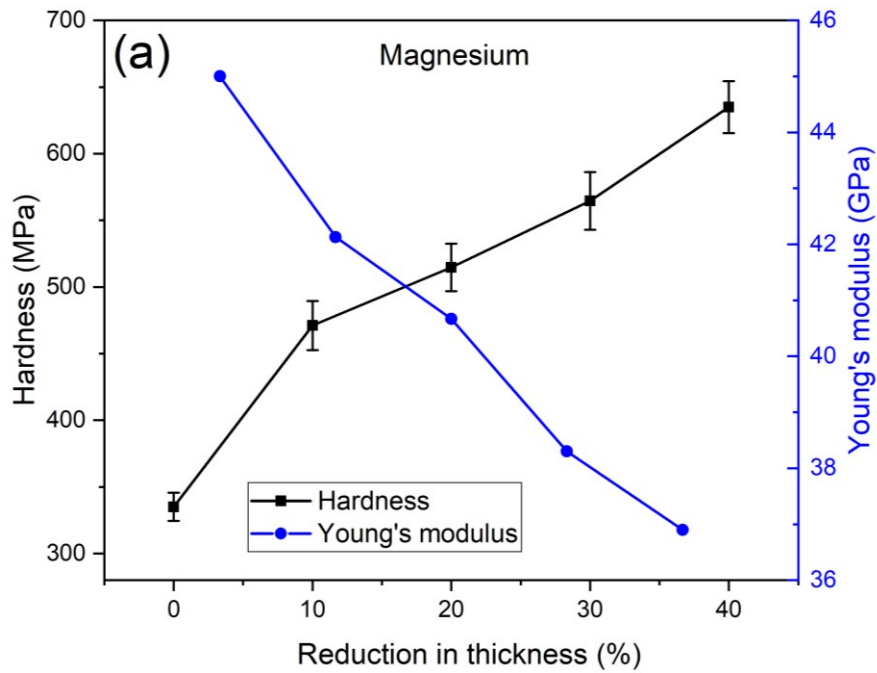
Figure 3.2. (a) Charpy impact energy and (b) stress-strain curves of the as-received Mg and Cu.

Based on the stress-strain curves [Fig. 3.2(b)] obtained from the tension tests at room temperature, the as-received Cu shows much larger elongation and strength than the Mg sample. As a result, the strain energy density of Cu up to failure is considerably larger than that of Mg, corresponding to much higher fracture toughness (K_{IC}).

Figure 3.3 illustrates changes in hardness and Young's modulus of Mg and Cu caused by cold work. Values of the measured hardness and Young's modulus are given in Table 3.2. Due to the strain-hardening effect resulting from interactions of strain-introduced lattice imperfections such as dislocation tangling, the cold work increased the hardness of the metals as expected. However, Young's moduli of the metals decreased as the cold work was applied. The decrease in Young's modulus is ascribed to the deformation-introduced lattice defects or imperfections such as dislocations, micro-voids, and micro-void induced micro-cracks, which negatively affect the crystalline integrity and the broken atomic chains or damaged lattice network weaken the average atomic bond strength [26, 81-82].

To obtain relevant information on the cold work induced lattice imperfections, Mg and Cu samples without cold work and with cold work by 20% reduction in thickness, respectively, were examined under the scanning electron microscope. The samples were polished followed by etching using etchants described in Experimental Details. Fig. 3.4 illustrates surface morphologies of the samples. As shown, cold work resulted in micro-cracks in the deformed Mg. Due to its HCP structure with only three slip systems, Mg has a higher probability to generate micro-cracks during severe plastic deformation, since large strain may not be well accommodated by the limited slip systems alone and micro-cracking would thus participate in the

deformation process [83]. The situation is different for FCC Cu having 12 slip systems, which has much larger ductility than Mg (see Fig. 3.2). Cu is capable of accommodating plastic deformation by operation of its 12 slip systems. No micro-cracks were observed on the surface of the deformed Cu but etch pits are present on the rough surface. Etch pits are likely the ends of dislocations that could be visualized after etching [84, 85] and the rough surface with irregular pits should be a sign of a heavily deformed surface with high-density dislocations.



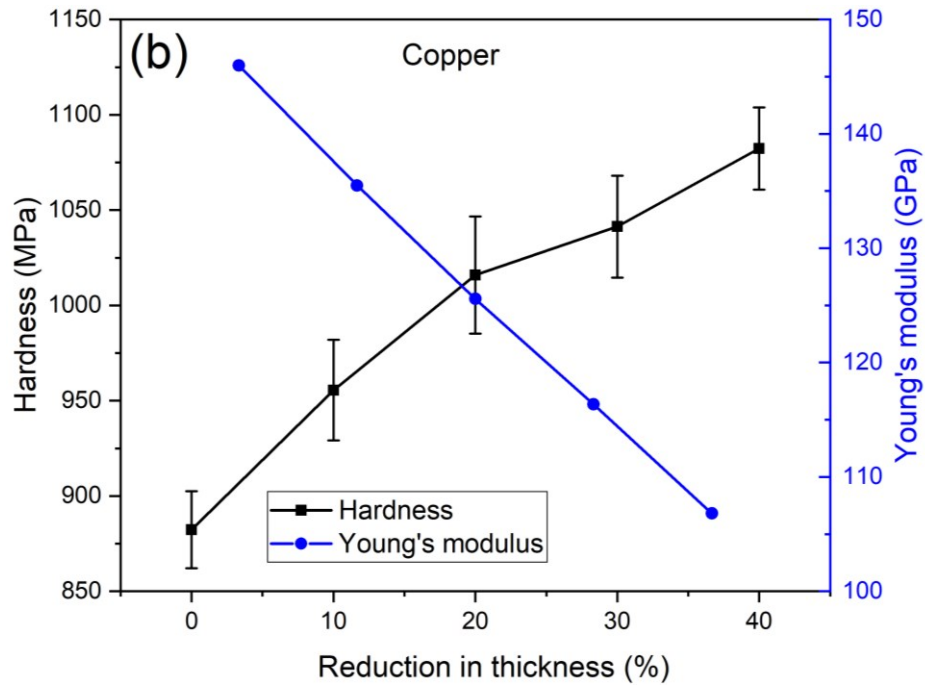


Figure 3.3. Variations in Rockwell hardness and Young's modulus with respect to cold work reduction: (a) Magnesium and (b) Copper.

Table 3.2. Hardness (MPa) and Young's Modulus (GPa) for Cu and Mg samples with at 0%, 10%, 20%, 30%, 40% reduction in thickness.

	Hardness (MPa)		Young's Modulus (GPa)	
	Copper	Magnesium	Copper	Magnesium
0%	882.335 ± 20.2	335.007 ± 10.6	145.98	45
10%	955.508 ± 26.4	471.049 ± 18.5	135.49	42.13
20%	1015.907 ± 30.8	514.651 ± 17.9	125.57	40.67
30%	1041.304 ± 26.8	564.588 ± 21.7	116.34	38.3
40%	1082.291 ± 21.5	634.836 ± 19.5	106.81	36.9

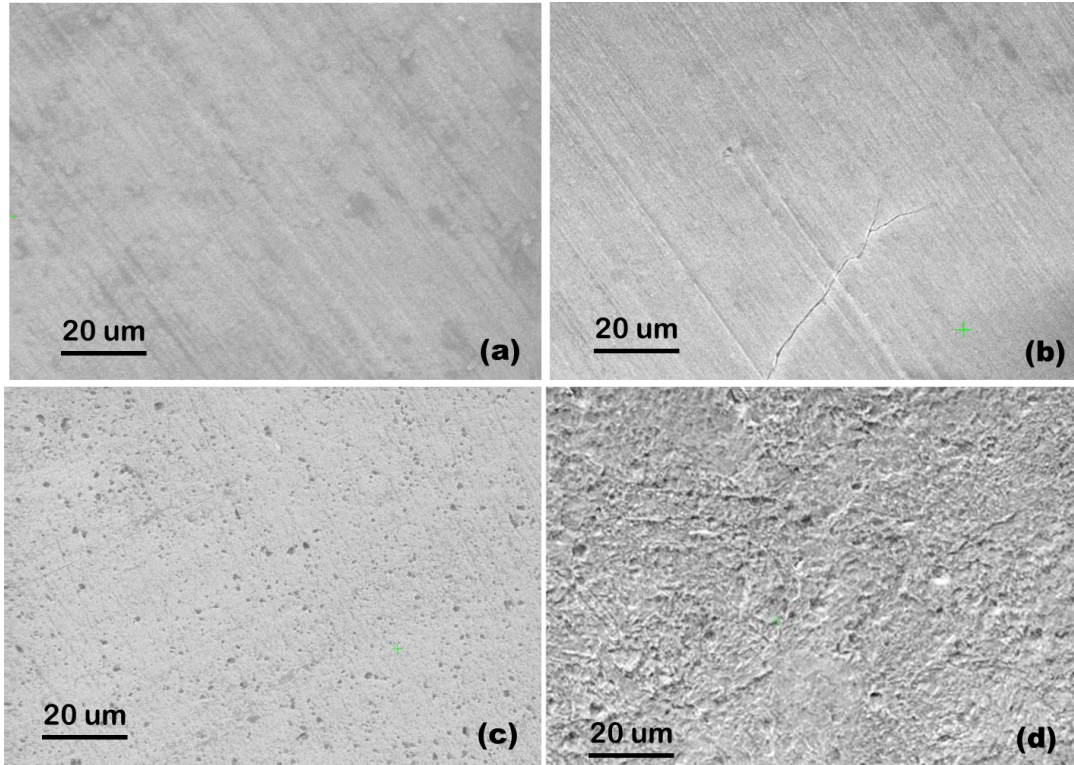


Figure 3.4. (a) Mg sample without cold work, (b) Mg sample cold worked by 20% reduction in thickness, (c) Cu sample without cold work, (d) Mg sample cold worked by 20% reduction in thickness; all samples were polished and then etched.

3.2.2. Wear behavior

Wear behaviors of the samples were evaluated by performing sliding wear tests under the conditions as described in Experimental Details. Volume losses of the samples were determined using the 3D profilometer by measuring the depth and width of the wear tracks caused by wear. Figs. 3.5 illustrates representative wear tracks on un-deformed Mg and Cu samples with cross-sectional profiles, respectively, caused by sliding wear under a contact force of 5N. Based on the dimensions of the wear tracks, the softer Mg showed very poor wear resistance with a much deeper and wider wear track, compared to that of the harder Cu. Besides, the worn surface of Mg

is rougher, which should be ascribed to its low fracture toughness (see Fig. 3.2), since wear of a less tough surface may involve more fracture and local delamination, thus leading to larger roughness.

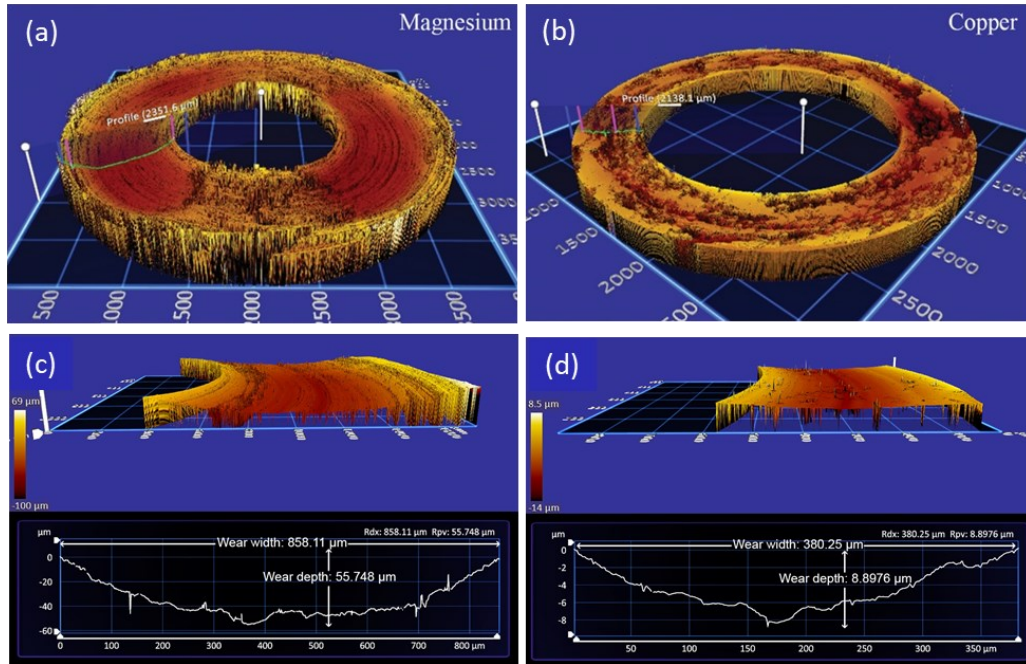
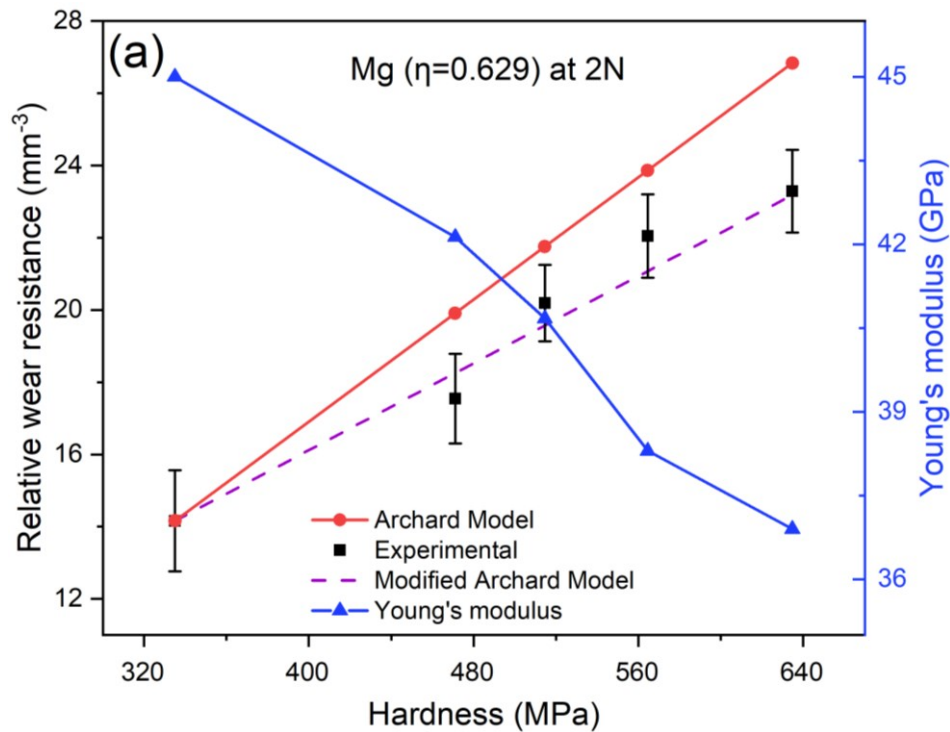
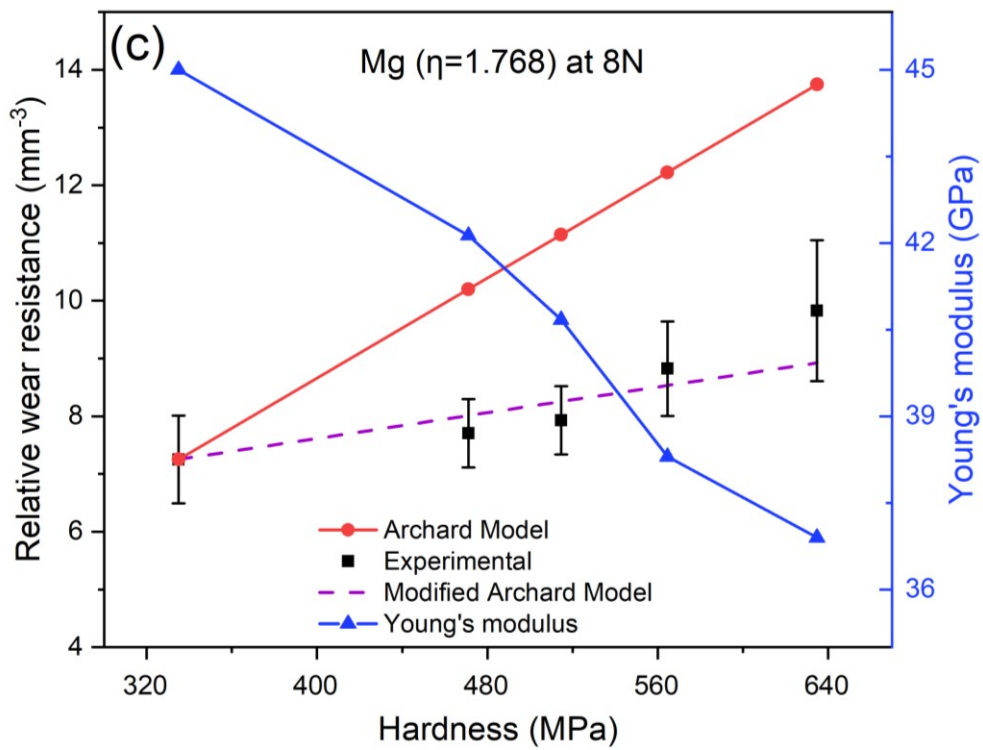
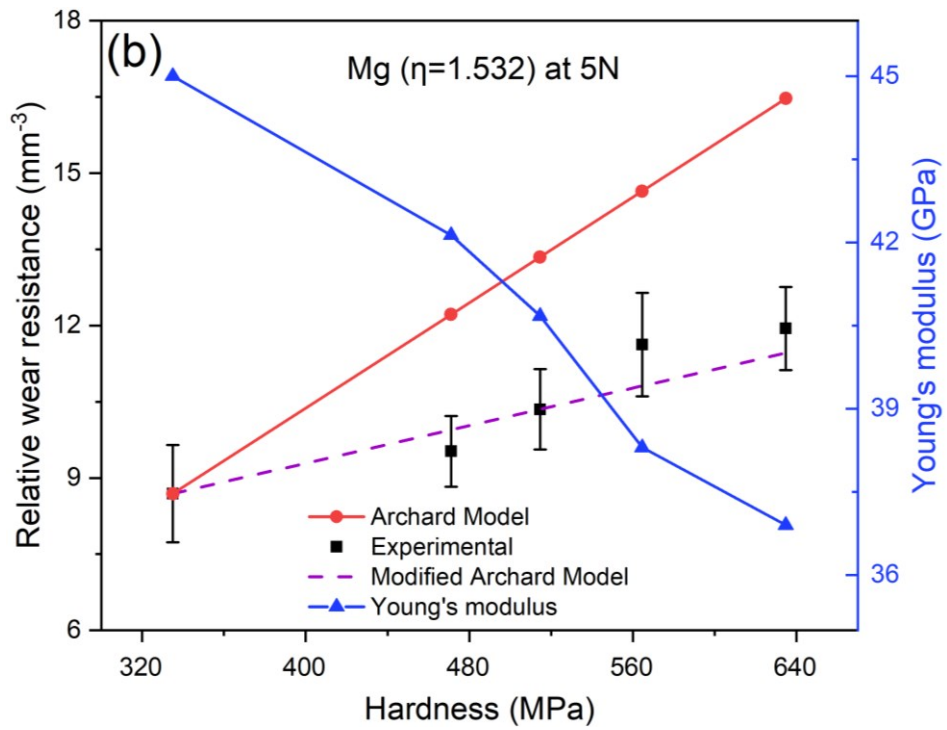


Figure 3.5. 3D wear track profiles and cross-sectional dimensions of undeformed (a, c) Mg and (b, d) Cu samples caused by wear under 5N load at a sliding speed of 2 cm/s.

Figures 3.6 (a-d) illustrate relative wear resistances and Young's moduli of cold worked Mg samples with respect to hardness tested under different loads. Figures 3.7 (a-d) provide similar information for the Cu samples. The wear resistance versus hardness curves was calculated using the wearing energy model i.e., eq. (3.2). Experimentally determined data points of the wear resistance are shown in the figures, which were used to determine the value in eq. (3.2). In the figures, the wear

resistance versus hardness predicted using the Archard equation is also shown for comparison. One may see that the wear resistance of the samples predicted by the Archard equation are larger than the experimentally measured ones. In other words, the Archard equation overestimates the benefit of cold work on the wear resistance, since it only relates the wear resistance to the apparent hardness without taking into consideration that the increased hardness by cold work is gained at the expense of Young's modulus.





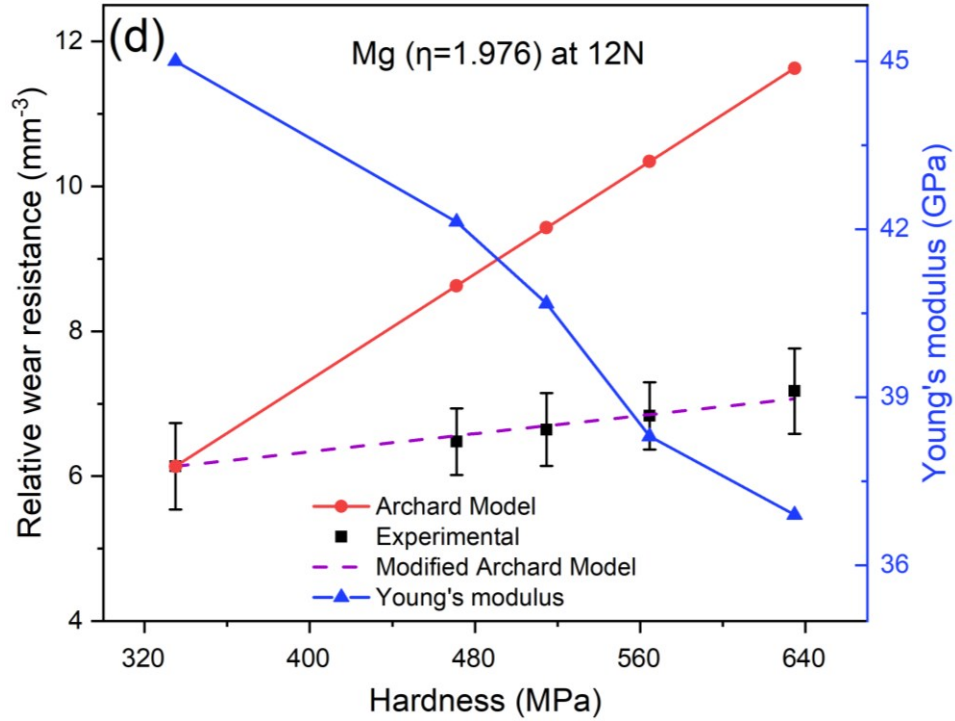
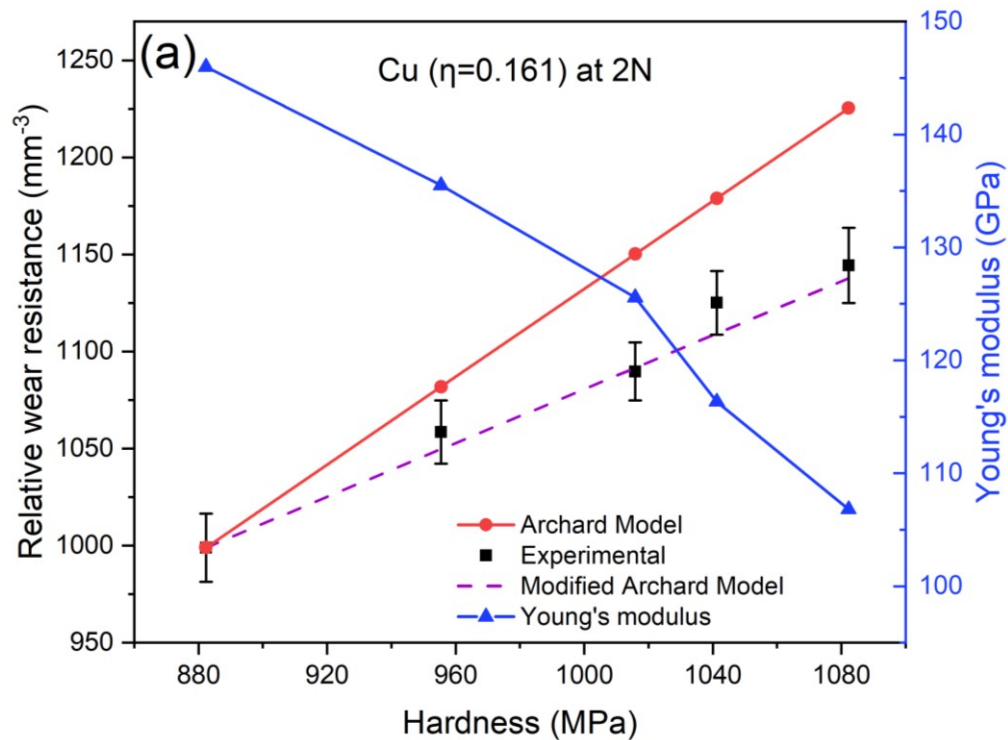
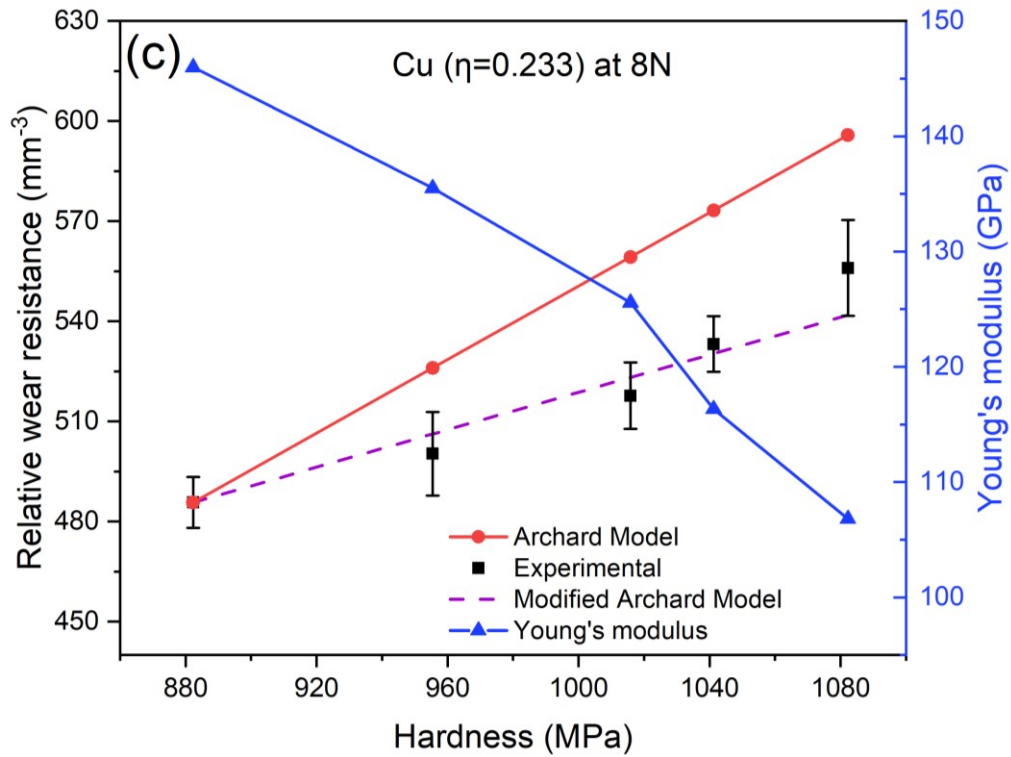
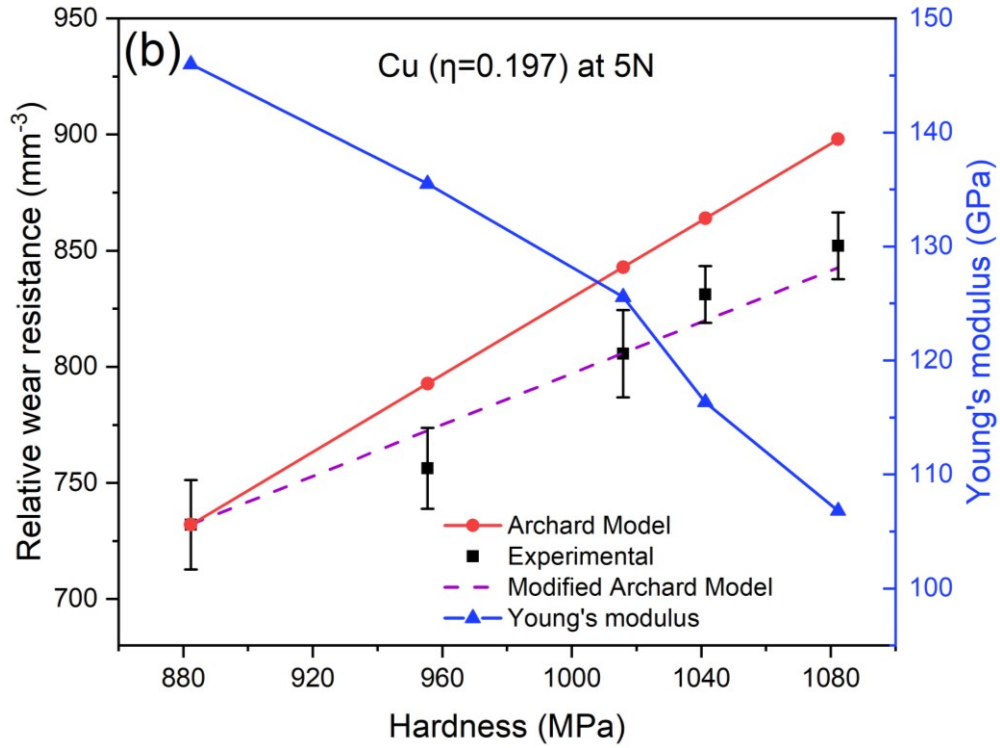


Figure 3.6. (a-d) Curves of relative wear resistance of non-deformed deformed Mg samples versus apparent hardness, predicted by Archard's equation. Experimentally measured data points are presented, which were used to determine the η value in the wearing energy model [eq. (3.2)]. Wear resistance \sim hardness curves given by eq. (3.2) are presented by dashed purple lines; Variations in Young's modulus with respect to hardness are also given. The wear tests were performed under (a) 2N, (b) 5N, (c) 8N, (d) 12N for samples with 0%, 10%, 20%, 30%, 40% reduction in thickness, respectively.

As shown, the experimentally determined wear resistance is lower than that predicted by the Archard equation. This is attributed to the decrease in Young's modulus, corresponding to the weakening of the atomic bonding caused by the deterioration of the crystal integrity as defects are introduced by plastic deformation [26, 81, 82, 86]. The decrease in Young's modulus leads to an increase in volume loss and thus a lowered wear resistance as eq. (3.2) indicates. This has been well illustrated by the relative wear resistance \sim hardness curves given by eq. (3.2), in which the η value was determined based on the experimentally determined volume losses.





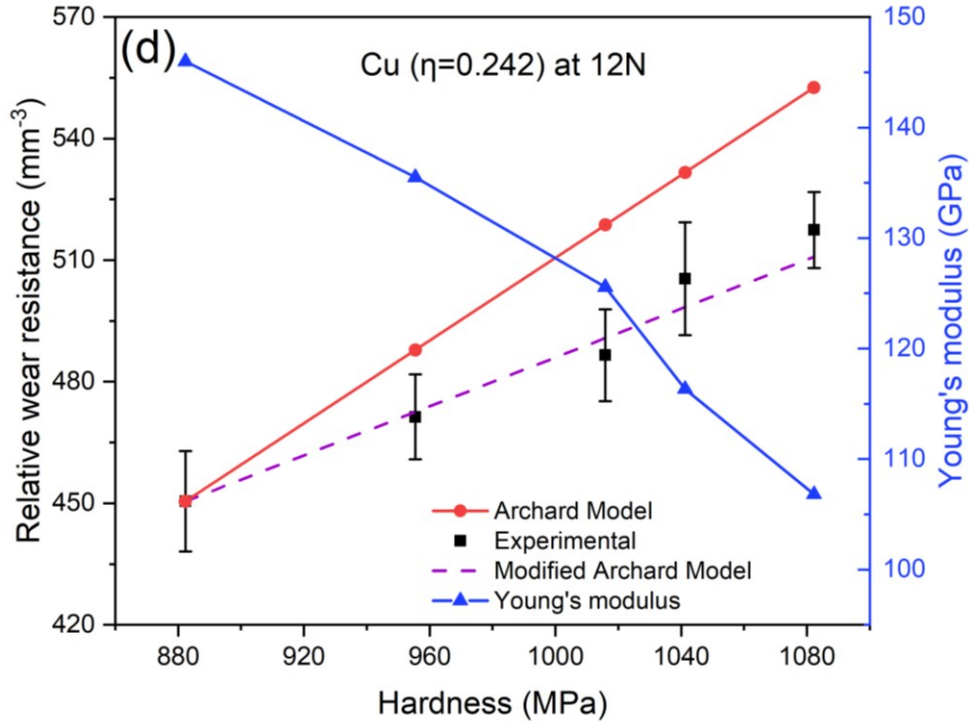


Figure 3.7. (a-d) Curves of relative wear resistance of non-deformed and deformed Cu samples versus apparent Rockwell hardness, predicted by Archard's Model. Experimentally measured data points are presented, which were used to determine the η value in the wearing energy model [eq. (3.2)]. Wear resistance ~ hardness curves given by eq. (3.2) are presented by dashed purple lines; Variations in Young's modulus with respect to hardness are also given. The wear tests were performed under (a) 2N, (b) 5N, (c) 8N, (d) 12N for samples with 0%, 10%, 20%, 30%, 40% reduction in thickness, respectively.

The degree or severity of such a negative influence of decreased Young's modulus on wear resistance is reflected by η value in the wearing energy model as shown in equation 3.2. The measured relative wear resistances were fitted with this

equation so that η values of the Mg and Cu samples tested under different loads can be determined. The results of the analysis are shown in figure 3.8. As shown, Mg has larger η values than Cu under different loads and the η value increases as the load are increased.

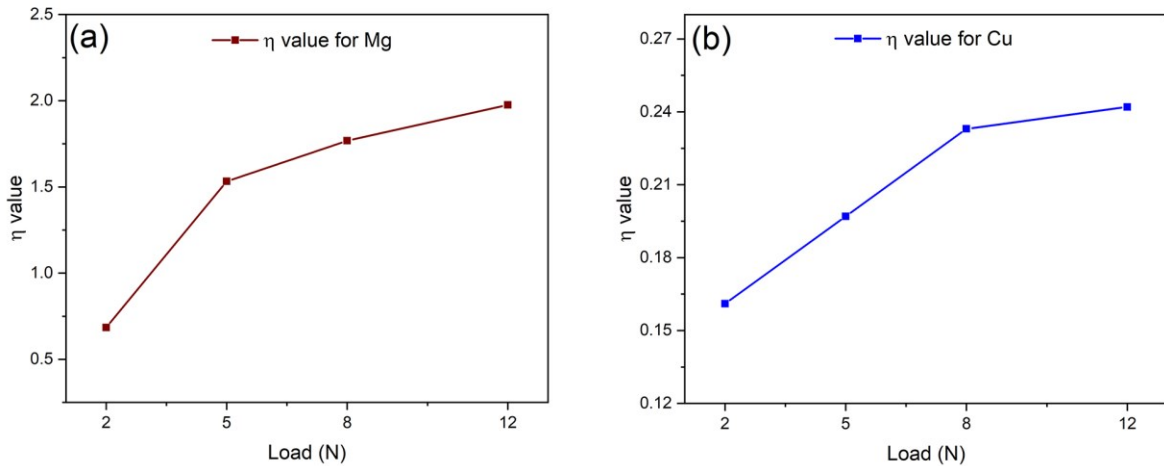


Figure 3.8. Variations in η value versus with the applied load for (a) Mg (HCP) and (b) Cu (FCC).

According to eq. (3.2), a larger η corresponds to a more negative effect of the decreased Young's modulus on the wear resistance. The η values of Mg larger than those of Cu under different loads suggest that Mg benefits less from cold work or strain hardening. This is understandable; since Mg with an HCP structure has limited slip systems corresponding to poor ductility [Fig. 3.2(b)], it has a higher probability of forming micro-cracks caused by cold work, which are more detrimental to the stress-bearing capability and fracture toughness [81]. Cu has an FCC structure with many more slip systems, rendering this metal more flexible with less deterioration of crystalline integrity than Mg during cold work. As a result, copper would benefit more from cold work or strain-hardening.

It is interesting to notice that the η value increases with the load as figure 3.8 illustrates. This dependence of η on the applied load is explainable. Similar to the enlarged decrease in Young's modulus as the amount of cold work is increased, during wear under larger loads, Young's modulus will continuously deteriorate and a larger load would speed up such deterioration, magnifying the role of cold work in lowering Young's modulus or weakening the atomic bonding. Thus, this material-dependent coefficient is also influenced by the applied load.

3.3. Conclusion

The wear resistance of metals is increased by cold work, but the increment is considerably smaller than that predicted by the Archard equation. The lower Young's modulus due to lattice defects introduced by plastic deformation, which deteriorate crystalline integrity and hence weaken the average atomic bonding, is attributed to the reduced advantage of strain-hardening to wear resistance.

Cu (FCC) benefits more from strain-hardening than Mg (HCP) because the latter has fewer slip systems and cold work in materials with lower fracture toughness is more likely to result in micro-voids and micro-cracking. Mg shows a larger value of η than Cu, which is a coefficient in the wearing energy model, reflecting a higher degree or severity of the negative influence of cold work on Young's modulus of Mg and corresponding wear resistance.

Chapter IV:

The unsuitability of generalizing the H/E ratio as an index for the wear resistance of materials

Hardness has long been regarded as a predominant factor for the wear resistance of materials. One of the widely used wear models is known as Archard's equation [9], which suggests a reverse relationship between the wear resistance and hardness as eq.(3.1) expresses. The wear coefficient K in the equation is used to compare the wear resistance of different materials, which is estimated mainly by experiments. Influences of other properties of a material on its resistance to wear, e.g., Young's modulus, shear modulus, and Poisson's ratio under specific wear conditions, could be included in the wear coefficient for a more accurate wear prediction. As an example, in a recently proposed wear model based on Archard's equation, Young's modulus is included [24]. There were also attempts to develop more general models for wear prediction [13,15, 87]. Since many wear models are proposed based on the contact geometry, which is mainly dependent on hardness, limitations exist because they do not directly deal with the wearing stress and failure process. Hardness alone only partially reflects the wear resistance of materials [24].

Efforts have been made to relate Young's modulus (E) to the wear resistance. One of the earlier attempts to use the H/E ratio for evaluating the wear resistance was made by Oberle [88]. The dependence of the wear resistance on the H/E ratio is adopted likely based on the consideration that materials with higher H/E ratios may

absorb more energy elastically with less damage. More studies are focused on the influence of E on the contact or indentation geometry, though plastic deformation dominates the contact [89-91], which may influence the wear resistance. The H/E ratio has often been used as an index to evaluate and rank wear resistance of materials and coatings/films [89, 92-98]. As a matter of fact, H and E are closely related. A material having a lower E has weaker atomic bonding, which negatively influences the hardness. Such a relationship complicates the dependence of the wear resistance on the H/E ratio. A recent molecular dynamics modeling study shows that the H/E ratio overestimates the wear resistance of strain-hardened materials and shows the inconsistency between the H/E ratio and the wear resistance of strain-free metals [99]. Thus, generalizing the dependence of the wear resistance on the H/E ratio is questionable. In the literature, the H/E ratio is frequently used as an index of wear resistances without sufficient justification in terms of its limitation in the application. This could lead to misleading information when investigating the mechanism for the wear of materials in different modes as well as when designing or modifying wear-resistant materials. It is thus of significance to show the limitation of this ratio as a measure of the wear resistance. This chapter reports an experimental study on the relationship between the H/E ratio and the wear resistance of cold worked metals to demonstrate this point.

Cold work is one of the approaches to increase the hardness of materials by mechanical deformation through, e.g., rolling and forging. The increase in hardness is achieved by the formation of lattice defects such as dislocations and their interactions, e.g., mutual pinning or tangling of dislocations. However, cold work can

decrease E due to the deterioration of the lattice integrity, which weakens the interatomic bonding [26]. Thus, the increased H/E ratio may not well reflect the wear resistance. Cold work could have negligible or even negative effects on the wear resistance [100-104]. In this study, relevant experiments were performed to determine the relationship between the H/E ratio and the wear resistance, using Mg and Cu as sample materials. Results of the study do show the limitation of the H/E for ranking wear resistance of materials.

4.1. Experimental

4.1.1. Materials and sample preparation

Sample preparation and deformation methods are similar to those described in Chapter 3. Annealed copper and Mg plates were provided by McMaster-Carr (Elmhurst, USA) and Alfa Aesar (Tewksbury, USA), respectively. The plates were cut into rectangular pieces, which were covered by cast iron blocks and then plastically deformed through repeated hammering to reduce their thickness homogeneously by 10, 20, 30, and 40%, respectively.

The cold worked samples were polished with SiC abrasive papers up to 1200 grit, cleaned using acetone solution, and then etched. The etchant for Cu was a mixture of 50 ml distilled water and 50 ml nitric acid, while that for Mg was a mixture of 10 ml acetic acid, 70 ml ethanol, 10 ml distilled water, and 6 grams of picric acid. After etching, samples were washed under flowing water and dried quickly with an airflow. Surfaces of the samples were characterized using a Zeiss EVO M10 SEM.

4.1.2. Mechanical testing

Young's moduli of the samples were determined using a Resonance Frequency and Damping Analyzer (RFDA, made by IMCE, Belgium). The hardness of the samples was measured using a Rockwell indenter (Zwick Roell Indentec, UK). Electron work functions (EWFs) of the samples were measured using a scanning Kelvin probe (KP Technology, UK). EWF is the minimum energy needed to move electrons at the Fermi level from inside a metal to its surface, which is a measure of the atomic bond strength of the metal [57].

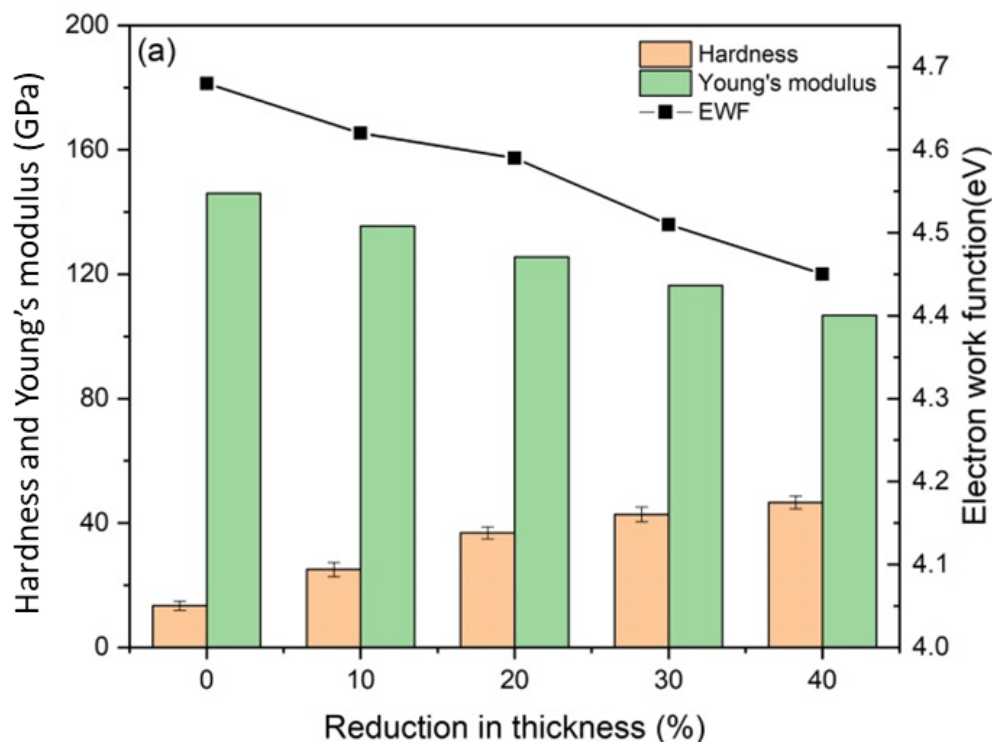
4.1.3. Sliding wear test

For wear tests, samples of 1.5 cm x 3 cm in dimensions were cut from the deformed metals, polished with SiC papers up to 1200 grit, cleaned with acetone solution, and then dried with an air flow. Sliding wear test was performed on a pin-on-disc tribometer (CSM Instruments) at room temperature. The pin was a ball with its diameter = 3 mm. The wear tests were performed at 20 mm/s over 12.5 meters under forces of 5N and 8N, respectively. A 3D Optical Surface Profilometer (Zygo Corporation, USA) was used to determine the volume loss based on the dimensions of wear track. The relative wear resistance is defined as 1/volume loss. Standardized wear resistance of a deformed sample is defined as the ratio of its relative wear resistance to that of a non-deformed one.

4.2. Results and Discussion

4.2.1. Mechanical properties

Values of E, H, and EWF of Cu and Mg with respect to the reductions of sample thickness are presented in Fig. 4.1. As illustrated, Cu has a higher hardness and Young's modulus than Mg. Hardness is increased by the cold work, whereas E changes in an opposite direction. The trend of variation in EWF is like that of E for both the metals, which is understandable since E and EWF are closely related [57]. EWF is correlated with the electron density [57], which can be decreased by lattice defects [105]. As shown and discussed below, lattice imperfections lose the crystal lattice, leading to decreased electron density and thus EWF. The decrease in EWF is an indication of the weakening of metallic bond strength [24].



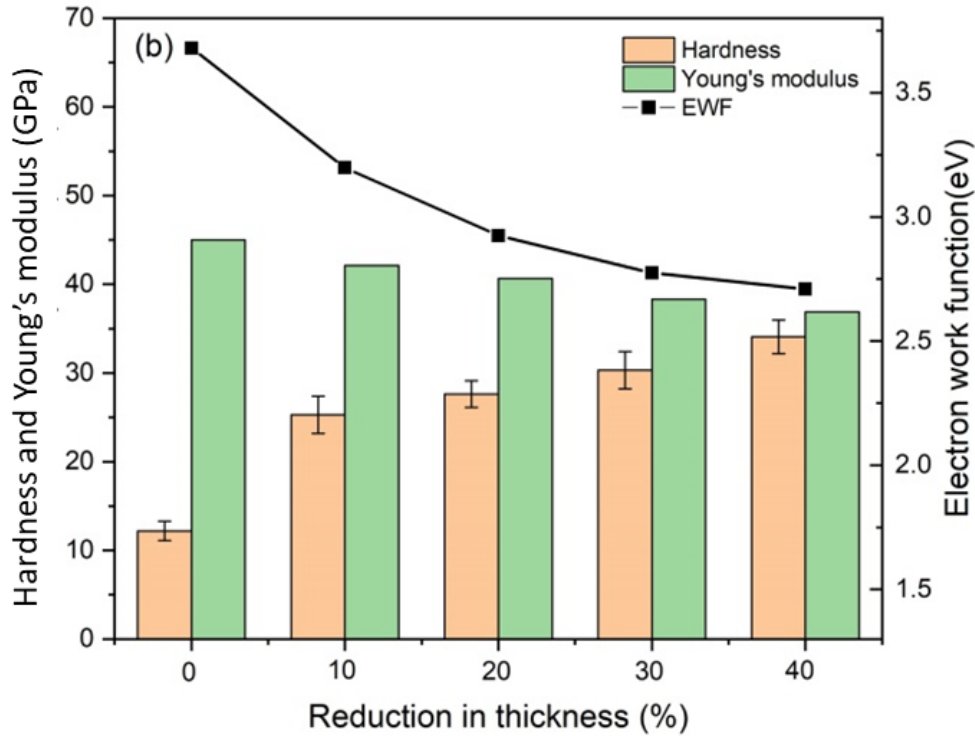


Figure 4.1. Variations in H , E , and EFW of (a) Cu and (b) Mg, with respect to the reductions in the thickness of 0%, 10%, 20%, 30%, and 40%, respectively.

4.2.2. Microstructural characterization

The decreases in EWF of Mg and Cu are ascribed to the formation of strain-induced lattice imperfections such as dislocations, micro-cracks, and micro-voids, all of which can lower EWF due to the deterioration of the lattice integrity and correspondingly lowered electron density [26]. The cold work induced imperfections can be seen in SEM images (figure 4.2). Figs. 4.2 (a) - (c) illustrate non-deformed Mg and Mg samples with 20% and 40% reductions in thickness, respectively. As shown, cold work resulted in micro-cracks in deformed Mg. This may happen because hcp Mg has only three slip systems, leading to low toughness and thus a higher probability of generating micro-cracks during the deformation processes of Mg and

its alloys [106-107]. Figs. 4.2 (d)–(f) illustrate non-deformed Cu and Cu samples with 20% and 40% reductions in thickness, respectively. No micro-cracks were observed on the surface of the deformed Cu due to its fcc structure with higher ductility but etch pits are present on the etched surface. Etch pits are likely the ends of dislocations that could be visualized after etching [85, 108] and the rough surface with irregular pits should be a sign of a heavily deformed surface with high-density dislocations.

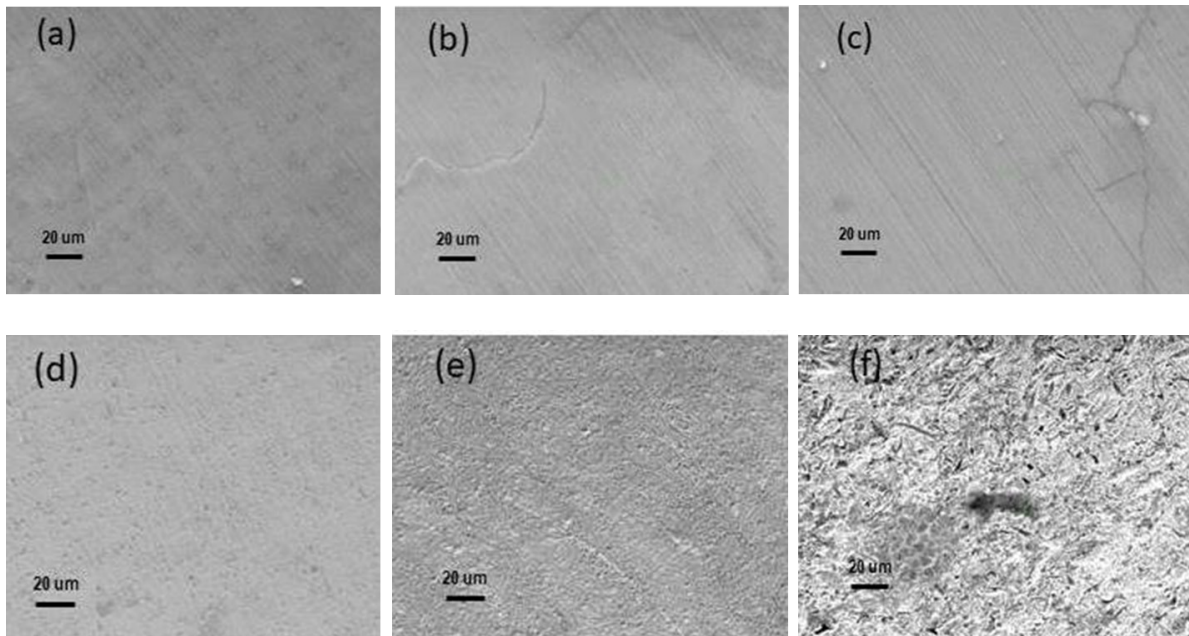
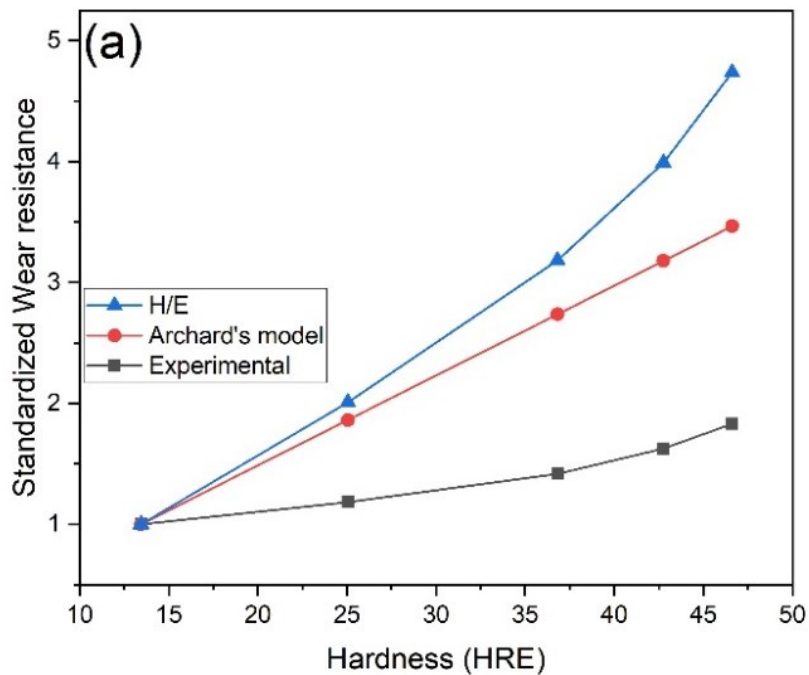
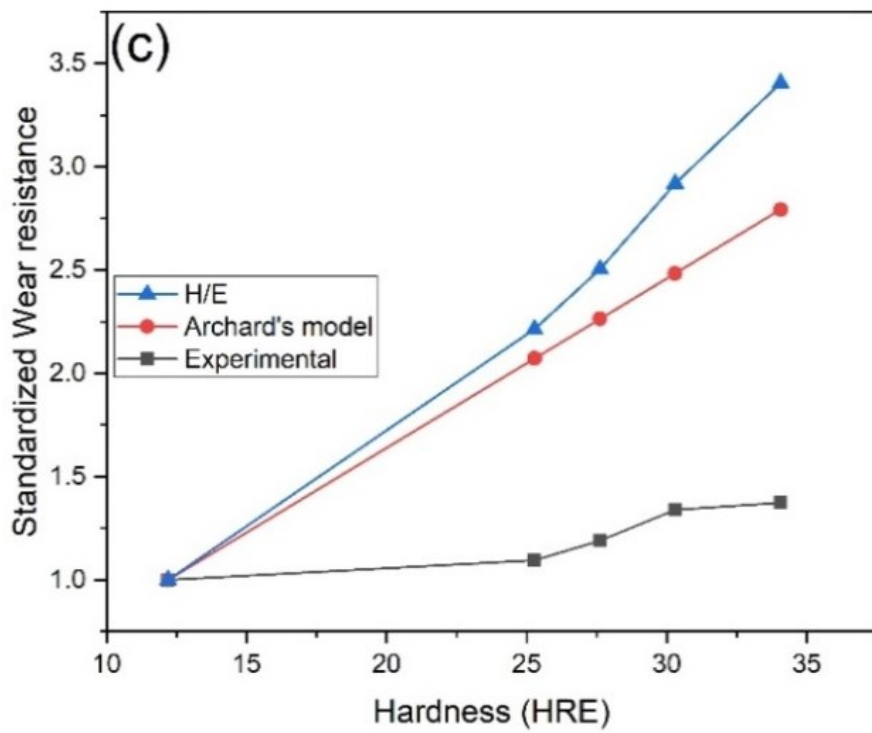
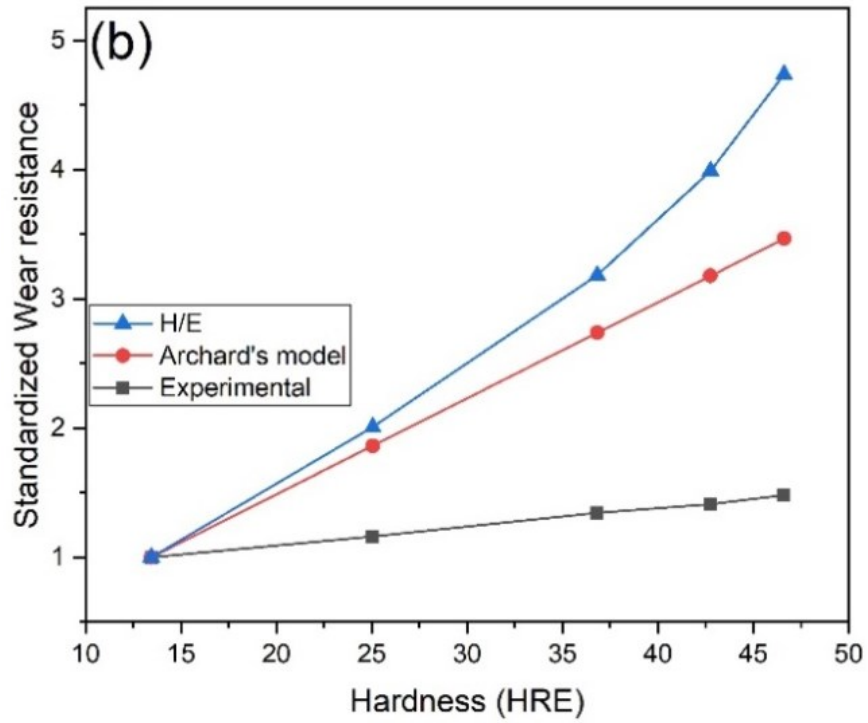


Figure 4.2. SEM images of (a) non-deformed Mg, (b) Mg with 20% reduction in thickness, (c) Mg with 40% reduction in thickness; (d) non-deformed Cu, (e) Cu with 20% reduction in thickness, and (f) Cu with 40% reduction in thickness. The surfaces were etched.

4.2.3. Wear behavior

Figure 4.3 shows the measured standardized wear resistances, corresponding H/E ratios, and those predicted by Archard's equation for the samples tested at two loads, 5N and 8N, respectively. As shown, the wear resistance of Cu and Mg were increased by cold work. However, the H/E ratio and the wear resistance predicted by Archard's equation significantly overestimate the wear resistance. Archard's equation without E involved gives higher wear resistance than the experimental value. The wear resistances represented by the H/E ratios are even higher, since the cold work increases H but decreases E, leading to larger H/E ratios.





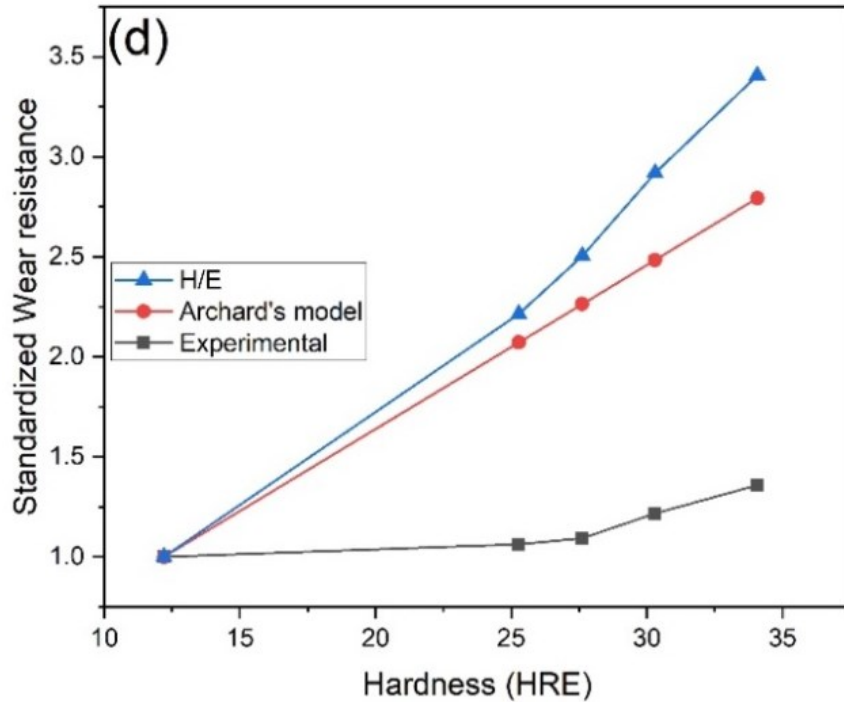


Figure 4.3. Standardized wear resistances determined experimentally, corresponding H/E ratios and those predicted by Archard's equation versus the apparent hardness for cold worked Cu and Mg tested at two loads: (a) Cu_5N, (b) Cu_8N, (c) Mg_5N and (d) Mg_8N.

The decrease in Young's modulus (E) caused by cold work results from deformation-lattice imperfections, e.g., dislocations, vacancies, vacancy cluster, and micro-cracks that may be initiated by vacancy clusters or micro-voids. Although mutual interactions among lattice imperfections can increase hardness as known the strain-hardening, the imperfections lose the crystal lattice, leading to lattice discontinuity which weakens the atomic bonding [26]. Dislocations can increase the average atomic spacing, making it deviate from the equilibrium one, thus decreasing the atomic bond strength as well [24]. Fig. 4.4 schematically illustrates how the

atomic bond strength or bond energy (ϵ_b) is reduced in a loosened lattice, which correspondingly decreases the Young's modulus.

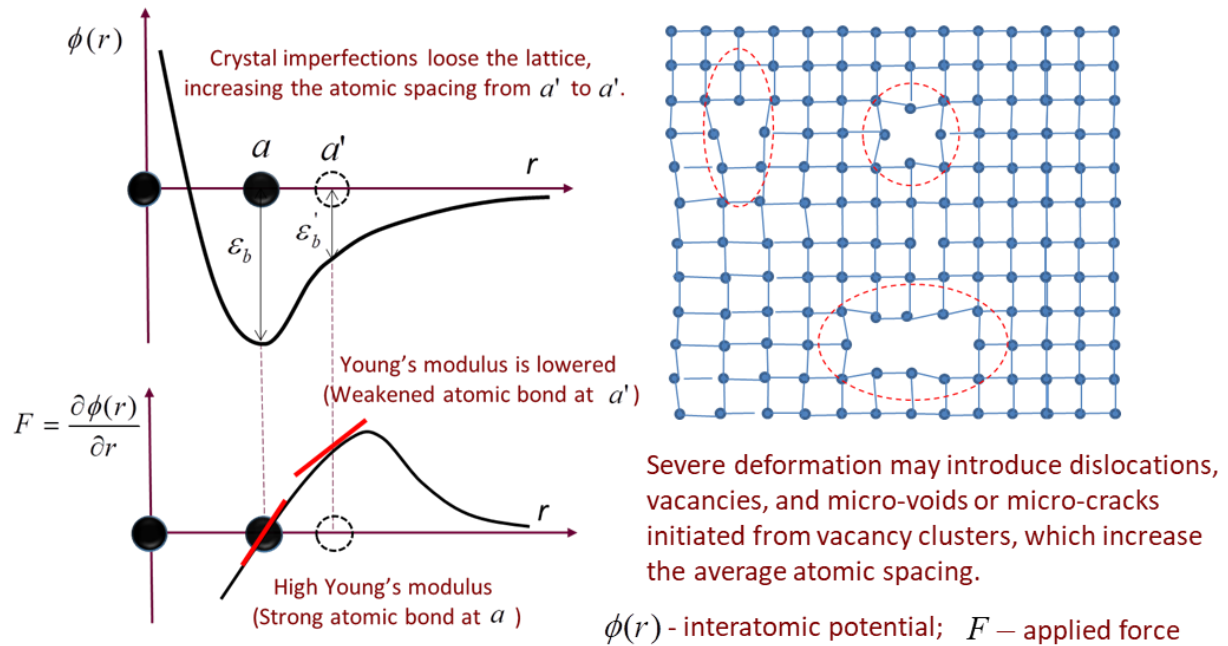


Figure 4.4. Plastic deformation may introduce dislocations, vacancies, and micro-voids or micro-cracks that may be initiated from vacancy clusters during severe plastic deformation. The lattice imperfections lose the crystal lattice, leading to weakened atomic bonding and correspondingly decreased Young's modulus.

Cu is more wear-resistant than Mg due to its higher H and E, although the standardized wear resistance i.e., the ratio of the wear resistance of deformed sample to that of non-deformed one does not directly show this difference. Besides, the fewer slip systems of Mg make it prone to micro-cracking, which are more detrimental to its resistance to wear.

Based on the experimental results, the H/E ratio should not be generalized as an index for the wear resistance, although it may work for specific cases. In fact, even in strain-free states, the H/E ratio also shows discrepancy when used to rank the wear resistance of metals [99].

As a remark, the elastic deformation has limited influence on the asperity contact geometry during the wear of metallic materials in which plastic deformation dominates. Thus, Young's modulus is not expected to have a strong influence on the wear of metals or alloys in most cases. The situation could change for ceramic materials and coatings or thin films since ceramic materials have little or limited plastic deformation before fracture. Thus, H/E ratio may reflect the wear resistance for some cases but should not be generalized as an 'index' of wear resistance.

The authors would like to clarify that in the present study the elastic modulus is considered when dealing with wear of the metals in which plastic deformation plays a predominant role. The plastic deformation originates from defect activities such as the operation of slip systems involving the generation and movement of dislocations. The energy barrier to the defect generation and movement is determined by the atomic bond strength, which can be reflected by the elastic modulus. The generated dislocations and other defects, e.g., vacancy or vacancy clusters, lower the lattice integrity and thus decrease the average atomic bond strength that is reflected by the lowered elastic modulus, leading to decreased wear resistance. In the present study, the elastic modulus is not used to deal with contact geometry but to represent the variations in atomic bond strength caused by plastic deformation.

4.3. Conclusions

We demonstrated that the H/E ratio should not be used as a generalized indicator of wear resistance using cold worked Mg and Cu as an example. Cold working increases the hardness of materials, which improves wear resistance. However, cold working deteriorates the crystal integrity by introducing lattice imperfections, resulting in a lower Young's modulus and weaker atomic bonding. The H/E ratio overestimates the wear resistance of the metals even more than Archard's equation.

Chapter V

Influence of Bauschinger effect on wear of cold-worked Cu and Mg during unidirectional and bidirectional sliding wear

Wear process is influenced by mechanical properties of the materials, operating conditions, and the geometry of the wearing components in contact. In the case of metallic specimens, the type of loading condition can affect the strain-hardening process and greatly influence the intensity of the wear damage. One such type of phenomenon based on the loading condition is called the Bauschinger's effect. When a metallic material is loaded uniaxially in one direction into the plastic region, then unloaded to zero stress level, followed by reloading in the reverse direction, the material may be yielded at a stress level lower than its original yield strength. This direction-dependent, asymmetrical, and anisotropic yield behavior is known as the Bauschinger effect, after Johann Bauschinger who first reported this phenomenon in 1886 [60]. Figure 5.1 is the schematic representation of Bauschinger's effect.

After this discovery, the Bauschinger effect has been widely studied. Bauschinger's findings involved only the basic phenomenon and that directional behavior in the stress-strain relationship is much more complex after further studies [109-111].

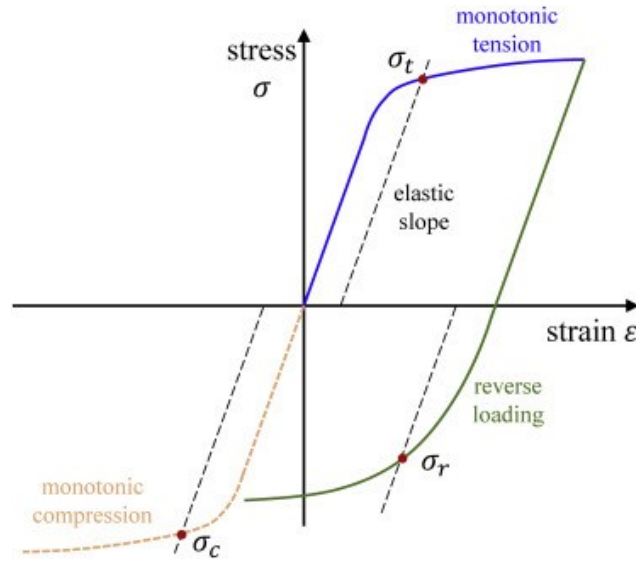


Figure 5.1. Schematic illustration of Bauschinger effect in metallic materials [112]

Out of the different theories which try to explain this phenomenon, after the discovery of the presence of Bauschinger's effect in single crystals, the dislocation theory has been studied most extensively. One of the initial approaches towards the dislocation theory was proposed by Mott [68] and Seeger [69]. They suggested that during pre-deformation of any metallic material, long-range stresses are built up because of the formation of the dislocation pile up at the barriers like grain boundaries which are capable enough to restrict the dislocation movement. Due to this restricted dislocation movement, the back stresses generated by the dislocation pileup will accommodate the dislocation motion in the opposite/reverse direction.

When this dislocation pileup interacts with the dislocations which are further mobilized on the slip plane, immobile and sessile Lomer–Cottrell junctions are generated. These junctions prevent the movement of other dislocations in their slip planes which can restrict the pileup from moving back after unloading because it is

important for the pileups to stay there after unloading to assist the reverse movement.

The second approach towards the dislocation theory was proposed by Orowan [62]. He and his group concluded that due to the reversal of the deformation, the entire stress-strain relationship changes and there is some permanent softening induced in the metal which depends on the amount of softening is dependent on the magnitude of the back stresses. Also, after heating the pre-deformed specimens above their recrystallization temperature, the anisotropic behavior was diminished. This proved that there are other factors governing the Bauschinger effect other than back stresses. During reverse loading, dislocations formed will cancel out or annihilate the dislocations with opposite signs after coming in contact, thus lowering the yield strength and strain hardening of the metal[113-119]. Dislocation density also lowers during the annihilation process which helps prevent any further mechanical damage to the material [120-122].

The wear resistance of Cu-40%Zn alloy was tested by Tang et al. [120] under unidirectional and bidirectional conditions using a steel wheel as the abrader. For the bidirectional process, the rotation of the steel wheel was changed after a fixed number of rotations. They concluded that the amount of volume loss for the Cu-40%Zn alloy in the unidirectional abrasion process was higher as compared to the bidirectional one because of the lowered strain hardening effect in the bidirectional sliding. Also, wear resistance was enhanced with the frequency of the direction change during rotation. In another study by Tang et al. [121], they used a ceramic

counter face for the Cu-40% Zn and the results were different showing that the amount of material loss increased with the direction reversal. Higher frequency resulted in more material loss.

Previously, we investigated the wear behavior of cold worked Cu and Mg in unidirectional sliding wear conditions from the viewpoint of the newly derived wearing energy model [24, 122]. In this study, we investigate the effect of the Bauschinger effect during the bidirectional sliding wear and compare it against the unidirectional and the effect of the direction change frequency on the wear resistance of the cold worked Cu and Mg.

5.1. Experimental

5.1.1. Materials and methodology

Materials used for the current study are Cu (99.99% pure) plates which has an FCC structure and Mg (99.8% pure) cylinders which has an HCP structure in their annealed state without any preexisting deformation. These copper plates and magnesium cylinders were cut into small rectangular plates using an automatic wire-cutting machine. For cold working of Cu and Mg, the small rectangular plates prepared in the above step were placed between two cylindrical cast iron blocks (40 mm in diameter), and a flat circular faced hammer weighing 10lbs. was used at an impact speed of 6-8 m/s. The materials under study are comparably softer hence are easily deformed. To maintain homogeneity during cold working, hammering was done in small cycles with each cycle consisting of 5 impacts. Both Cu and Mg were cold worked to get the required reduced thickness of 10%, 20%, 30%, and 40%.

These thicknesses were carefully measured after every hammering cycle using a Vernier caliper.

After cold working, the plates were polished with silicon carbide emery paper up to 4000 grits, cleaned with water followed by acetone, and then pressurized air was used to clean the sample surface and then stored in a desiccator. For the sliding wear test, rectangular plates with dimensions of 15 mm × 20 mm were used. For surface morphology analysis, Cu was etched with a mixture of 50 ml nitric acid and 50 ml distilled water, Mg was etched using acetic-picral which is a mixture of 5 ml acetic acid, 100 ml ethanol, 10 ml distilled water, and 6 g of picric acid for 3-5 seconds. After etching, they were washed instantly under flowing water to prevent over-etching and then dried with airflow.

Young's modulus of all samples was measured using a non-destructive acoustic instrument with RFDA basic software provided by IMCE (Genk, Belgium) under flexural mode. The hardness of the samples was determined using a Zwick Roell Indentec Hardness Testing Machine. Rockwell scale B (HRB) of Cu samples was determined using a 1/16 in (1.59 mm diameter) steel ball as an indenter under a load of 100kgf. Rockwell scale E (HRE) of Mg samples was determined using a 1/8 in (3.18 mm diameter) steel ball as an indenter under a load of 100kgf. Indentations were made across the rectangular samples to get the mean value. The obtained Rockwell hardness values were converted into SI units (MPa) and are presented in Table 3.2.

5.1.2. Sliding wear test and Characterization

Dry sliding wear tests were performed on a computerized pin-on-disc Rtec MFT-5000 Tribometer (Rtec, San Jose, US) using a 5.953 mm diameter silicon nitride (Si_3N_4) ball at room temperature. All the wear tests were performed at a normal load of 5N for 10 minutes with a sliding speed of 4 cm/s. For unidirectional sliding, the above-mentioned parameters were used and for bidirectional sliding wear tests, a cyclic number (CN) was introduced to measure the number of times the direction changes during the sliding wear process. CN=0 signifies unidirectional sliding, while CN=5 signifies that the direction is changed 5 times during the entire sliding wear test. For bidirectional sliding tests, we used CN=5, CN=10, CN=20, and CN=30. Figure 2 shows the experimental setup for the sliding wear test in unidirectional and bidirectional processes.

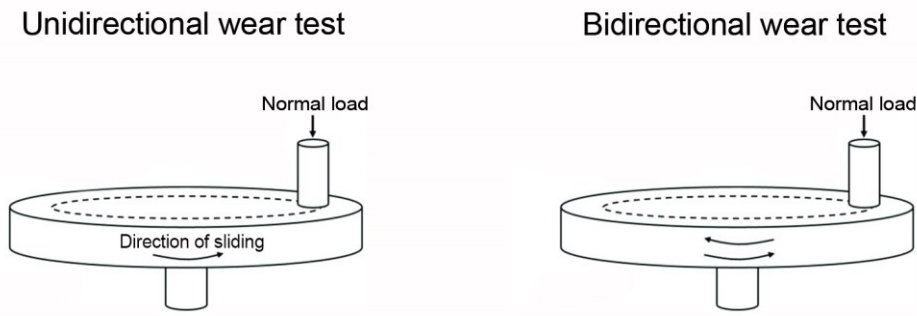


Figure 5.2. *Schematic illustration of unidirectional and bidirectional sliding wear tests*

Each test was repeated a minimum of three times. Wear volume was calculated by measuring the dimensions of the wear track using a 3D Optical Surface Profilometer made by Zygo Corporation (Middlefield, CT, USA). The wear track

morphology was analyzed using EVO MA10 Scanning Electron Microscope equipped with an Energy-Dispersive Spectrometer (EDS).

5.2. Results and Discussion

5.2.1. Mechanical properties

Hardness and Young's modulus measurements are given in table 3.1. Hardness values increased with cold work due to strain hardening of the samples due to the interaction and tangling of the dislocations formed during the cold work. However, Young's modulus of the samples lowered with the intensity of cold work. This lowering of Young's modulus is mainly linked to the strain-induced lattice defects or imperfections like dislocations, micro-voids, and micro-void induced micro-cracks, which negatively affect the crystalline integrity, and the broken interatomic chains or distorted lattice network weaken the average interatomic bond strength [26, 81, 82, 86].

5.2.2. Microstructural characterization

To understand the effect of cold work on the surface morphology of Cu and Mg, samples were etched and examined under the scanning electron microscope, which is shown in Figs. 5.3 and 5.4, respectively. For both Cu and Mg, the samples under examination were strain-free (0% thickness reduction) and experienced the largest deformation (40% thickness reduction). Respectively, which were observed under the SEM at low (400X) and high magnification (5200X). Cu having an FCC structure possesses more slip systems with higher ductility than Mg, which did not show any microcracks after cold working (Fig. 5.3), while microcracks were observed on cold

worked Mg (see Fig. 5.4 (b)) which has an HCP structure having a lower number of slip systems to accommodate plastic deformation caused by the cold work [83]. However, in the cold worked Cu, persistent slip bands (PSB) [124] can be observed as shown by the white dashed line in figure 5.3 (d) which are not seen in undeformed Cu. There are pits on the Cu surface (Fig. 5.3(b)) which are mainly due to the etchant.

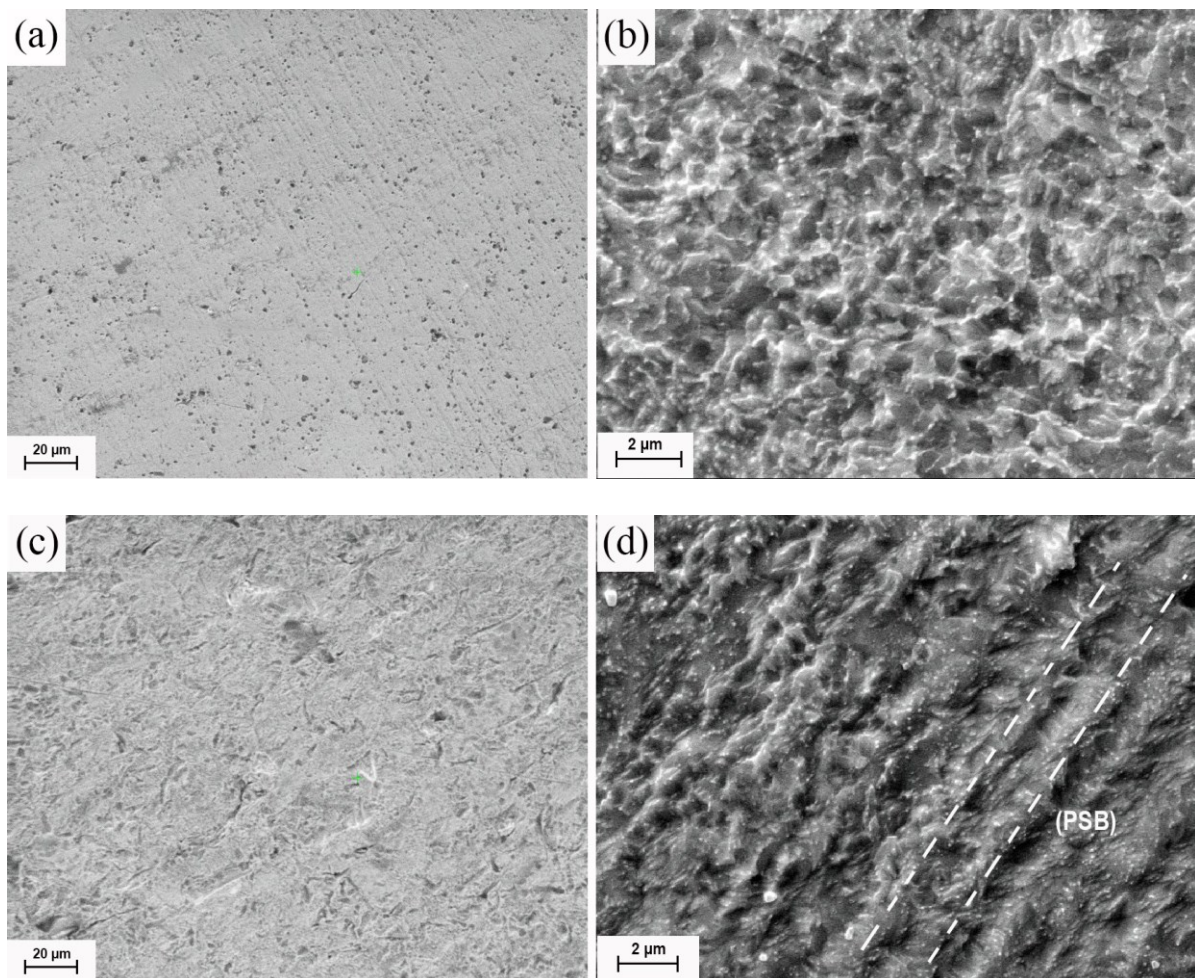


Figure 5.3. SEM images of etched (a) undeformed Cu (400X), (b) undeformed Cu (5200X), (c) cold worked Cu up to 40% reduction in thickness (400X), (d) cold worked Cu up to 40% reduction in thickness (5200X).

During Mg surface observation, a mix of microcracks and microvoids were observed in the cold worked sample as illustrated in figures 5.4 (b, c). These microcracks and microvoids can be linked to adjacent imperfections, which may trigger cracking and extend cracks leading to failure due to the stress concentration at the crack tip. The number of imperfections like the microvoids and microcracks increased, observed on the Mg surface as the amount of cold work was increased.

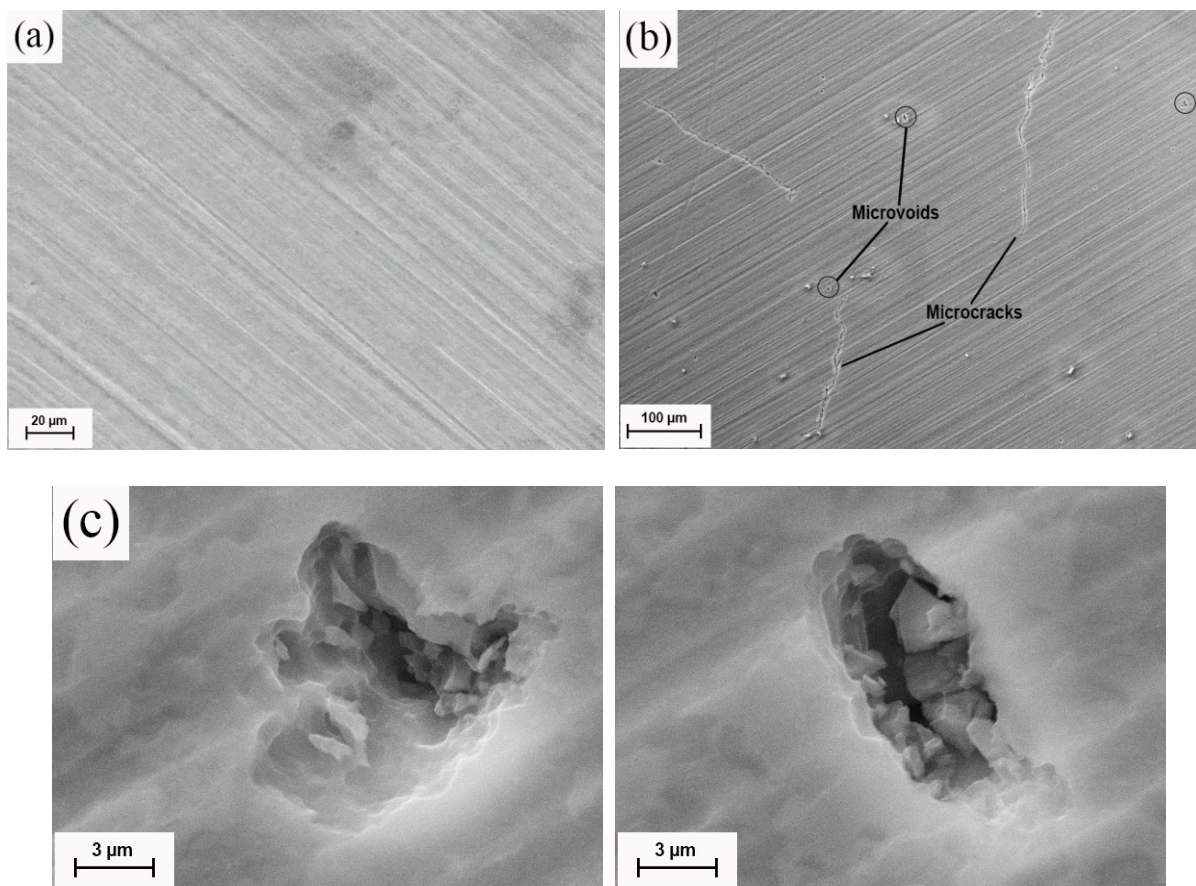


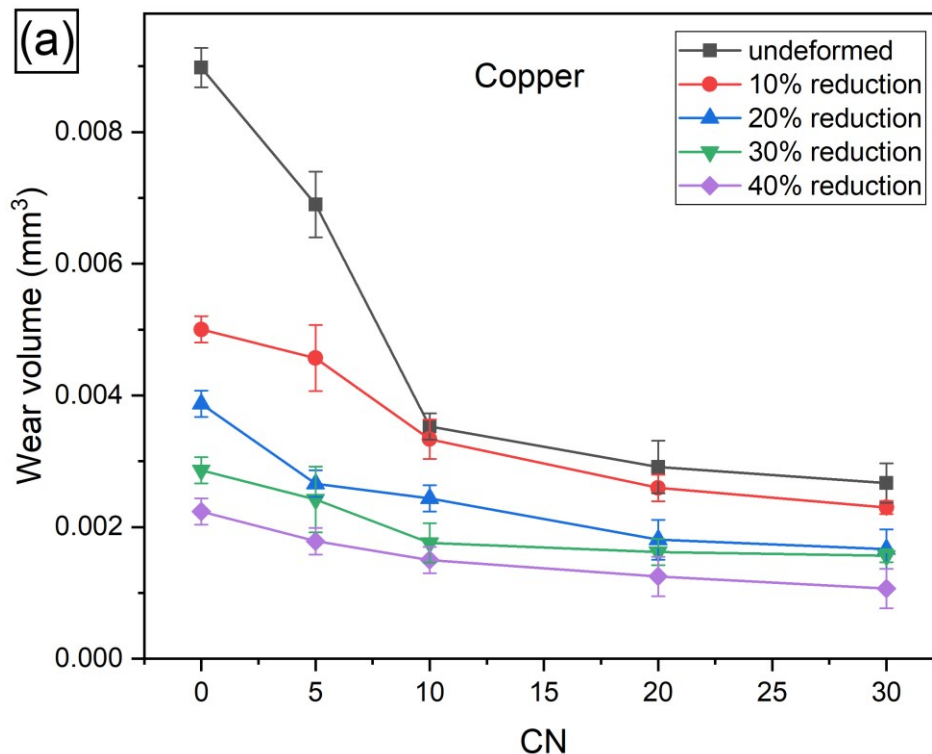
Figure 5.4. SEM images of etched (a) undeformed Mg, (b) cold worked Mg with 40% reduction in thickness, (c) Micro voids present cold worked Mg (40%).

5.2.3. Wear characteristics

Wear volume losses of both the cold worked Cu and Mg samples with different amounts of thickness reductions tested under both unidirectional and bidirectional sliding wear conditions are shown in figure 5.5. For both the metals, their wear volume losses are higher during the unidirectional sliding wear tests than those caused by bidirectional sliding wear tests. During bidirectional sliding wear, the wear volume loss decreased with the increased frequency of change in sliding direction or the Cyclic Number (CN). For Cu, at higher CN values like CN=20 and 30, the wear volume became stable which was not the case for Mg. Cold worked Cu has more dislocations which can easily tangle to each other and cause dislocation pileup and tangling saturation, thus early reaching the stability of such a barrier to dislocation movement. From figure 5.5 (a), one may see that the percentage change in the wear volume for undeformed Cu samples from unidirectional (CN=0) to bidirectional (CN=30) is 70.2% and for 40% cold worked sample it was around 50%. Also, after a certain amount of cold work (20%) the percentage change in the wear volume also became stable. As the intensity of cold work increases, we can see that Bauschinger's effect is less profound due to the presence of dislocation pileups and existing dislocation tangling whereas in an undeformed sample there are fewer dislocations which makes the Bauschinger effect occur easily.

The situation is the opposite for Mg. According to figure 5.5 (b), the percentage change in wear volume of undeformed Mg from unidirectional (CN=0) to bidirectional (CN=30) is 24%, while that of 40% cold worked sample is about 41%. The smaller percentage change of the undeformed Mg may be ascribed to the

presence of fewer slip systems of Mg. For cold worked Mg, there are two possible factors promoting the Bauschinger effect: 1) the pre-generated dislocations cause local lattice distortion, which might facilitate the formation of new defects such as dislocations and possible deformation twinning during bidirectional sliding when the wearing stress is reversed; 2) the cold work generated microvoids and microcracks provide empty spaces inside the Mg sample, which may also facilitate the generation of new dislocations and possible deformation twinning from the internal surface of micro-voids [124]. As the wear tests were performed at room temperature without any airflow to reduce the frictional heating at the contacting surfaces, the Bauschinger effect could be more visible as the dislocations become easier to be generated and moved at elevated temperatures, as which the materials were more or less softened [125].



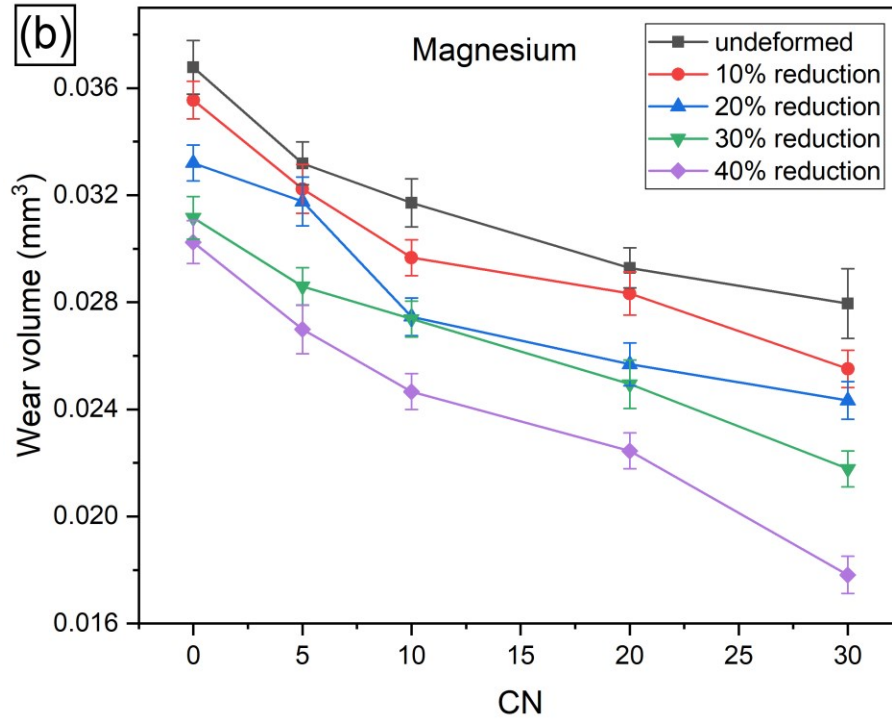
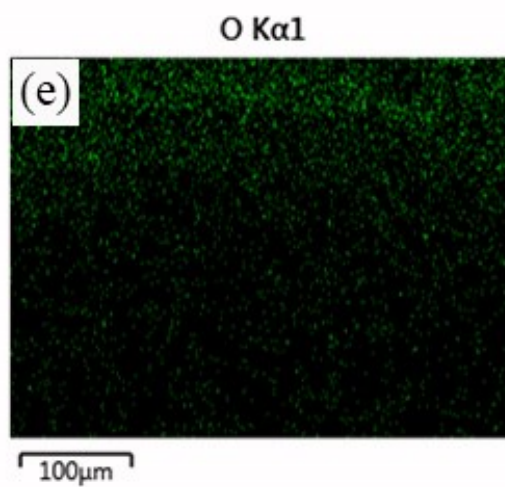
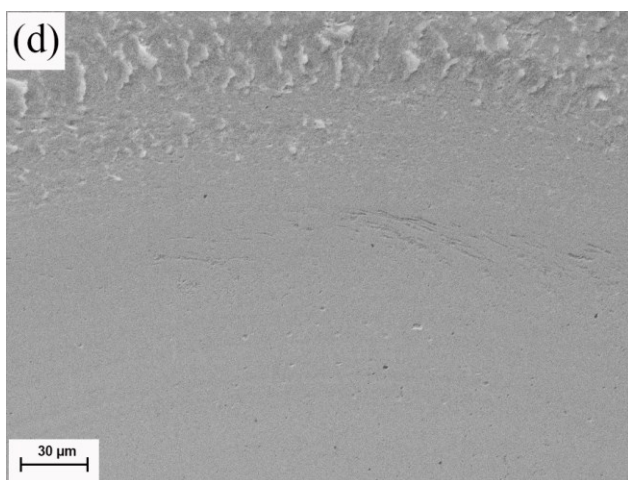
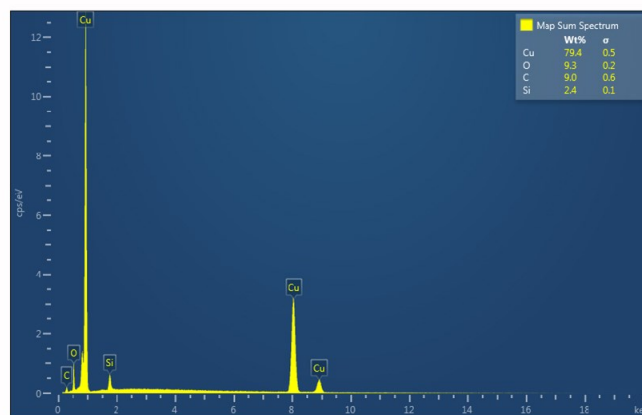
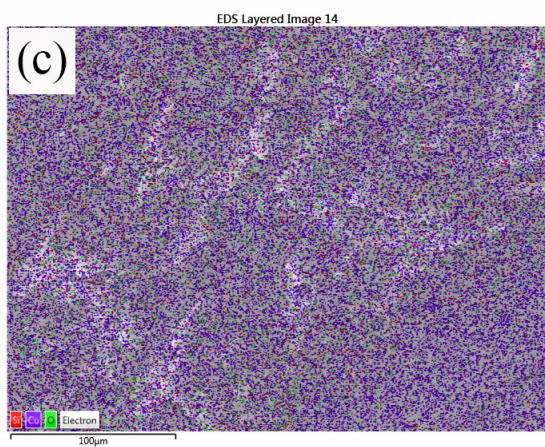
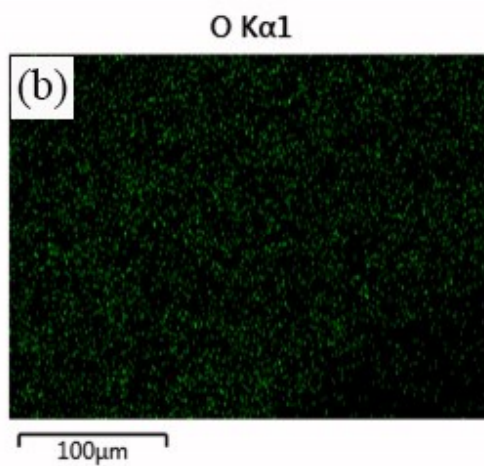
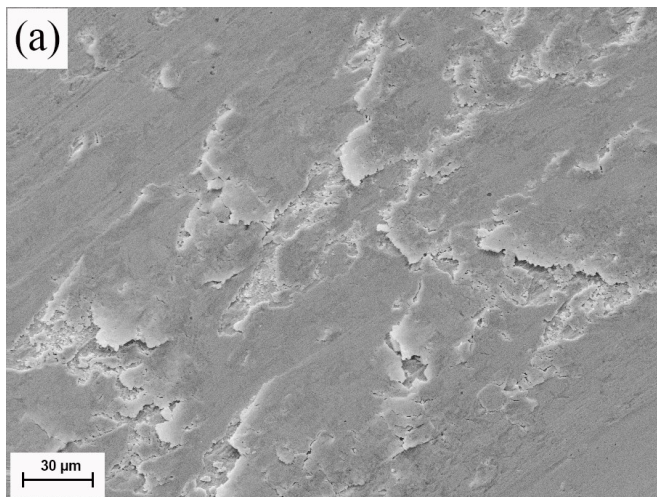


Figure 5.5. *Wear volume (mm³) versus CN (Cyclic number) for Cu and Mg of 0%, 10%, 20%, 30%, 40% reduction in thickness.*

It should be mentioned and discussed the formation of tribo-oxides, which may increase the local hardness of the wear track [127] and thus help reduce wear. The formed oxide scale could more or less influence the Bauschinger effect. Figure 5.6 shows the SEM and EDX analysis of the wear track of cold worked Cu (20% reduction in thickness) in both unidirectional and bidirectional sliding (CN=30).

Figure 5.6 (a-c) shows that the distribution of oxides examined through EDX analysis and relatively larger surface coverage is observed on the worn surface experiencing bidirectional sliding, compared to that on the surface worn by unidirectional sliding (figure 5.6 (d-f)).



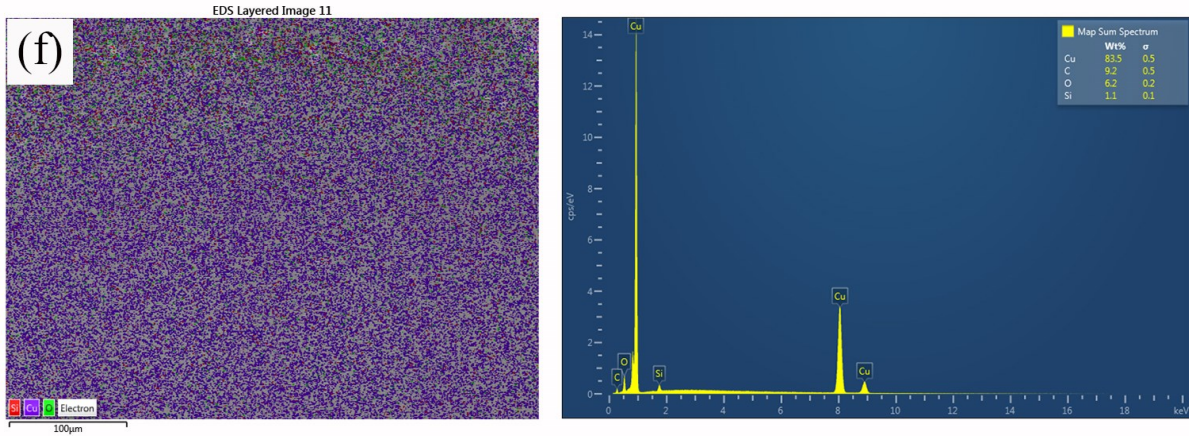
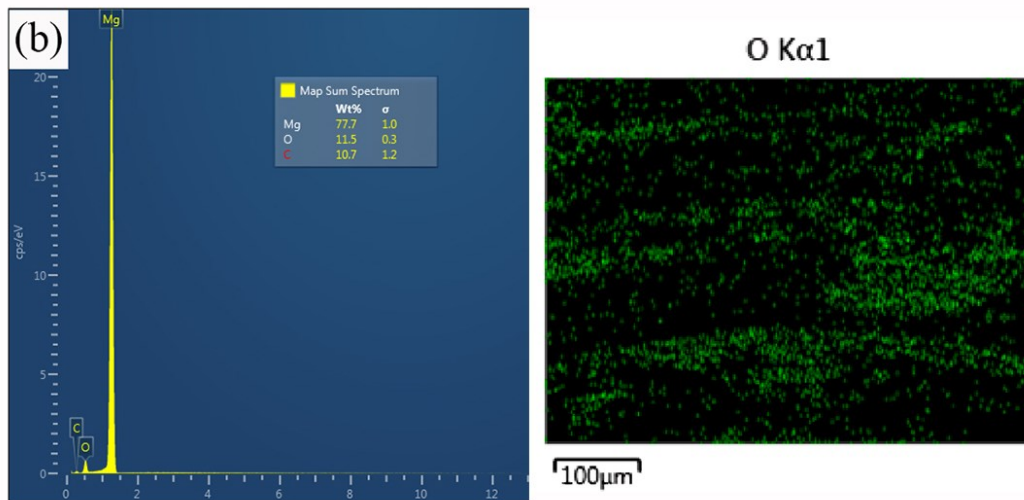
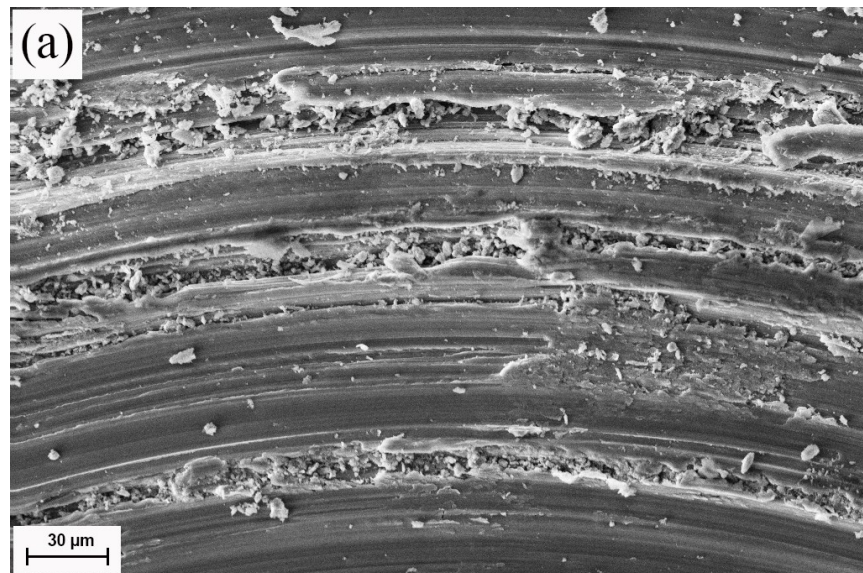


Figure 5.6. (a) SEM image of wear track of cold worked Cu (20%) caused by bidirectional sliding (CN=30), (b) oxygen composition of the wear track on the cold-worked Cu during bidirectional sliding, (c) EDX map and spectrum of cold worked Cu experienced bidirectional sliding, (d) SEM image of wear track on the cold-worked Cu (20%) caused by unidirectional sliding, (e) oxygen composition of the wear track on the cold worked Cu experience unidirectional sliding, (f) EDX map and spectrum of cold worked Cu experience unidirectional sliding.

The smaller coverage of oxide on worn surfaces under the unidirectional sliding could be due to the unidirectional wearing force that may enhance the plowing effect and scratch off the oxide scale. While during the bi-directional sliding, the reversal of wearing force could weaken such scratch-off effect, since the Bauschinger effect could also apply to the dislocation process at the metal/oxide interface. The larger coverage of the oxide scale on the worn surface may help reduce local stress concentration, thus reducing the wear damage [128]. In other words, the formation of oxide scales could further benefit the resistance of the sample to bi-directional sliding wear attack.

The above phenomenon was also observed in case of Mg. Figure 5.7 illustrates the wear tracks of cold worked Mg caused by unidirectional and bidirectional sliding wear tests. Similar to the case of Cu, the amount of oxygen (wt. %) present on worn surfaces is higher during bidirectional sliding, implying more oxide scales retained on the wear track, for which the reason has been discussed in the previous paragraph. With less oxide on the surface, the plowing effect appeared more severe on the worn surface caused by the unidirectional sliding wear.



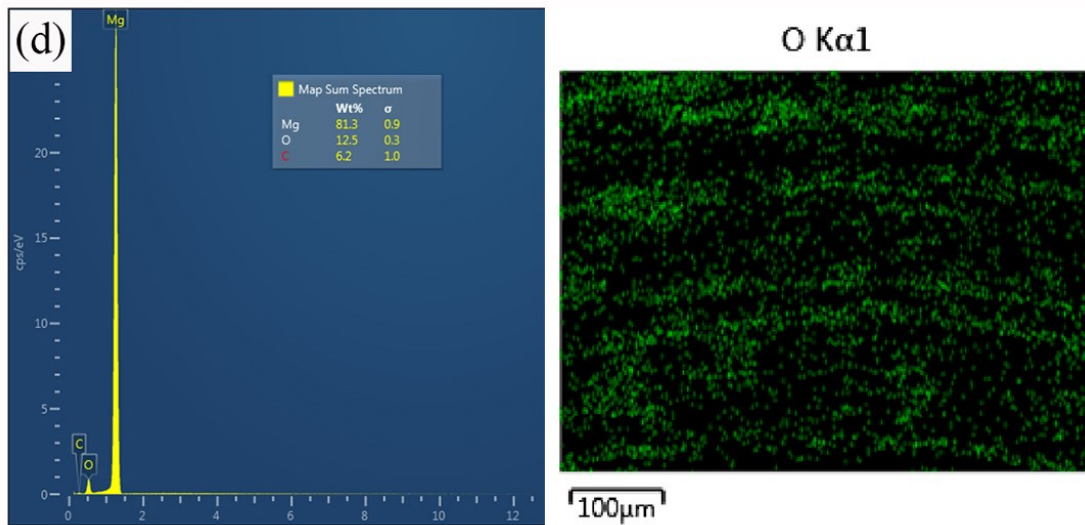
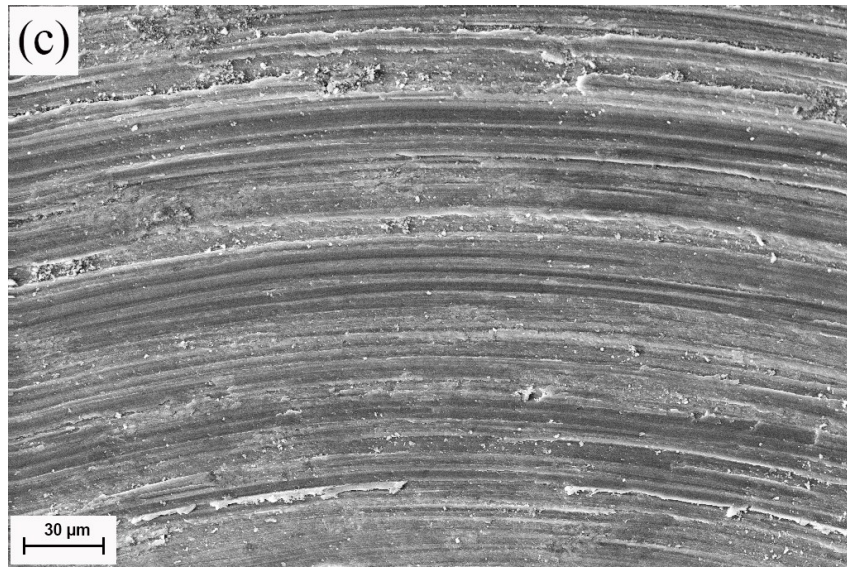


Figure 5.7. SEM images and EDX analysis of wear track on (a, b) cold- worked Mg (40%) caused by unidirectional sliding and (c, d) that caused by bidirectional sliding (CN=30).

Figure 5.8 shows the 3D wear track profiles for both samples with no deformation and with the maximum deformation at CN=0 and CN=30, respectively. The wear track profiles show the wear tracks dimensions which are used to determine the overall wear volume loss caused by sliding wear under different

conditions. In Cu samples, larger volume loss is caused by unidirectional sliding (CN=0). The wear width is significantly smaller in the case of bidirectional sliding for any given deformation, which can be ascribed, as discussed earlier, to the wearing stress reversal that results in less build-up of dislocations towards failure. The Mg with an HCP structure shows smaller difference in dimensions between wear tracks caused by unidirectional and bi-directional wear tests, respectively (Fig. 5.9), corresponding to the less profound Bauschinger effect as discussed earlier due to its fewer slip system.

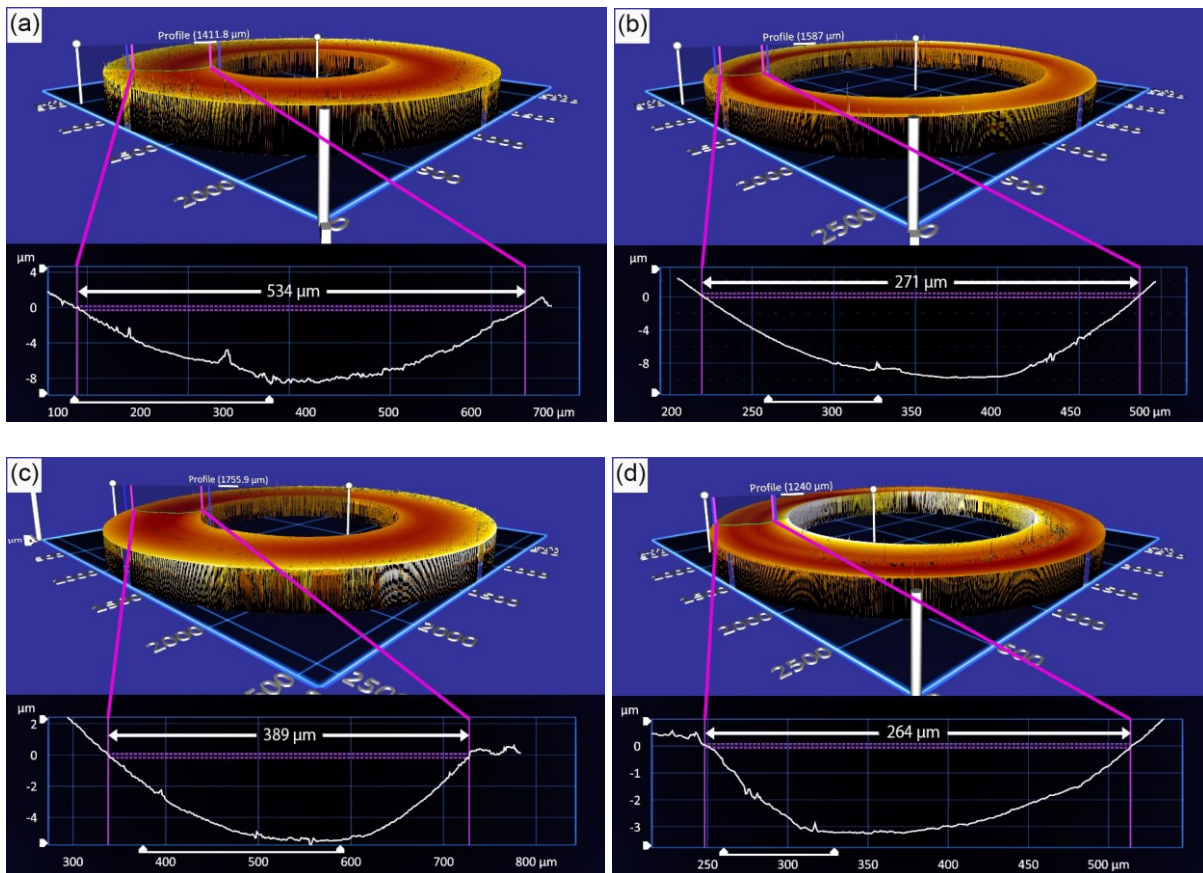


Figure 5.8. 3D profile of the wear tracks along with the wear width and depth curve for (a) Cu 0% [CN=0], (b) Cu 0% [CN=30], (c) Cu 40% [CN=0], Cu 40% [CN=30].

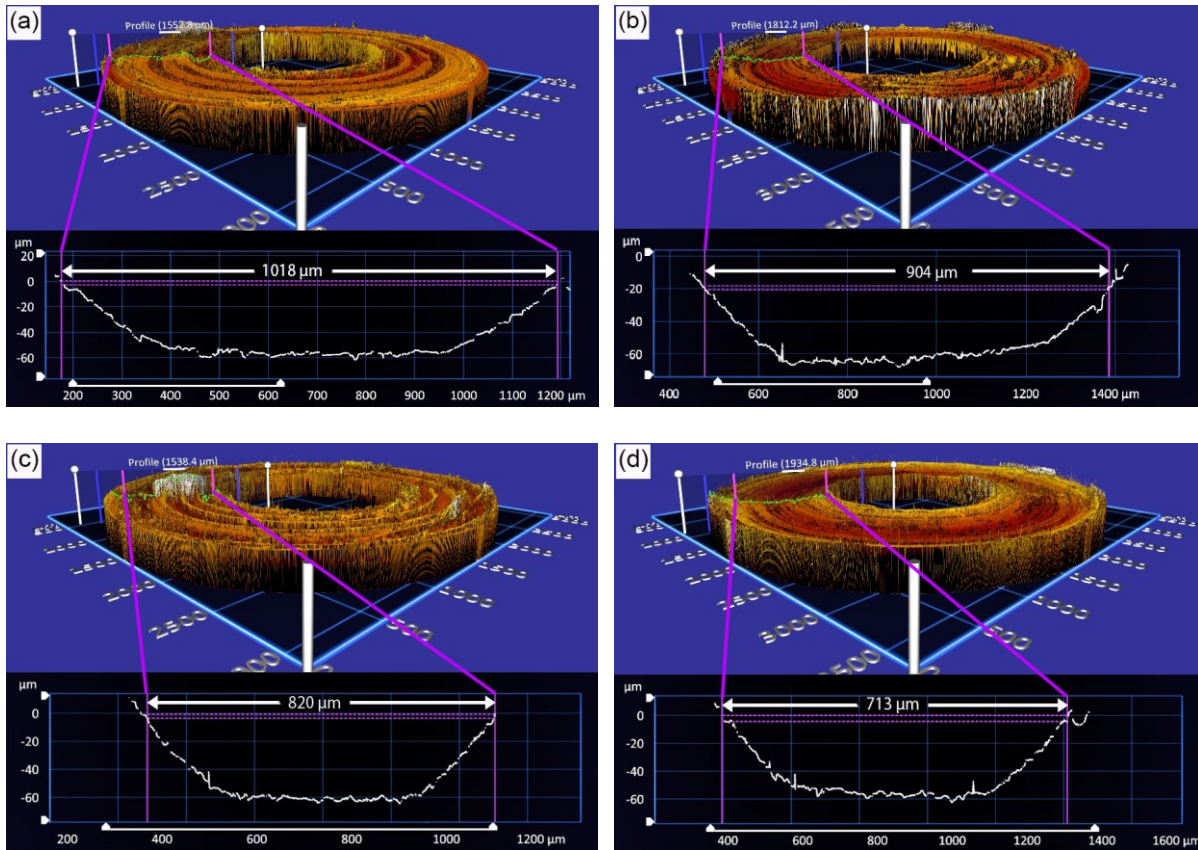


Figure 5.9. 3D profile of the wear tracks along with the wear width and depth curve for (a) Mg 0% [CN=0], (b) Mg 0% [CN=30], (c) Mg 40% [CN=0], Mg 40% [CN=30].

5.3. Conclusions

Bidirectional sliding results in less wear volume loss, which decreases as the frequency of changing the sliding direction increases. This decrease in wear volume is primarily due to the Bauschinger effect, which occurs when the wearing stress is reversed, causing dislocation reversible movement and annihilation (canceling out of dislocations with opposite sign). In comparison to undeformed Cu, cold work increased dislocation density, which resulted in a higher probability of dislocations

tangling, resulting in a less pronounced Bauschinger effect. The percentage change in wear volume remained relatively consistent at 20 percent cold work.

Cold worked Mg samples had a larger percentage wear volume change than undeformed Mg samples. It's mostly due to the fact that there are fewer dislocations and less dislocation pipe up, which means there's more room for reversible dislocation movement when the wearing stress is reversed. The presence of microvoids and microcracks further aids the Bauschinger effect by allowing reversible dislocation movement with less restraint for creating new dislocations with the opposite sign as the wearing load is reversed. During the wear tests, oxidation occurred on both Cu and Mg samples due to frictional heating. For both Cu and Mg, the oxygen levels induced by bidirectional sliding were greater than those caused by unidirectional sliding. Wear was reduced due to the formation of a tribo-oxide layer.

Chapter VI

General Conclusions

The outcomes of the present research are summarized and concluded in this chapter, with answers to the primary research questions. The main contributions of this research are described and future work that could be carried out for further understanding and potential applications will also be discussed.

6.1. Part I: Clarification of the puzzled effects of cold work on wear of metals from the viewpoint of wearing energy consumption

6.1.1 Concluding results

Strain-hardening increases the hardness of metallic materials and thus benefits their wear resistance. However, strain-hardening introduces lattice imperfections, which deteriorate the crystalline integrity and diminish such benefits. As a result, the strain-hardening may not benefit the wear resistance as large as expected such as that predicted by the Archard model/equation. In this study, the effects of cold work on resistances of Cu (FCC) and Mg (HCP) to abrasive wear were investigated under the ambient condition. The metal samples were deformed by homogeneous hammering to reduce their thickness to different percentages. Corresponding hardness values and Young's moduli of the deformed and undeformed samples were measured. Pin-on-disc sliding wear tests were performed under different loads at room temperature. The different responses of the samples to abrasive wear were

analyzed from the viewpoint of wearing energy consumption and crystalline structure. The following conclusions are drawn:

- 1) The cold work increases the wear resistance of the metals, but such an increase is considerably smaller than that predicted by the Archard equation.
- 2) The reduced benefit of strain-hardening to wear resistance is attributed to the lowered Young's modulus due to lattice imperfections introduced by plastic deformation, which deteriorate the crystalline integrity and thus weaken the average atomic bonding.
- 3) The strain-hardening benefits Cu (FCC) more than Mg (HCP) since the latter has limited slip systems and the cold work more likely results in micro-voids and micro-cracking in materials with lower fracture toughness.
- 4) Mg shows a larger value of η than Cu, which is a coefficient in the wearing energy model, reflecting a higher degree or severity of the negative influence of cold work on Young's modulus of Mg and corresponding wear resistance.
- 5) η value increases with increasing the applied load. This happens because during wear, Young's modulus continuously deteriorates, and a larger load would speed up such deterioration.

6.1.2 Future recommendations

Similar tests can be performed on metallic materials with different crystal structures and microstructures. With proper second phases and microstructure features, it is possible to tune η , e.g., to a negative value, to obtain enlarged benefits of material hardening to the wear resistance. This is worth being investigated. The benefits of different hardening mechanisms, such as precipitation-hardening,

solution-hardening, and others, etc., to the wear resistance, should be investigated as well based on the wearing energy consumption, which would help select the optimal hardening process to achieve the largest benefits.

6.2. Part II: The unsuitability of generalizing the H/E ratio as an index for the wear resistance of materials

6.2.1. Concluding results

Using cold worked Mg and Cu as an example, we demonstrate that the H/E ratio should not be generalized as an index for wear resistance. With cold work, the hardness of the materials increases, which is beneficial to the wear resistance. However, the cold work deteriorates the crystal integrity by introducing lattice imperfections, leading to decreased Young's modulus corresponding to weakened atomic bonding. The H/E ratio overestimates the wear resistance of the metals even more than Archard's equation.

6.2.2. Future recommendations

It would be of interest to expand the scope of this research to other types of material with different crystal structures and microstructures, such as ceramic materials, composites, and coatings or thin films, to obtain further understanding. Using metal-matrix composite reinforced by ceramic particles as an example, the reinforcing phase may increase both the hardness and Young's modulus. In this case, how H/E varies with the wear resistance can be systematically investigated to further assess this ratio for possible use in wear analysis and representation.

6.3. Part III: Influence of Bauschinger effect on the wear behavior of cold-worked Cu and Mg during unidirectional and bidirectional sliding wear

6.3.1. Concluding results

In this study, influences of the Bauschinger effect on the wear behavior of cold-worked Cu and Mg during unidirectional and bidirectional sliding wear tests were investigated. Mg and Cu were cold worked to different amounts (0%, 10%, 20%, 30%, 40% reduction in thickness) and their hardness and Young's modulus were measured after polishing. Sliding wear tests were performed in unidirectional and bidirectional with different frequencies of changing the sliding direction (CN=0, 5, 10, 20, 30) to investigate the effect of wear stress reversal on the wear behavior of the cold worked Cu and Mg. The wear tracks were analyzed using a 3D profilometer and characterized by SEM and EDX analysis, including oxidation caused by frictional heating. The following conclusions were drawn:

- 1) Hardness values of Cu and Mg samples increased with cold work due to the strain hardening effect while Young's modulus decreased caused by the strain-induced defects such as dislocations, microcracks, and microvoids.
- 2) Wear volume loss is smaller during bidirectional sliding, which further lowers the frequency of changing the sliding direction. This decrease in the wear volume is mainly due to the Bauschinger effect in which, on reversing the wearing stress, dislocation reversible movement and annihilation takes place (canceling out of dislocations with opposite sign).

- 3) Cold work in Cu increased dislocation density, which led to a higher probability of dislocations tangling, so less profound Bauschinger effect as compared to undeformed Cu. After 20% cold work, the percentage change in wear volume was relatively stable.
- 4) In Mg, the percentage wear volume change was higher in cold worked samples as compared to undeformed Mg. It's mainly because of fewer dislocations and less dislocation pipe up, which left more space for reversible movement of dislocations on reversal of wearing stress. The presence of microvoids and microcracks also facilitate the reversible dislocation movement with less constraint for generating new dislocations with an opposite sign as the wearing stress is reversed, thus aiding the Bauschinger effect.
- 5) Due to frictional heating, oxidation occurred on both Cu and Mg samples during the wear tests. The oxygen amounts on Cu and Mg samples caused by bidirectional sliding were larger than those caused by unidirectional for both Cu and Mg. The formed tribo-oxide layer helped reduce wear.
- 6) The smaller coverage of oxide on worn surfaces caused by the unidirectional sliding could be due to the unidirectional wearing force that may enhance the plowing effect and scratch off the oxide scale. While during the bi-directional sliding, the reversal of wearing force could weaken such scratch-off effect, since the Bauschinger effect may also apply to the dislocation process at the metal/oxide interface. The larger coverage of the oxide scale on the worn surface may help reduce local stress concentration, thus reducing the wear damage. In other words, the formation of oxide scales could further benefit the resistance of the sample to bi-directional sliding wear attack.

6.3.2. Future recommendations

During sliding testing, the surface temperature can be raised, which may lead to local annealing such as recovery, recrystallization, and grain growth. Such changes could influence the Bauschinger effect and such the wear behavior. This is worth being investigated in order well control the wear of materials.

Similar to the above two parts, bidirectional and unidirectional sliding wear can be performed on metals with different crystal structures, alloys, and composites. A higher frequency of directional change ($CN > 30$) can also be used to observe the saturation level of the reversal of dislocation motion. Different counter bodies like steel balls or any other ceramic other than silicon nitride can also be used to observe any difference in the wear behavior.

In addition, one could take advantage of the Bauschinger effect to optimize machining efficiency for the manufacturing industry. For instance, the cutting efficiency could be considerably affected using unidirectional cutting or bidirectional cutting. Furthermore, the material of the counterpart should also affect the Bauschinger effect, since there is a large difference in adhesive force between metal-metal pair and ceramic-metal pair. This can be investigated to effectively control industrial wear, optimize tribological systems, and improve machining processes.

Bibliography

- [1] Reye Th. Zur Theorie der Zapfenreibung. Der Civilingenieur, 4: 235–255 (1860).
- [2] Xin, L., Han, Y., Ling, L., Lu, Y., & Shoji, T. (2021). Surface Oxidation and Subsurface Microstructure Evolution of Alloy 690TT Induced by Partial Slip Fretting Corrosion in High-Temperature Pure Water. *Acta Metallurgica Sinica (English Letters)*, 34(4), 543-554.
- [3] Gu, Y., Xia, K., Wu, D., Mou, J., & Zheng, S. (2020). Technical characteristics and wear-resistant mechanism of nano coatings: a review. *Coatings*, 10(3), 233.
- [4] Zhou, K., Keer, L. M., Wang, Q. J., & Hua, D. Y. (2011). Size prediction of particles caused by chipping wear of hard coatings. *Wear*, 271(7-8), 1203-1206.
- [5] Feng, X., Lu, C., Jia, J., Xue, J., Wang, Q., Sun, Y., ... & Yi, G. (2020). High temperature tribological behaviors and wear mechanisms of NiAl–NbC–Ag composites formed by in-situ decomposition of AgNbO₃. *Tribology International*, 141, 105898.
- [6] Singh, K., Tiwari, M., & Mahato, A. (2020). Evolution of regimes of wear in zircaloy-4/inconel-600 contact subjected to fretting loading. *Tribology International*, 147, 106274.
- [7] Kruschov M M. Resistance of metals to wear by abrasion, as related to hardness. London: Proc. Conf. Lubrication and wear, Institution Mech. Eng. 655–659 (1957)
- [8] Krushchov M M, Babichev M A. Investigation of wear of metals. Moscow: Russian Academy of Sciences, 1960.

- [9] Archard J F. Contact and rubbing of flat surfaces. *Journal of Applied Physics* 24: 981–988 (1953).
- [10] Archard J F, Hirst W. The wear of metals under unlubricated conditions. *Proc. R. Soc. London A* 236: 397–410 (1956).
- [11] Burwell, J. T., and C. D. Strang. "Metallic wear." *Proceedings of the Royal Society of London. Series A. Mathematical and Physical Sciences* 212.1111 (1952): 470-477.
- [12] R. Holm, *Electrical Contacts* (H. Gerbers, Stockholm, 1946).
- [13] F. P. Bowden and D. Tabor, *Friction and Lubrication of Solid* (Clarendon Press, Oxford, 1950).
- [14] D. H. Buckley, *Surface Effects in Adhesion, Friction, Wear, and Lubrication* (Elsevier, New York, 1981).
- [15] Rabinowicz E.: *Friction and Wear of Materials*. Wiley, New York (1965; 2nd ed., 1995).
- [16] N. P. Suh, *Sliding Wear of Metals, Tribophysics* (Prentice-Hall, Inc., 1986), Chap. 5.
- [17] A. Zmitrowicz, *J. Theor. Appl. Mech.* 44, 219 (2006).
- [18] K. C. Ludema and L. Ajayi, *Friction Wear Lubrication: A Textbook in Tribology*, 2nd ed. (CRC Press, Boca Raton, 2018).
- [19] I. Hutchings and P. Shipway, *Sliding Wear, Tribology—Friction and Wear of Engineering Materials*, 2nd ed. (Butterworth-Heinemann, Oxford, 2017), Chap. 5.
- [20] D. A. Rigney, "Sliding wear of metals," *Annu. Rev. Mater. Sci.* 18, 141–163 (1988).

- [21] D. Y. Li and A. Wear, in ASM Handbook, Friction, Lubrication, and Wear Technology, edited by G. E. Totten (ASM International, Materials Park, 2017), Vol. 18, pp. 44073–40002.
- [22] F. P. Bowden and D. Tabor, R. Soc. Proc. A 169, 391 (1939).
- [23] E. Rabinowicz, J. Appl. Phys. 22, 1373 (1951).
- [24] Li, D.Y., Pan, Hongbo: A wearing energy model. J. of Applied Physics 128, 195105 (2020).
- [25] Grover, R.; Carthy, B. Mc; Zhao, Y.; Jabbour, G. E.; Sarid, D.; Laws, G. M.; Takulapalli, B. R.; Thornton, T. J.; Gust, D. (2004). Kelvin probe force microscopy as a tool for characterizing chemical sensors. Applied Physics Letters, 85(17), 3926
- [26] Li, Q., Hua, G., Lu, H., Yu, B., Li, D.Y.: Understanding the Effect of Plastic Deformation on Elastic Modulus of Metals Based on a Percolation Model with Electron Work Function. JOM 70, 1130–1135 (2018).
- [27] Orlova, T.S., Ankudinov, A.V., Mavlyutov, A.M., Resnina, N.N.: Effect of Grain Boundaries on the Electron Work Function of Ultrafine Grained Aluminum. Rev. on Adv. Mater. Sci. 57, 110-115 (2018).
- [28] Li, W., Li, D.Y.: On the correlation between surface roughness and work function in copper. The Journal of Chemical Physics 122, 064708 (2005).
- [29] Khisamov, R.K., Safarov, I.M., Mulyukov, R.R., Yumaguzin, Y.M.: Effect of grain boundaries on the electron work function of nanocrystalline nickel. Phys. Solid State 55, 1–4 (2013).

- [30] Li, W., Li, D.Y.: In situ measurements of simultaneous electronic behavior of Cu and Al induced by mechanical deformation. *Journal of Applied Physics* 99, 073502 (2006).
- [31] Karanjule, D., Bhamare, S., Rao, T.: Effect of Cold Drawing Pass Schedule on Mechanical Properties and Microstructure of ST 52 during Cold Drawing of Seamless Tubes and its Influence on Springback, *Advances in Science Technology and Engineering Systems Journal* 2, 1202-1210 (2017).
- [32] Yu, H.Y.: Variation of elastic modulus during plastic deformation and its influence on springback. *Materials & Design* 30, 846–850 (2009).
- [33] ASTM. ASTM G40 - Standard Terminology Relating to Wear and Erosion. ASTM (2017).
- [34] Glaeser, W. A. Friction and Wear. *IEEE Trans. Parts, Hybrids, Packag.* 7, 99–105 (1971).
- [35] Kato, K. Classification of wear mechanisms/models. *Proc. Inst. Mech. Eng. Part J J. Eng. Tribol.* 216, 349–355 (2002).
- [36] Raymond, G. B. *Mechanical wear fundamentals and testing*. Marcel Dekker Inc., 61 USA (2004). doi:doi:10.1201/9780203021798.fmatt
- [37] Varenberg, M. Towards a unified classification of wear. *Friction* 1, 333–340 (2013).
- [38] Yamamoto, T. & Buckley, D. H. *Wear mechanism based on adhesion*. (1982).
- [39] Kato, K. Abrasive wear of metals. *Tribol. Int.* 30, 333–338 (1997).
- [40] Phiri, R. R., Philip Oladijo, O., & Akinlabi, E. T. (2018). Thin films in tribology. *Proceedings of the International Conference on Industrial Engineering and Operations Management*, 2018(NOV), 140-146.

- [41] William D. Callister, David G. Rethwisch. *Materials Science and Engineering: An Introduction* 9th Edition, Wiley; 9 edition (December 4, 2013), ISBN-13: 978-1118324578.
- [42] Dmitri Kopeliovich, *Mechanisms of wear*: Substech.com
https://www.substech.com/dokuwiki/doku.php?id=mechanisms_of_wear
- [43] J. L. González-Velázquez, *Mechanical Behavior and Fracture of Engineering Materials*, *Structural Integrity* 12.
- [44] H Strunk; R Frydman (1975). Jog dragging in edge dislocations with application to plastic deformation and internal friction. , 18(1), 143–148.
- [45] William, F. H. & Hosford, H. *Mechanical behavior of materials*. USA Univ. Michigan. Google Sch. (2005).
- [46] 49. Cheng, Y. T. & Cheng, C. M. Scaling approach to conical indentation in elasticplastic solids with work hardening. *J. Appl. Phys.* 84, 1284–1291 (1998).
- [47] Kleemola, H.J., Nieminen, M.A. On the strain-hardening parameters of metals. *Metall Mater Trans B* 5, 1863–1866 (1974).
- [48] Lasalmonie, A., Strudel, J.L. Influence of grain size on the mechanical behaviour of some high strength materials. *J Mater Sci* 21, 1837–1852 (1986).
- [49] C.H Cáceres; D.M Rovera (2001). Solid solution strengthening in concentrated Mg–Al alloys. , 1(3), 0–156.
- [50] Martin, J. W. (2012). *Precipitation Hardening: Theory and Applications*. United Kingdom: Elsevier Science.
- [51] Morral, F. R. (1977). *Dispersion Strengthening of Metals*. United States: Metals and Ceramics Information Center.

- [52] Christian, J. L. (1967). Fiber-strengthened Metallic Composites. United States American Soc. for Testing and Materials.
- [53] Comprehensive Materials Processing. (2014). Netherlands: Elsevier Science.
- [54] Kittel C. Introduction to Solid State Physics (8th ed.) John Wiley and Sons. 2015, ISBN: 978-1-119-45416-8.84
- [55] Torre C. PHYS 3700: Introduction to Quantum Statistical Thermodynamics. Utah State University, 2015. Retrieved August 2021.
- [56] Luo Y, Tang Y, Chung TF, Tai CL, Chen CY, Yang JR, Li DY. Electron work function: an indicative parameter towards a novel material design methodology. Scientific Reports, 2021, 11: 11565.
- [57] Hua, G., Li, D.Y.: Generic relation between the electron work function and Young's modulus of metals. Appl. Phys. Lett. 99, 041907 (2011).
- [58] Larisa-Emilia C, Sherri J, Saman S, Michael T. Work-function measurement by high-resolution scanning Kelvin nanoprobe. Measurement Science and Technology, 2007, 18(3): 567–578.
- [59] Fernández Garrillo P. A., Grévin B., Chevalier, N., Borowik, Ł. Calibrated work function mapping by Kelvin probe force microscopy. Review of Scientific Instruments. 2018. 89(4): 043702.
- [60] Bauschinger, J: About the change in the elastic limit and strength of iron and steel through stretching and squeezing, through heating and cooling and through often repeated stress. Communications from the mechanical-technical laboratory of the Royal Technical University in Munich, 13 (1886) 1-116.

- [61] Woolley, R.L. (1953). LXIV. The Bauschinger effect in some face-centred and body-centred cubic metals. *The London, Edinburgh, and Dublin Philosophical Magazine and Journal of Science*, 44(353), 597–618.
- [62] Orowan E., *Symp. on Internal stresses and fatigue in metals*, Detroit, (1958) 59–80.
- [63] G. Masing: *Wiss. Ver. Siemens-Konzern*, 4 (1925), 244.
- [64] G. Masing and W. Mauksch: *Wiss. Ver. Siemens-Konzern.*, 5 (1926), 135.
- [65] E. Heyn, *Metall and Erz*, Heft 22, 22, November 1918, pp. 441-442 and 436-441.
- [66] R.K. (1950). *Plasticity of Crystals*. E. Schmid and W. Boas. F. A. Hughes & Co. Ltd., London. 1950. 353 pp. 222 illustrations. Index. Appendix. Bibliography. 35s. net. *The Journal of the Royal Aeronautical Society*, 54(479), 718-719.
- [67] Masing, G. (1923). Zur Heyn'schen Theorie der Verfestigung der Metalle durch verborgen elastische Spannungen. *Wissenschaftliche Veröffentlichungen Aus Dem Siemens-Konzern*, 231–239.
- [68] N.F. Mott, A theory of work-hardening of metal crystals *Phil Mag*, 43 (346) (1952), pp. 1151-1178.
- [69] A. Seeger, *Dislocation and Mechanical Properties of Crystals*, John-Wiley and Sons, New York, 1957, pp. 243.
- [70] Madhavan, R., Bellon, P., Averbach, R.S.: Wear resistance of Cu/Ag multilayers: a microscopic study. *ACS Appl. Mater. Interfaces* 10, 15288–15297 (2018).
- [71] Fischer, A., Dudzinski, W., Gleising, B., Stemmer, P.: Analyzing mild- and ultra-mild sliding wear of metallic materials by transmission electron microscopy. In: Dienwiebel, M., de Barros, M.I. (eds.) *Advanced Analytical Methods in Tribology, Triboanalytics*, pp. 29–59. Springer, Berlin (2018).

- [72] Li, X.Y., Tandon, K.N.: Microstructural characterization of mechanically mixed layer and wear debris in sliding wear of an Al alloy and an Al based composite. *Wear* 245, 148–161 (2000).
- [73] Popov, Valentin: Generalized Archard law of wear based on Rabinowicz criterion of wear particle formation, *Mechanical Engineering* 17 39 – 45 (2019).
- [74] Straffelini, G.: *Friction and Wear-Methodologies for Design and Control*, Springer, Switzerland, 2015.
- [75] Rabinowicz E.: The effect of size on the looseness of wear fragments. *Wear* 2, 4–8 (1958).
- [76] Popova, E., Popovl, V.L., Kim, Dae-Eun: 60 years of Rabinowicz’ criterion for adhesive wear, *Friction* 6, 341–348 (2018).
- [77] Rabinowicz, E., Dunn, L. A., and Russell, P. G.: A Study of Abrasive Wear Under Three-Body Conditions, *Wear* 4, 345–355 (1961).
- [78] Dorini, F.A., Pintaude, G., and Sampaio, R: Maximum Entropy Approach for Modeling Hardness Uncertainties in Rabinowicz’s Abrasive Wear Equation, *Journal of Tribology* 136 021607-1 (2014).
- [79] Atkins, A. G.; Slice–push, formation of grooves and the scale effect in cutting. *Interface Focus*, 6, 20160019 (2016).
- [80] ASTM E399-20., Standard Test Method for Linear-Elastic Plane-Strain Fracture Toughness of Metallic Materials. ASTM International. West Conshohocken, PA. www.astm.org (2020).
- [81] Kumar, Vikas, Li, Lei, Gui, Hailian, Wang, Xiaogang, Huang, Qingxue, Li, Qingyang, Mokdad, Fatma, Chen, D.L., Li ,D.Y.: Tribological properties of AZ31

- alloy pre-deformed at low and high strain rates via the work function. *Wear* 414-415, 126-135 (2018).
- [82] Friedel, J.: XLVI. Anomaly in the rigidity modulus of copper alloys for small concentrations. *The London, Edinburgh, and Dublin Philosophical Magazine and Journal of Science* 44, 444-448 (1953).
- [83] Wagner, L.: Mechanical surface treatments on titanium, aluminum and magnesium alloys. *Materials Science and Engineering A263*, 210-216 (1999).
- [84] Imashimizu, Yuji, Watanabé, Jirô: Morphology of Dislocation Etch Pits on the (111) Surface of Cu Crystals, *Transactions of the Japan Institute of Metals* 24, 1-8 (1983).
- [85] Hockey, B. J., Mitchell, J. W.: Etch pit studies of dislocation arrangements resulting from the deformation of single crystals of copper 7.5 at.% aluminium alloys, *Philosophical Magazine* 26, 409-423 (1972).
- [86] Mott, N.F.: CXVII. A theory of work-hardening of metal crystals. *The London, Edinburgh, and Dublin Philosophical Magazine and Journal of Science* 43, 1151-1178 (1952).
- [87] G.W. Rowe, *Friction, Wear and Lubrication: Terms and Definitions*, OECD, Paris, 1968.
- [88] T.L. Oberle, *Wear of metals*, *J. Occup. Med.* 3 (1951) 438-439.
- [89] W. Ni, Y.-T. Cheng, M.J. Lukitsch, A.M. Weiner, L.C. Lev, D.S. Grummon, Effects of the ratio of hardness to Young's modulus on the friction and wear behavior of bilayer coatings, *Appl. Phys. Lett.* 85 (2004) 4028-4030.
- [90] G. Pintaude, Introduction of the ratio of the hardness to the reduced elastic modulus for abrasion, *Tribology - Fundamentals and Advancements* (2013),

- [91] David Labonte, Lenz Anne-Kristin, Michelle L. Oyen, *Acta Biomater.* 57 (2017) 373–383.
- [92] C. Rebholz, A. Leyland, J. Schneider, A. Voevodin, A. Matthews, Structure, hardness, and mechanical properties of magnetron-sputtered titanium–aluminium boride films, *Surf. Coating. Technol.* 120-121 (1999) 412–417.
- [93] A. Amri, Z.-T. Jiang, X. Zhao, Z. Xie, C.-Y. Yin, N. Ali, N. Mondinos, M.M. Rahman, Tailoring the physicochemical and mechanical properties of optical copper–cobalt oxide thin films through annealing treatment, *Surf. Coating. Technol.* 239 (2014) 212–221.
- [94] M. Hawryluk, Z. Gronostajski, P. Widomski, M. Kaszuba, J. Ziembra, J. Smolik, Influence of the application of a PN Cr/CrN hybrid layer on the improvement of the lifetime of hot forging tools, *J. Mater. Process. Technol.* 258 (2018) 226–238.
- [95] Wenzheng Zhai, Lichun Bai, Runhua Zhou, Xueling Fan, Guozheng Kang, Yong Liu, Kun Zhou, Recent progress on wear-resistant materials: Designs, properties, and applications, *Adv. Sci.* 8 (2021) 2003739.
- [96] Xiulin Jia, Cuicui Ji, Jiangbo Cheng, Yiping Shan, Songya Tian, Erosive wear resistance evaluation with the hardness after strain-hardening and its application for a high-entropy alloy, *Wear* (2018) 178–182, 398-399.
- [97] Li Li, Suyan Zhao, Nannan Zhang, Yanhui Guo, Hongyan Gan, Enhanced Wear Resistance of Iron-Based Alloy Coating Induced by Ultrasonic Impact, *Coatings* 9 (2019) 804.

- [98] Huanlong Hu, Li Zhong, Wen Sun, Ruitao Li, Hua Li, Khiam Aik Khor, Friction and wear behaviors of reduced graphene oxide- and carbon nanotube-reinforced hydroxyapatite bioceramic, *Front. Mater* 11 (2020), 564624.
- [99] Yunqing Tang, Hongbo Pan, D.Y. Li, Contribution of cold work to the wear resistance of materials and its limitation – a study combining molecular dynamics modeling and experimental investigation, *Wear* 476 (2021) 203650.
- [100] S.A. Kouhanjani, A. Zare-Bidaki, M. Abedini, N. Parvin, Influence of prior cold working on the tribological behavior of Cu–0.65wt.%Cr alloy, *J. Alloys Compd.* 480 (2009) 505–509.
- [101] A. Khodabakhshi, V. Abouei, N. Mortazavi, S.H. Razavi, H. Hooshyar, M. Esmaily, Effects of cold working and heat treatment on microstructure and wear behaviour of Cu–Be alloy C17200, *Tribology - Materials, Surfaces & Interfaces* 9 (2015) 118–127.
- [102] K.-H. Zum Gahr, Wear by hard particles, *Tribol. Int.* 31 (1998) 587–596.
- [103] Z. Bojar, P. Jozwik, C. Pakowski, Abrasive wear of Ni₃Al - based intermetallic alloy, *Int. J. Appl. Mech. Eng.* 9 (2004) 21–26.
- [104] K. Edalati, M. Ashida, Z. Horita, T. Matsui, H. Kato, Wear resistance and tribological features of pure aluminum and Al–Al₂O₃ composites consolidated by high-pressure torsion, *Wear* 310 (2014) 83–89.
- [105] W. Li, D.Y. Li, Variations of work function and corrosion behaviors of deformed copper surfaces, *Appl. Surf. Sci.* 240 (2005) 388–395.
- [106] Zhaoxuan Wu, W.A. Curtin, The origins of high hardening and low ductility in magnesium, *Nature* 526 (2015) 62–67.

- [107] Chao He, Yujuan Wu, Liming Peng, Ning Su, Li Xue, Kun Yang, Yongjie Liu, Shucheng Yuan, Renhui Tian, Cyclic deformation and correspondent crack initiation at low-stress amplitudes in Mg–Gd–Y–Zr alloy, *Materials* 11 (2018) 2429.
- [108] F.J. Young Jr., Etch pits at dislocations in copper, *J. Appl. Phys.* 32 (1961) 192.
- [109] A. H. Cottrell, "Dislocations and Plastic Flow in Crystals", 1953 (Oxford University Press), pp. 111 and 132.
- [110] S. N. Buckley, and K. M. Entwistle, *Acta Metall.* 1956.4, pp.352.
- [111] H. G. Van Bueren, *Imperfections in Crystal*, 1960 (Amsterdam), pp.240.
- [112] Zebang Zheng, Rui Li, Mei Zhan, Gaihan Yuan, Hongrui Zhang, Yudong Lei, Daniel S. Balint, The effect of strain rate asymmetry on the Bauschinger effect: A discrete dislocation plasticity analysis, *Journal of Materials Research and Technology*, Volume 16, 2022, Pages 1904-1918.
- [113] Stewart, D., Cheong, K.S.: Molecular dynamics simulations of dislocations and nanocrystals. *Curr. Appl. Phys.* 8, 494–497 (2008).
- [114] Wu, P., Xu, X., Rengarajan, V., Zwieback, I.: Propagation and density reduction of threading dislocations in SiC crystals during sublimation growth silicon carbide 2008. *Mater. Process. Devices* 1069, 83–88 (2008).
- [115] Nye, J.F.: Unfolding higher-order wave dislocation clusters and catastrophe theory. *J. Opt. A Pure Appl. Opt.* 10, 075010 (2008).
- [116] Fang, H., Horstemeyer, M.F., Baskes, M.I., Solanki, K.: Atomistic simulations of Bauschinger effects of metals with high angle and low angle grain boundaries. *Comput. Methods Appl. Mech. Eng.* 193, 1789–1802 (2004).

- [117] Srivatsan, T.S.: The low-cycle fatigue and cyclic fracture behaviour of 7150 aluminium alloy. *Int. J. Fatigue* 13, 313–321 (1991).
- [118] Hecker, M., Thiele, E., Holste, C.: X-ray diffraction analysis of internal stresses in the dislocation structure of cyclically deformed nickel single crystals. *Mater. Sci. Eng. A* 234, 806–809 (1997).
- [119] Yue, L., Zhang, H., Li, D.Y.: A molecular dynamics study of nano twined copper under two-directional sliding. *Scripta Mater.* 63, 1116–1119 (2010).
- [120] C.Y. Tang, D.Y. Li, G.W. Wen, Bauschinger's effect in wear of materials, *Tribol. Lett.* 41 (3) (2011) 569–572.
- [121] C. Tang, D.Y. Li, G.W. Wen, A follow-up study on Bauschinger's effect in bidirectional wear of Cu-40% Zn against different types of counter-face, *Tribol. Lett.* 43 (1) (2011) 101–106.
- [122] C. Tang, J.M. Wang, G.W. Wen, Y. Wang, D.Y. Li, Bauschinger effect in wear of Cu-40Zn alloy and its variations with the wear condition, *Wear* 271 (9–10) (2011) 1237–1243.
- [123] Kumar, A., Li, D.Y. Clarification of the Puzzled Effects of Cold work on Wear of Metals from the Viewpoint of Wearing Energy Consumption. *Tribol Lett* 70, 3 (2022).
- [124] Caceres, C. H.; Lukac, P.; Blake, A. (2008). Strain hardening due to {10 12} twinning in pure magnesium. *Philosophical Magazine*, 88(7), 991–1003.
- [125] Zhang, Z.F.; Wang, Z.G.; Su, H.H. (1999). Observations on persistent slip bands transferring through a grain boundary in a copper bicrystal by the electron channelling contrast in scanning electron microscopy technique. *Philosophical Magazine Letters*, 79(5), 233–240.

- [126] Xu, Z., Li, D. Y., & Chen, D. L. (2021). Effect of Ti on the wear behavior of AlCoCrFeNi high-entropy alloy during unidirectional and bi-directional sliding wear processes. *Wear*, 476, 203650.
- [127] N. El-Tayeb (1994). The variation of hardness and wear coefficient in sliding wear of copper and aluminum alloys. , 174(1-2), 63–69. doi:10.1016/0043-1648(94)90087-6.
- [128] Iulian Radu; D.Y. Li (2005). Investigation of the role of oxide scale on Stellite 21 modified with yttrium in resisting wear at elevated temperatures. , 259(1-6), 453–458.

Appendix

A brief introduction to a wearing energy model

A wearing energy model was developed to deal with wear attack from a viewpoint of energy consumption [1], which is the deformation energy absorbed up to failure. When a material is cold worked, although the apparent hardness is increased due to the strain-hardening effect, the introduced defects deteriorate the atomic bonding, which diminishes the benefit of the increased hardness to the wear resistance. Such an effect is related to the ratio of residual strain in the pre-deformed state (ε_p) to the failure strain (ε_f) as ($\varepsilon_p/\varepsilon_f$) which can be correlated to the variation in Young's modulus (E) via its relationship with electron work function (φ) [1, 2].

Use tension test as an example, the specific deformation energy of an undeformed or strain-free sample up to failure is represented by the area under the stress-strain curve (ABDE); while that for a pre-deformed or cold worked one is smaller (FCDE) due to the decrease in ductility or failure strain from ε_f to $\varepsilon_f - \varepsilon_p$, although the yield strength increases from σ_y of the strain-free sample to σ'_y of the cold worked one as figure 1 illustrates [1].

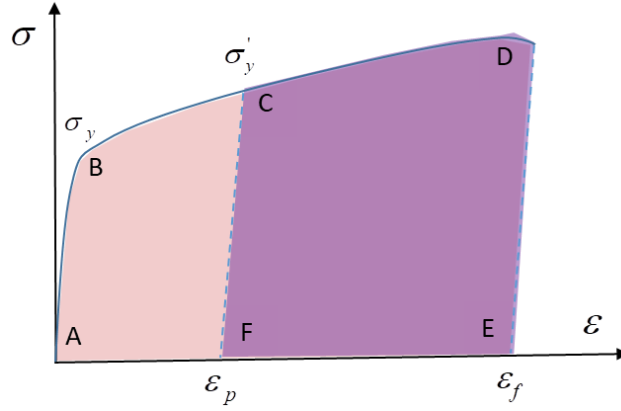


Figure 1. Stress-strain curve showing the energy consumed by an un-deformed sample (area ABDE) and pre-deformed sample (area FCDE) up to failure during tension test.

In the model, the wear rate i.e., the volume loss per unit sliding distance ($v = V/D$) of a material is larger if its energy consumption rate i.e., the wearing energy consumed per unit sliding distance ($w = W/D$) is smaller. It would take more energy to wear a strain-free material than to wear a deformed material which absorbs less energy for a fixed volume loss. Thus, we have [1]

$$v_f \cdot w_f = v_p \cdot w_p \quad (2)$$

Or

$$\frac{v_p}{v_f} = \frac{w_f}{w_p} \quad (3)$$

where f stands for strain-free state and p for the plastically deformed state. Here, $w_f \approx \sigma_f \varepsilon_f \approx \frac{1}{3} H_o \varepsilon_f$ (where, $\sigma_y \approx \frac{1}{3} H$ [3]) and $w_p \approx \sigma'_y (\varepsilon_f - \varepsilon_p) \approx \frac{1}{3} H (\varepsilon_f - \varepsilon_p)$. The wear energy consumption ratio, w_f/w_p , can be represented by the ratio of energy

consumption up to failure of un-strained sample to that of a deformed one i.e.

$$\sigma_y \varepsilon_f / \sigma'_y (\varepsilon_f - \varepsilon_p) \approx H_o \varepsilon_f / H (\varepsilon_f - \varepsilon_p) [1].$$

The wear rate of a deformed material can thus be expressed as

$$v_p = \frac{v_f w_f}{w_p} \cong \frac{v_f H_o \varepsilon_f}{H (\varepsilon_f - \varepsilon_p)} \quad (4)$$

From Archard's equation,

$$\frac{V}{D} = K \frac{L}{H_o} = v_f \quad (5)$$

Substitute v_f in eq.(5) into eq.(4), we have

$$v_p = \frac{v_f w_f}{w_p} \cong \frac{v_f H_o \varepsilon_f}{H (\varepsilon_f - \varepsilon_p)} = K \frac{L}{H (1 - \frac{\varepsilon_p}{\varepsilon_f})} \quad (6)$$

During plastic deformation, dislocations are generated, which lower the density of the material and weaken the atomic bond strength [4, 5-7]. Since the elastic modulus is dependent on the interatomic bond strength, the weakened atomic bonds due to cold working lowers the Young's modulus [8-11]. Via the relationships among the Young's modulus, electron work function, and strain energy, the $\varepsilon_p / \varepsilon_f$ ratio can be related to the ratio of Young's modulus of plastically deformed material (E) to that of strain-free one (E_o),

$$\eta \ln \left(\frac{E}{E_o} \right) = - \left(\frac{\varepsilon_p}{\varepsilon_f} \right) \quad (7)$$

where η is an adjusting parameter used to capture possible influences on the relationship between these two ratios, e.g., crystal structure, microstructure, type of deformation (tension, rolling, etc.), and formation of other defects such as microvoids. With this relationship, eq.(6) can be turned to

$$v_p = K \frac{L}{H[1 + \eta \ln(E/E_0)]} \quad (8)$$

or a form similar to Archard equation in which the wearing energy consumption has been considered,

$$V = K \frac{L \cdot D}{H[1 + \eta \ln(E/E_0)]} \quad (9)$$

The effect of cold work on wear can be well captured by looking at the deterioration of the crystal integrity caused by the cold work or plastic deformation.

References

- [1] Li, D.Y., Pan, Hongbo: A wearing energy model. *J. of Applied Physics* **128**, 195105 (2020).
- [2] Hua, G., Li, D.Y.: Generic relation between the electron work function and Young's modulus of metals. *Applied Physics Letters* **99**, 041907 (2011).
- [3] Zhang, P., Li, S. X., Zhang, Z. F.: *Mater. Sci. Eng. A* **529**, 62 (2011).
- [4] Li, Q., Hua, G., Lu, H., Yu, B., Li, D.Y.: Understanding the Effect of Plastic Deformation on Elastic Modulus of Metals Based on a Percolation Model with Electron Work Function. *JOM* **70**, 1130–1135 (2018).

- [5] Orlova, T.S., Ankudinov, A.V., Mavlyutov, A.M., Resnina, N.N.: Effect of Grain Boundaries on the Electron Work Function of Ultrafine Grained Aluminum. *Rev. on Adv. Mater. Sci.* **57**, 110-115 (2018).
- [6] Li, W., Li, D.Y.: On the correlation between surface roughness and work function in copper. *The Journal of Chemical Physics* **122**, 064708 (2005).
- [7] Khisamov, R.K., Safarov, I.M., Mulyukov, R.R., Yumaguzin, Y.M.: Effect of grain boundaries on the electron work function of nanocrystalline nickel. *Phys. Solid State* **55**, 1–4 (2013).
- [8] Li, W., Li, D.Y.: In situ measurements of simultaneous electronic behavior of Cu and Al induced by mechanical deformation. *Journal of Applied Physics* **99**, 073502 (2006).
- [9] Karanjule, D., Bhamare, S., Rao, T.: Effect of Cold Drawing Pass Schedule on Mechanical Properties and Microstructure of ST 52 during Cold Drawing of Seamless Tubes and its Influence on Springback, *Advances in Science Technology and Engineering Systems Journal* **2**, 1202-1210 (2017).
- [10] Yu, H.Y.: Variation of elastic modulus during plastic deformation and its influence on springback. *Materials & Design* **30**, 846–850 (2009).
- [11] Yamaguchi, K., Adachi, H., Takakura, N.: Effects of plastic strain and strain path on Young's modulus of sheet metals. *Metals and Materials* **4**, 420–425 (1998).